



5-2010

## **A Fully Integrated High-Temperature, High-Voltage, BCD-on-SOI Voltage Regulator**

Benjamin Matthew McCue  
bmccue@utk.edu

Follow this and additional works at: [https://trace.tennessee.edu/utk\\_gradthes](https://trace.tennessee.edu/utk_gradthes)



Part of the [VLSI and Circuits, Embedded and Hardware Systems Commons](#)

---

### **Recommended Citation**

McCue, Benjamin Matthew, "A Fully Integrated High-Temperature, High-Voltage, BCD-on-SOI Voltage Regulator. " Master's Thesis, University of Tennessee, 2010.  
[https://trace.tennessee.edu/utk\\_gradthes/646](https://trace.tennessee.edu/utk_gradthes/646)

This Thesis is brought to you for free and open access by the Graduate School at TRACE: Tennessee Research and Creative Exchange. It has been accepted for inclusion in Masters Theses by an authorized administrator of TRACE: Tennessee Research and Creative Exchange. For more information, please contact [trace@utk.edu](mailto:trace@utk.edu).

To the Graduate Council:

I am submitting herewith a thesis written by Benjamin Matthew McCue entitled "A Fully Integrated High-Temperature, High-Voltage, BCD-on-SOI Voltage Regulator." I have examined the final electronic copy of this thesis for form and content and recommend that it be accepted in partial fulfillment of the requirements for the degree of Master of Science, with a major in Electrical Engineering.

Benjamin J. Blalock, Major Professor

We have read this thesis and recommend its acceptance:

Benjamin J. Blalock, Leon M. Tolbert, Syed K. Islam

Accepted for the Council:

Carolyn R. Hodges

Vice Provost and Dean of the Graduate School

(Original signatures are on file with official student records.)

To the Graduate Council:

I am submitting herewith a thesis written by Benjamin Matthew McCue entitled “A Fully Integrated High-Temperature, High-Voltage, BCD-on-SOI Voltage Regulator.” I have examined the final electronic copy of this thesis for content and form and recommend that it be accepted in partial fulfillment of the requirements for the degree of Master of Science, with a major in Electrical Engineering.

Benjamin Blalock, Major Professor

We have read this thesis  
and recommend its acceptance:

---

Syed Islam

---

Leon Tolbert

---

Benjamin Blalock

Accepted for the Council:

---

Carolyn R. Hodges  
Vice Provost and Dean of the Graduate School

(Original signatures are on file with official student records.)

A Fully Integrated High-Temperature,  
High-Voltage, BCD-on-SOI Voltage Regulator

A Thesis  
Presented for the  
Master of Science Degree  
The University of Tennessee Knoxville

Benjamin Matthew McCue  
May 2010

Copyright © 2009 by Benjamin Matthew McCue  
All rights reserved.

# Acknowledgments

I would like to acknowledge my graduate committee Dr. Leon Tolbert, Dr. Syed Islam, and Dr. Benjamin Blalock for their insight, support, and dedication to educating future engineers. Having the knowledge and support of a very strong faculty greatly enhances the ability to prepare oneself for a career in electrical engineering.

I would also like to recognize the peer support of the entire Integrated Circuits and System Laboratory (ICASL) team. Their continued assistance with course work and research made pursuing post-graduate education a rewarding experience. A special thanks to ICASL members Robert Greenwell and Ross Chun.

Also, I would like to reiterate the support I received from my major professor Dr. Blalock. Without his support, financially and intellectually, reaching this point in my education would not have been possible. Dr. Blalock prepares his students for engineering careers as well as any student could hope.

Lastly, I would like to thank my family for their unconditional support. My wife, Jenna, followed me every step of the way through this demanding process. I would like to thank my late father, David, for his inspiration to choose a career in electrical engineering, and while he is not here now, I know he is proud.

# Abstract

Developments in automotive (particularly hybrid electric vehicles), aerospace, and energy production industries over the recent years have led to expanding research interest in integrated circuit (IC) design toward high-temperature applications. A high-voltage, high-temperature SOI process allows for circuit design to expand into these extreme environment applications. Nearly all electronic devices require a reliable supply voltage capable of operating under various input voltages and load currents. These input voltages and load currents can be either DC or time-varying signals. In this work, a stable supply voltage for embedded circuit functions is generated on chip via a voltage regulator circuit producing a stable 5-V output voltage. Although applications of this voltage regulator are not limited to gate driver circuits, this regulator was developed to meet the demands of a gate driver IC. The voltage regulator must provide reliable output voltage over an input range from 10 V to 30 V, a temperature range of  $-50\text{ }^{\circ}\text{C}$  to  $200\text{ }^{\circ}\text{C}$ , and output loads from 0 mA to 200 mA. Additionally, low power stand-by operation is provided to help reduce heat generation and thus lower operating junction temperature. This regulator is based on the LM723 Zener reference voltage regulator which allows stable performance over temperature (provided proper design of the temperature compensation scheme). This circuit topology and the SOI silicon process allow for reliable operation under all application demands. The designed voltage regulator has been successfully tested from  $-50\text{ }^{\circ}\text{C}$  to  $200\text{ }^{\circ}\text{C}$  while demonstrating an output voltage variation of less than 25 mV under the full range of input voltage. Line regulation tests from 10 V to 35 V show a 3.7-ppm/V supply sensitivity. With the use of a high-temperature ceramic output capacitor, a 5-nsec edge, 0 to 220 mA, 1- $\mu\text{sec}$  pulse width load current induced only a 55 mV drop in regulator output voltage. In the targeted application, load current pulse widths will be much shorter, thereby improving the load transient performance. Full temperature and input voltage range tests reveal the no-load supply current draw is within 330  $\mu\text{A}$  while still providing an excess of 200 mA of load current upon demand.

# Contents

<b>1. Introduction.....</b>	<b>1</b>
1.1. Motivation .....	1
1.2. Thesis Organization.....	1
<b>2. Background and Literature Review .....</b>	<b>2</b>
2.1. Voltage Regulator Background .....	2
2.2. LM723 Voltage Regulator Topology .....	4
2.2.1. LM723 Reference Generator Circuit.....	4
2.2.2. LM723 Operational Amplifier Circuit .....	6
2.3. LM723 Design Review .....	8
<b>3. Voltage Regulator Design and Simulation.....</b>	<b>9</b>
3.1. Voltage Regulator Design .....	9
3.1.1. Pre-Regulator.....	10
3.1.2. Reference Generator.....	13
3.1.3. Operational Amplifier .....	16
3.1.4. Output Stage .....	19
3.2. Voltage Regulator Simulation .....	20
3.2.1. Operational Amplifier .....	20
3.2.2. Input Voltage Start-Up .....	21
3.2.3. Line Regulation .....	22
3.2.4. Load Regulation .....	25
3.2.5. Temperature Characteristic .....	29
3.2.6. Load Transient.....	33
3.2.7. Line Transient.....	37
<b>4. Post-Fabrication Verification .....</b>	<b>41</b>
4.1. Voltage Regulator Testing Set-Up .....	41
4.2. Input Voltage Start-Up .....	43
4.3. Line Regulation .....	44
4.4. Load Regulation .....	47



4.5. Temperature Characteristic .....	50
4.6. Load Transient.....	54
4.7. Line Transient .....	59
<b>5. Conclusions.....</b>	<b>64</b>
5.1. Thesis Summary .....	64
5.2. Future Work .....	64
<b>References.....</b>	<b>66</b>
<b>Vita.....</b>	<b>68</b>

# List of Figures

Figure 2.1. Series Voltage Regulator .....	3
Figure 2.2. LM723 Voltage Reference Generator Circuit .....	5
Figure 2.3. LM723 Operational Amplifier Circuit .....	6
Figure 2.4. LM723 Operational Amplifier Circuit – AC Equivalent .....	7
Figure 3.1. 4-Stage Voltage Regulator Topology .....	10
Figure 3.2. Pre-Regulator Circuit.....	11
Figure 3.3. Reference Generator Circuit.....	13
Figure 3.4. Operational Amplifier Circuit .....	17
Figure 3.5. Output Stage .....	19
Figure 3.6. Operational Amplifier Loop Transmission .....	21
Figure 3.7. Simulated Voltage Regulator Start-Up.....	22
Figure 3.8. Simulated $V_{DD}$ Line Regulation.....	23
Figure 3.9. Simulated $V_{PRE}$ Line Regulation.....	24
Figure 3.10. Simulated $V_{REF}$ Line Regulation.....	24
Figure 3.11. Simulated $I_{REG}$ Line Regulation .....	25
Figure 3.12. Simulated $V_{DD}$ Load Regulation.....	26
Figure 3.13. Simulated $V_{PRE}$ Load Regulation.....	27
Figure 3.14. Simulated $V_{REF}$ Load Regulation.....	27
Figure 3.15. Simulated $I_{PRE}$ Load Regulation.....	28
Figure 3.16. Simulated $I_{REG}$ Load Regulation.....	28
Figure 3.17. Simulated $V_{DD}$ Temperature Characteristic .....	30
Figure 3.18. Simulated $V_{PRE}$ Temperature Characteristic .....	31
Figure 3.19. Simulated $V_{REF}$ Temperature Characteristic .....	31

Figure 3.20. Simulated $I_{PRE}$ Temperature Characteristic .....	32
Figure 3.21. Simulated $I_{REG}$ Temperature Characteristic .....	32
Figure 3.22. Simulated $I_{SUPPLY}$ Temperature Characteristic .....	33
Figure 3.23. Simulated $-50\text{ }^{\circ}\text{C}$ Load Transient .....	34
Figure 3.24. Simulated $25\text{ }^{\circ}\text{C}$ Load Transient .....	35
Figure 3.25. Simulated $200\text{ }^{\circ}\text{C}$ Load Transient .....	36
Figure 3.26. Simulated $-50\text{ }^{\circ}\text{C}$ Line Transient .....	38
Figure 3.27. Simulated $25\text{ }^{\circ}\text{C}$ Line Transient .....	39
Figure 3.28. Simulated $200\text{ }^{\circ}\text{C}$ Line Transient .....	40
Figure 4.1. Voltage Regulator Layout .....	41
Figure 4.2. Voltage Regulator Post-Fabrication .....	42
Figure 4.3. Voltage Regulator Test Board .....	42
Figure 4.4. Measured Voltage Regulator Start-Up .....	43
Figure 4.5. Measured $V_{DD}$ Line Regulation .....	45
Figure 4.6. Measured $V_{PRE}$ Line Regulation .....	45
Figure 4.7. Measured $V_{REF}$ Line Regulation .....	46
Figure 4.8. Measured $I_{REG}$ Line Regulation .....	46
Figure 4.9. Measured $V_{DD}$ Load Regulation .....	48
Figure 4.10. Measured $V_{PRE}$ Load Regulation .....	48
Figure 4.11. Measured $V_{REF}$ Load Regulation .....	49
Figure 4.12. Measured $I_{PRE}$ Load Regulation .....	49
Figure 4.13. Measured $I_{REG}$ Load Regulation .....	50
Figure 4.14. Measured $V_{DD}$ Temperature Characteristic .....	51
Figure 4.15. Measured $V_{PRE}$ Temperature Characteristic .....	52
Figure 4.16. Measured $V_{REF}$ Temperature Characteristic .....	52

Figure 4.17. Measured $I_{PRE}$ Temperature Characteristic .....	53
Figure 4.18. Measured $I_{REG}$ Temperature Characteristic .....	53
Figure 4.19. Measured $I_{SUPPLY}$ Temperature Characteristic .....	54
Figure 4.20. Load Transient Test Set-Up.....	55
Figure 4.21. Measured $-50\text{ }^{\circ}\text{C}$ Load Transient .....	56
Figure 4.22. Measured $25\text{ }^{\circ}\text{C}$ Load Transient .....	57
Figure 4.23. Measured $200\text{ }^{\circ}\text{C}$ Load Transient .....	58
Figure 4.24. Line Transient Test Set-Up .....	59
Figure 4.25. $v_{pulse}$ Line Transient Signal .....	60
Figure 4.26. Measured $-50\text{ }^{\circ}\text{C}$ Line Transient .....	61
Figure 4.27. Measured $25\text{ }^{\circ}\text{C}$ Line Transient .....	62
Figure 4.28. Measured $200\text{ }^{\circ}\text{C}$ Line Transient .....	63

# 1. Introduction

## *1.1 – Motivation*

Research centered around hybrid-electric vehicles continues to expand as the need to reduce dependence on fossil fuels increases. The electric motors in these vehicles show drastic increases in automotive fuel efficiency when compared to standard combustion engines. The extreme environment presented by these hybrid-electric engines can produce temperatures approaching 200 °C [1]. Of the many electrical components required in the implementation of these vehicles, high power DC-DC converters and DC-AC inverters are the cornerstone of generating drive-capable energy from battery power [1]. These energy converters require large drive currents to efficiently operate. The gate driver is a device that provides transient currents to the gates of these power devices [2]. Central to the implementation of the gate driver is the need for a stable voltage supply for its switching circuits [2]. Load current and input voltage variations create a demand for a voltage regulator capable of operating effectively over a variety of conditions. Current high-temperature voltage regulators capable of this operation do not yet effectively meet the demands of the gate driver circuits, which has led to the development of a LM-723 Zener reference-based voltage regulator in a high-temperature, high-voltage silicon-on-insulator (SOI) process (a commercially-available 0.8 micron SOI, BJT-CMOS-DMOS (BCD) process). In addition to the automotive application, the designed high-temperature voltage regulator has a wide range of potential applications which include aerospace and energy production industries. The uniqueness of this design stems from the wide operating temperature and wide input voltage range.

## *1.2 – Thesis Organization*

This thesis illustrates the design process for the implemented voltage regulator. The details of the LM723 voltage regulator (on which this design is based) are examined as well as design steps of the voltage regulator developed for the specific application. Simulation verification of the post-extraction design illustrates the design concepts in practice. Post-fabrication functionality testing over the entire range of operating conditions demonstrates properly functioning design

implementation. A design review highlights the performance capabilities of the voltage regulator while exploring potential design improvements.

## 2. Background and Literature Review

### 2.1 – Voltage Regulator Background

The general term “voltage regulator” simply describes a device that maintains a constant output voltage level regardless of outside influence (input voltage, load condition, temperature) [3]. Linear voltage regulator topologies (non-switching technology) are broken down into two main categories: series and shunt regulators. In general, series regulators provide better temperature performance than shunt regulators; the wide operating temperature for this voltage regulator project directs the choice of regulator topology to employ a series configuration [3]. The series regulator also allows for a greater input voltage to output voltage differential than the shunt regulator, and therefore, proves to be the obvious choice for the high input voltage used in this system [3]. The main components used in a series regulator consist of a reference voltage generator and an operational amplifier [4]. Figure 2.1 illustrates the implementation of a reference voltage generator and an operational amplifier to form a series voltage regulator. Resistors  $R_1$  and  $R_2$  are used to set the output voltage in relation to the reference voltage. The output voltage ( $V_{OUT}$ ) is related to the reference voltage ( $V_{REF}$ ) through the non-inverting, ideal op-amp equation (Equation 2.1) [4].

$$V_{OUT} = V_{REF} \cdot \frac{R_1 + R_2}{R_2} \quad (\text{Equation 2.1})$$

In general, the reference voltage in series voltage regulators can be generated from several circuits including bandgap voltage references and Zener voltage references [4]. To allow  $V_{OUT}$  to provide a stable, reliable output voltage, the op-amp used in the series voltage regulator must possess the typical qualities of a well-designed op-amp. Low op-amp drift and offset voltage are essential qualities for an op-amp to accurately regulate  $V_{OUT}$  according to Equation 2.1 [5]. The negative feedback loop (with attentive op-amp design) imposes a high impedance node at the input of the op-amp. Large op-amp input impedance is essential in minimizing loading effects presented on the reference generator.

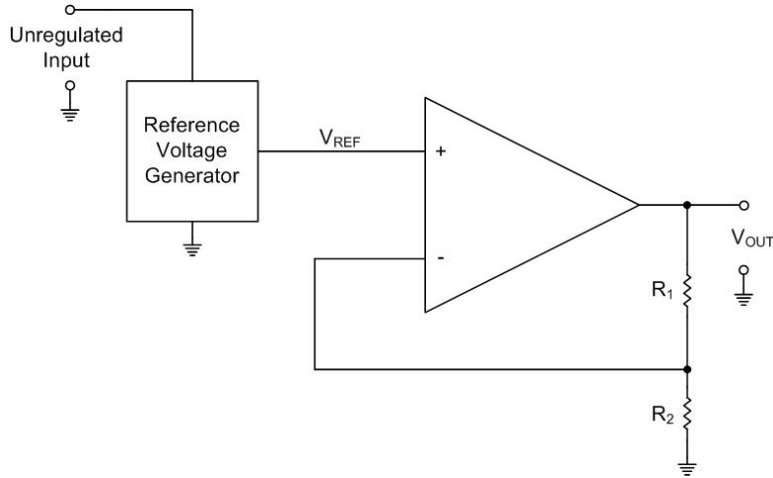


**Figure 2.1 – Series Voltage Regulator**

Similarly, the output of the op-amp must present a low impedance node. As with any op-amp, lowering output impedance increases op-amp current drive capability. Current drive capability is essential in any voltage regulator design due to the use of these circuits as voltage sources for variable load currents [4]. Equations 2.2 and 2.3 illustrate op-amp input impedance and output impedance, respectively.

$$R_{in} = r_i \cdot (1 + T_0) \quad (\text{Equation 2.2})$$

$$R_{out} = \frac{r_o}{(1+T_0)} \quad (\text{Equation 2.3}) \quad \text{where } T_0 = A_{OL} \cdot \frac{R_2}{R_1+R_2}$$

In Equations 2.2 and 2.3,  $A_{OL}$  is the mid-band, open-loop gain of the op-amp, and  $T_0$  is the mid-band loop transmission. Similarly,  $r_i$  and  $r_o$  are the mid-band, open-loop input and output resistances, respectively. As with most op-amp circuits, a large loop transmission allows negative feedback to drastically improve the performance of the op-amp. Exploring the relationship between  $V_{OUT}$  and  $R_{OUT}$  reveals that  $R_{OUT}$  is a function  $V_{OUT}$  as shown in Equation 2.4 (assuming  $A_{OL}$ ,  $V_{REF}$ , and  $r_o$  are constant) [4].

$$R_{OUT} = \frac{r_o}{A_{OL} V_{REF}} \cdot V_{OUT} \quad (\text{Equation 2.4})$$

Change in output current can be related to change in output voltage by Equation 2.5 [4].

$$\Delta V_{OUT} = R_{OUT} \cdot \Delta I_{OUT} \quad (\text{Equation 2.5})$$

Combining Equation 2.4 and Equation 2.5, illustrates the relationship between output voltage and output current (Equation 2.6).

$$\frac{\Delta V_{OUT}}{V_{OUT}} = \frac{r_o}{A_{OL} V_{REF}} \cdot \Delta I_{OUT} \quad (\text{Equation 2.6})$$

Equation 2.6 allows for load regulation calculations of a series regulator. A large open-loop gain improves load regulation and is essential in developing a voltage regulator capable providing an accurate voltage source under variable loads. Line regulation for a given series regulator is dependent on the reference generator circuit and will be examined in following sections [4].

## ***2.2 – LM723 Voltage Regulator Topology***

See reference [4] regarding section 2.2 discussion. The LM723 is a linear, series voltage regulator, which utilizes Zener diodes for reference voltage generation. This design utilizes BJT transistors throughout the topology. To better understand the LM723 design, each circuit section is examined at the transistor level.

### **2.2.1 – LM723 Reference Generator Circuit**

The circuit used to generate the reference voltage in the LM723 regulator design is shown in Figure 2.2. The current sink  $I_I$  is generated using a base-emitter referenced current source. The Zener diode  $D_I$  induces a relatively constant Zener breakdown voltage across  $R_1$ ,  $Q_I$ , and  $R_2$  of approximately 6.2 V. The bias current through  $Q_I$  is set by sizing resistors  $R_1$  and  $R_2$  according to Equation 2.7.

$$I_{C1} = -\frac{6.2 - V_{EB1}}{R_1 + R_2} \quad (\text{Equation 2.7})$$

Therefore, the magnitude of  $I_{C1}$  is approximately equal to 5.6 V divided by the total resistance in series with  $Q_I$ . The main advantage of this current biasing scheme is the independence of the generated bias current to input voltage. Current  $I_{C2}$  is mirrored from  $Q_I$  according to Equation 2.8 (assuming  $V_{EB}$  matching between devices).

$$I_{C2} = I_{C1} \frac{R_2}{R_3} \quad (\text{Equation 2.8})$$



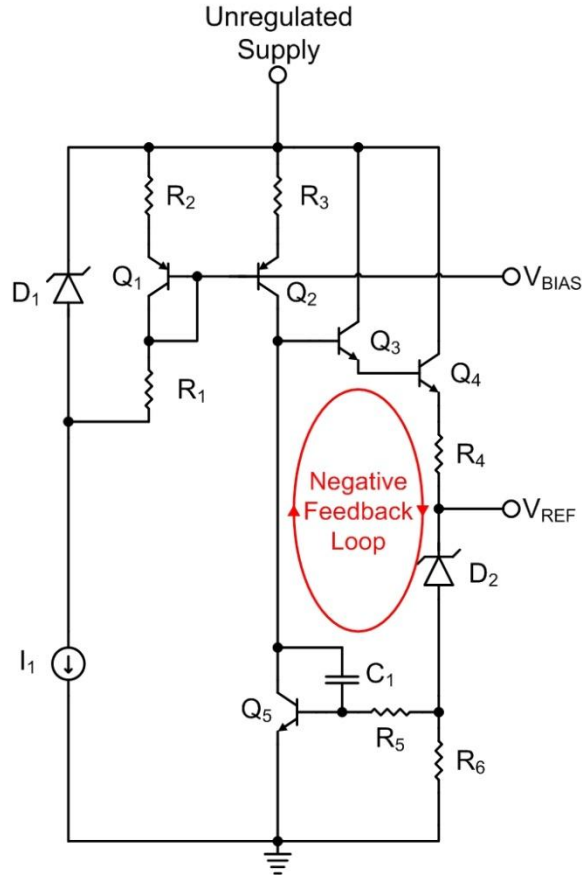


**Figure 2.2 – LM723 Reference Voltage Generator Circuit**

The current  $I_{C2}$  establishes the operating current for the voltage reference circuit composed of  $Q_3$ - $Q_5$ .  $I_{C5}$  is forced to match  $I_{C2}$  through the negative feedback loop. The current through  $D_2$  is set by resistor  $R_6$  according to Equation 2.9 (assuming negligible base currents).

$$I_{D2} = \frac{V_{BE5}}{R_6} \quad (\text{Equation 2.9})$$

The reference voltage,  $V_{REF}$ , is then equal to the sum of the Zener breakdown voltage of  $D_2$  and  $V_{BE5}$  (about 6.8 V).  $Q_3$  and  $Q_4$  form a Darlington pair to boost the loop gain, lowering the impedance at the reference voltage node. Reducing the impedance at the reference voltage node increases the drive capability of the reference generator circuit. Resistor  $R_4$  acts as a current limiter to protect the reference generator circuit from short circuit damage.  $R_5$  and  $C_1$  form a high frequency compensation network to reduce the bandwidth around the loop, which prevents oscillations in the feedback loop. The negative feedback loop provides output tracking and

allows changes at the reference voltage node to be referred to the current through  $D_2$ ; this feedback action corrects changes in reference voltage due to loading effects.

### 2.2.2 – LM723 Operational Amplifier Circuit

Following the voltage reference generator in the LM723 design, the operational amplifier sets and regulates the output voltage as a function of the reference voltage. Figure 2.3 shows the operational amplifier used in the LM723 design. This op-amp is a simple, two-stage feedback amplifier. A differential input pair ( $Q_{11}$ ,  $Q_{12}$ ) provides the gain stage for the op-amp, while the Darlington pair, common-collector stage ( $Q_{13}$ ,  $Q_{14}$ ) provides the low output impedance stage.  $V_{BIAS}$  in Figure 2.3 is generated from the base voltage of the current reference transistor ( $Q_1$ ) in the reference generator circuit. Resistors  $R_7$  and  $R_8$  set the ratios between the reference current through  $Q_1$  and the biasing currents used in the op-amp circuit. Currents  $I_{C6}$ ,  $I_{C7}$ , and  $I_{C8}$  match as long as  $R_7 = R_8$  and the emitter areas of  $Q_6$  and  $Q_7$  are equal.

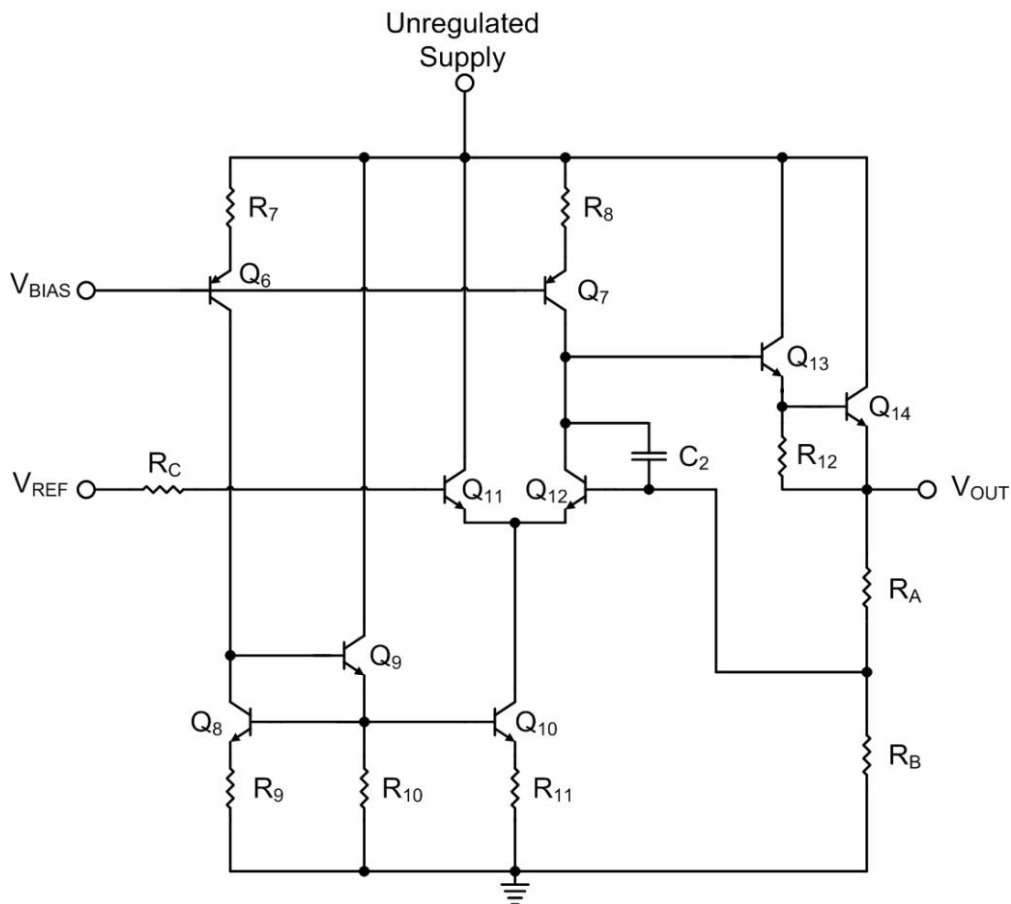


Figure 2.3 – LM723 Operational Amplifier Circuit

$Q_{10}$  is set to have twice the emitter area of  $Q_8$ , and  $R_{11}$  is sized at half the value of  $R_9$ . This device sizing sets  $I_{C10}$  to be twice the magnitude of  $I_{C8}$ . Setting the bias currents to these values allows  $I_{C11}$  to equal  $I_{C12}$ .  $Q_9$  provides current gain to minimize current mismatch due to base currents. This technique allows for better current matching and therefore, reduces offset error at the op-amp output. The load placed at  $V_{OUT}$  determines the current flowing through the Darlington pair  $Q_{14}$  and  $Q_{13}$ .  $R_{12}$  provides a constant current path through  $Q_{13}$ , so the output voltage will always be regulated. Capacitor  $C_2$  provides dominant pole compensation for the op-amp in the form of Miller capacitance. The induced pole reduces the bandwidth and improves stability. The AC equivalent circuit for the op-amp in Figure 2.3 is shown in Figure 2.4.  $R_{LEQ12}$  is calculated from Equation 2.10 and represents the load seen by  $Q_{12}$ .

$$R_{LEQ12} = r_{o7} \cdot (1 + g_{m7}R_8) \quad (\text{Equation 2.10})$$

The output impedance of the gain transistor,  $Q_{12}$ , is calculated assuming  $g_{m11} = g_{m12}$  through matching.

$$R_{o12} = (1 + g_{m12} \frac{1}{g_{m11}}) \cdot r_{o12} \quad (\text{Equation 2.11})$$

Using Equations 2.10 and 2.11, the open-loop gain is derived as demonstrated in Equation 2.12.

$$A_{OL} = \frac{|v_o|}{|v_i|} = \frac{|v_1|}{|v_i|} = \frac{g_{m12}}{2} \cdot (R_{o12} || R_{LEQ12}) \quad (\text{Equation 2.12})$$

The output resistance for the op-amp is determined by the impedance looking into the emitter of the Darlington pair.

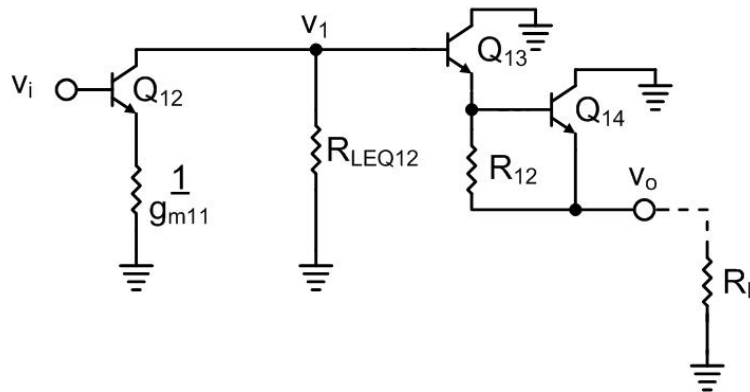


**Figure 2.4 – LM723 Operational Amplifier Circuit – AC Equivalent**

Equation 2.13 shows the calculation of this impedance (assuming  $R_{I2} \gg r_{\pi14}$ ).

$$r_o = \frac{1}{g_{m14}} + \frac{1}{\beta_{o14}} \cdot \left( \frac{1}{g_{m13}} + \frac{R_{o12} \parallel R_{LEQ12}}{\beta_{o13}} \right) \quad (\text{Equation 2.13})$$

Using Equations 2.12 and 2.13 in Equation 2.6 reveals the load regulation of the LM723 topology voltage regulator. Typical values for load regulation are on the order of 0.01-0.04 %; in other words, a 50-mA change in load current for a nominal 5-V output voltage results in an output voltage change of only 1-4 mV. The low output impedance of the op-amp allows the LM723 to exhibit this impressive resistance to loading conditions. The Miller compensation capacitor  $C_2$  sets the dominant pole and allows a 2-pole loop transmission approximation to be used (Equation 2.14).

$$T(s) = T_0 \left( \frac{1}{1 + \frac{s}{T_{mid} \cdot R_{LEQ12} \parallel R_{o12} \cdot C_2}} \cdot \frac{1}{1 + \frac{s}{R_{in12} \parallel R_A \parallel R_B (C_2 + C_{be12} + C_{bc12})}} \right) \quad (\text{Equation 2.14})$$

The single high-gain stage allows for pole splitting which ensures stability. The higher order poles and zeros are neglected, as they occur at frequencies much high than the unity gain frequency ( $f_{un}$ ) of the op-amp.

### 2.3 – LM723 Design Review

The LM723 is a well designed, reliable voltage regulator that has been in industrial use for many years [6]. Several LM723 design features must be considered to ensure the designed voltage regulator meets the demand of the gate driver circuits. First, the LM723 is designed to withstand temperatures up to 125 °C [6]. While its performance will most likely not degrade for temperatures marginally exceeding the rated operating temperature, the use of the gate driver voltage regulator in environments approaching 200 °C imposes significant strain on the classic LM723 design. In addition to the temperature requirements, the gate driver voltage regulator is subject to input voltage ( $V_{DDH} - V_{SSH}$ ) changes ranging from 10-30 V [2]. While the LM723 performs well under varying input voltage, the input conditions the gate driver project presents would result in an output voltage variation of 50-80 mV [6]. While this output voltage change may be acceptable for some applications, the design can be improved to perform more consistently over input voltage changes. Perhaps the most significant challenge to the LM723 design in the gate driver application is the transient load current imposed by the switching

circuits it is required to power. Essentially, the gate driver circuit impose large, switched-capacitor loads [2]. A slow voltage regulator response to a sudden load current demand results in a large deviation in regulator output voltage. Deviations in regulator output voltage can cause instability and gate driver error [2]. The transient current response of the classic LM723 design is not sufficient to supply the gate driver during a transient load [6]. Additionally, the required operating temperature of the gate driver project leads to an increased concern of on-chip heat generation. Also, the low  $\beta$  and  $g_m$  values (especially for the PNP devices) in the commercially-available, 0.8-micron process significantly reduce the attainable DC loop gain [5]. In summary, the LM723 provides a strong example for the design of the gate driver voltage regulator, but several significant design modifications are needed to ensure successful on-chip implementation.

## 3. Voltage Regulator Design and Simulation

### 3.1 – Voltage Regulator Design

The voltage regulator designed for the gate driver project consists of four stages: pre-regulator circuit, reference generator circuit, operational amplifier circuit, and output stage. The pre-regulator is supplied by  $V_{DDH}$  (10.0 V to 30.0 V) and outputs the pre-regulator voltage,  $V_{PRE}$ . The reference generator closely resembles the topology seen in Chapter 2, but several design alterations are implemented to improve regulator performance for the gate driver application. The generated reference voltage ( $V_{REF}$ ) is the most critical voltage for establishing a constant regulator output voltage ( $V_{DD}$ ). The operational amplifier is based on the design described Chapter 2 but with several significant design modifications to the LM723 design. The output of the operational amplifier is designated as  $V_{DD'}$ . The feedback signal from the voltage regulator output is input to the differential pair in the operational amplifier. The output stage of the voltage regulator is technically part of the operational amplifier, but the drastic changes from the topology seen in Chapter 2 warrant special consideration for this stage. The output stage receives the  $V_{DD'}$  signal from the operational amplifier. The output of this stage (and output of the overall voltage regulator) is designated as the output voltage,  $V_{DD}$ . The block diagram in Figure 3.1 illustrates the 4-stage voltage regulator topology as a fully-functional unit with important signals labeled..

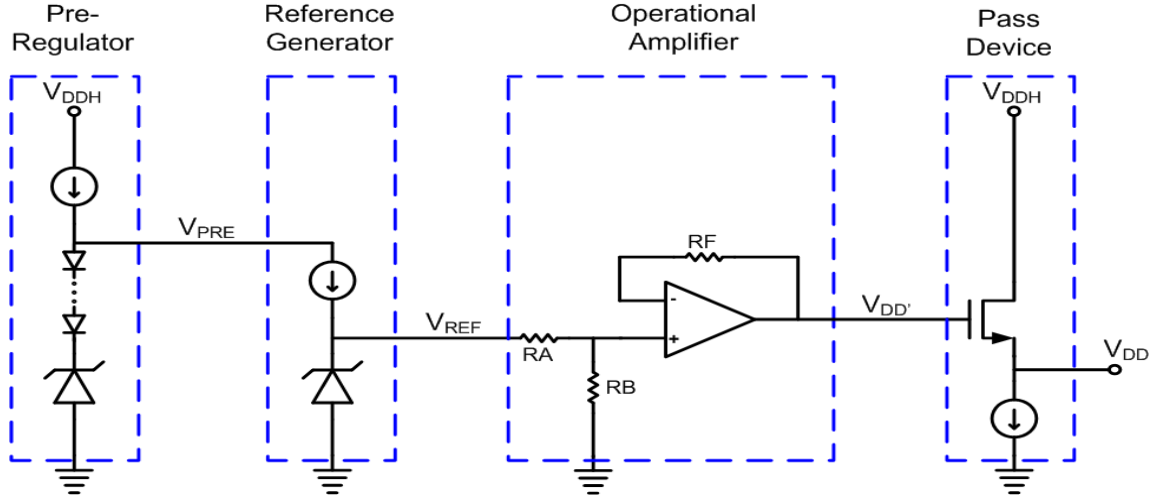


**Figure 3.1 – 4-Stage Voltage Regulator Topology**

### 3.1.1 – Pre-Regulator

The  $V_{DDH}$  input voltage supplied to the gate driver chip varies from 10 - 30 V; however, the commercially-available, 0.8-micron process offers BJT devices with an open-base, collector-emitter breakdown voltage of 15 V. To implement the BJT based LM723 design, a pre-regulator circuit is implemented to limit the voltage supplied to the remaining regulator stages. A Zener shunt regulator is used as a crude voltage regulator to generate  $V_{PRE}$ . Using this concept, the design of a pre-regulator is realized as seen in Figure 3.2. A threshold referenced current source ( $M1-M6$ ,  $R1$ ) generates the bias current for the pre-regulator circuit. This current is set by the threshold of  $M1$  and the resistor  $R1$  as illustrated in Equation 3.1 [4].

$$I_{D2} = I_{D1} = \frac{V_{TH1}}{R_1} \quad (\text{Equation 3.1})$$

This reference current,  $I_{D2}$ , is mirrored through the cascode current mirror,  $M3-M6$ , creating  $I_{D1}$ .  $M1_{SU}-M9_{SU}$  provide start-up for the current source to prevent the stable zero-current state [7].  $M7-M10$  mirror  $I_{D2}$  so that  $I_{D11} = I_{D12} = I_{D1}$ .  $M13$ ,  $M14$  are set to 10x the width of  $M11$ ,  $M12$ , so that  $I_{D13}$ ,  $I_{D14}$  are 10x the generated bias current.  $M11-M14$  are arranged in a wide-swing cascode configuration to allow  $V_{PRE}$  to swing very close to  $V_{DDH}$  [7]. In the wide-swing cascode configuration,  $M12$  is set to 5x the length of  $M11$  [7]. Equations 3.2a and 3.2b illustrate the required voltage difference between  $V_{DDH}$  and  $V_{PRE}$  for  $M13$  and  $M14$  to remain “on” [7].

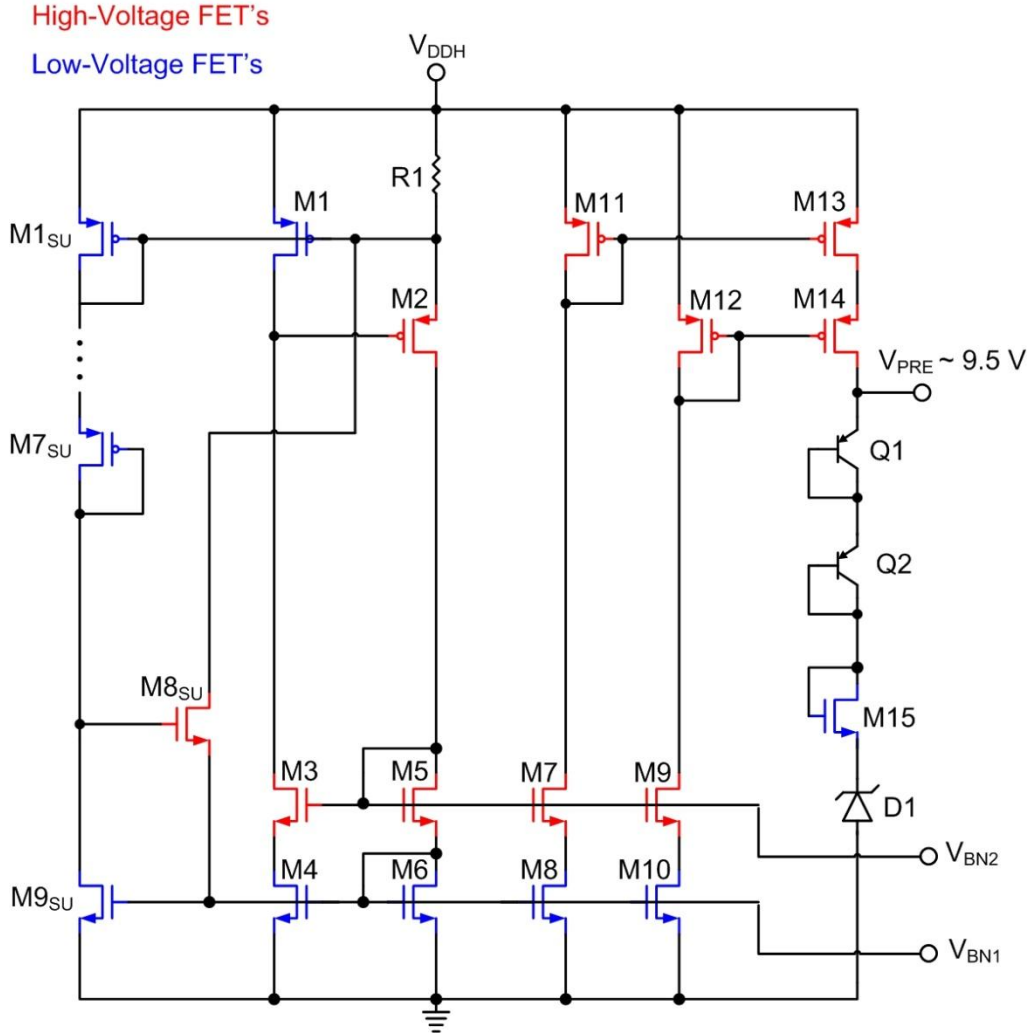


**Figure 3.2 – Pre-Regulator Circuit**

$$V_{DDH} - V_{PRE} \geq 2 \cdot V_{SD,sat\ 13,14} + |V_{TH13}| \quad (\text{Equation 3.2a, typical cascode})$$

$$V_{DDH} - V_{PRE} \geq 2 \cdot V_{SD,sat\ 13,14} \quad (\text{Equation 3.2b, wide-swing cascode})$$

When compared to a wide-swing cascode, a typical cascode configuration requires an additional threshold voltage to remain turned “on”. The additional voltage swing generated by the use of the wide-swing cascode is required for low  $V_{DDH}$  voltages because the regulator circuits require a supply voltage of at least 8.5 V (set to 9.5 V to account for model inaccuracy, process variation, and mismatch). The current source ( $M13, M14$ ) shunts current into the Zener diode, NMOS and PNP series configuration ( $Q1, Q2, M15, D1$ ). The breakdown voltage of  $D1$  in the

commercially-available, 0.8-micron process is about 6.2 V.  $Q1$ ,  $Q2$ , and  $M15$  add two  $V_{EB}$ , one  $V_{THN}$ , and one  $V_{DS,SAT}$  to the generated pre-regulated voltage as shown in Equation 3.3.

$$V_{PRE} = V_{D1,BD} + V_{THN15} + V_{DS,SAT15} + V_{EB1} + V_{EB2} \quad (\text{Equation 3.3})$$

The series configuration of  $Q1$ ,  $Q2$ ,  $M15$ , and  $D1$  provides the temperature-compensated voltage  $V_{PRE}$ . The high  $V_{DDH}$  voltage (up to 30 V) requires high-breakdown voltage devices to be used for the cascode devices. The remaining devices, however, do not have a large, induced drain-source voltage and are implemented using standard devices which provide better matching. Table 3.1 summarizes the devices used in the pre-regulator design.

**Table 3.1 – Pre-Regulator Device Specifications**

<b>Device</b>	<b>Device Type</b>	<b>Device Property</b>
$M1$	Low-Voltage PMOS	$\frac{80.0 \mu}{1.6 \mu}$
$M2, M11$	45-V P-Channel LDMOS	$\frac{20.0 \mu}{3.2 \mu}$
$M12$	45-V P-Channel LDMOS	$\frac{20.0 \mu}{16.0 \mu}$
$M13, M14$	45-V P-Channel LDMOS	$\frac{200.0 \mu}{3.2 \mu}$
$M3, M5, M7, M9$	45-V N-Channel LDMOS	$\frac{20.0 \mu}{3.2 \mu}$
$M4, M6, M8, M10$	Low-Voltage NMOS	$\frac{12.8 \mu}{1.6 \mu}$
$M15$	Low-Voltage NMOS	$\frac{80.0 \mu}{4.0 \mu}$
$M1_{SU}-M7_{SU}$	Low-Voltage PMOS	$\frac{1.6 \mu}{16.0 \mu}$
$M8_{SU}$	45-V N-Channel LDMOS	$\frac{20.0 \mu}{3.2 \mu}$
$M9_{SU}$	Low-Voltage NMOS	$\frac{12.8 \mu}{1.6 \mu}$
$R1$	Poly2	50 k $\Omega$
$D1$	Zener	6.2 V



Using the devices in Table 3.1 and the device properties from the commercially-available, 0.8-micron process documentation, the nominal bias currents are set as follows:  $I_{D4} = I_{D6} = I_{D8} = I_{D10} = I_{D9SU} = 20 \mu\text{A}$ ,  $I_{D13} = 200 \mu\text{A}$ .  $I_{D13}$  is mainly sourced to supply the remaining voltage regulator stages; however, 20-40  $\mu\text{A}$  of current remains to bias  $D1$ ,  $Q1$ ,  $Q2$ , and  $M15$ .  $V_{PRE}$  is established at 9.5 V, but varies slightly with changes in current draw from the remaining stages, temperature, and process variations.

### 3.1.2 – Reference Generator

The reference generator circuit (Figure 3.3) used in the voltage regulator design is powered from the pre-regulator circuit described in Section 3.1.1. In the reference generator circuit, current bias is generated by the base-emitter referenced current source composed of  $Q3$ - $Q6$  and  $R2$  while  $Q1_{SU}$ - $Q5_{SU}$  and  $M16$ - $M17$  provide start-up [4].  $Q7$  sinks the bias current through the parallel combination of  $D2$  and  $Q8$ .

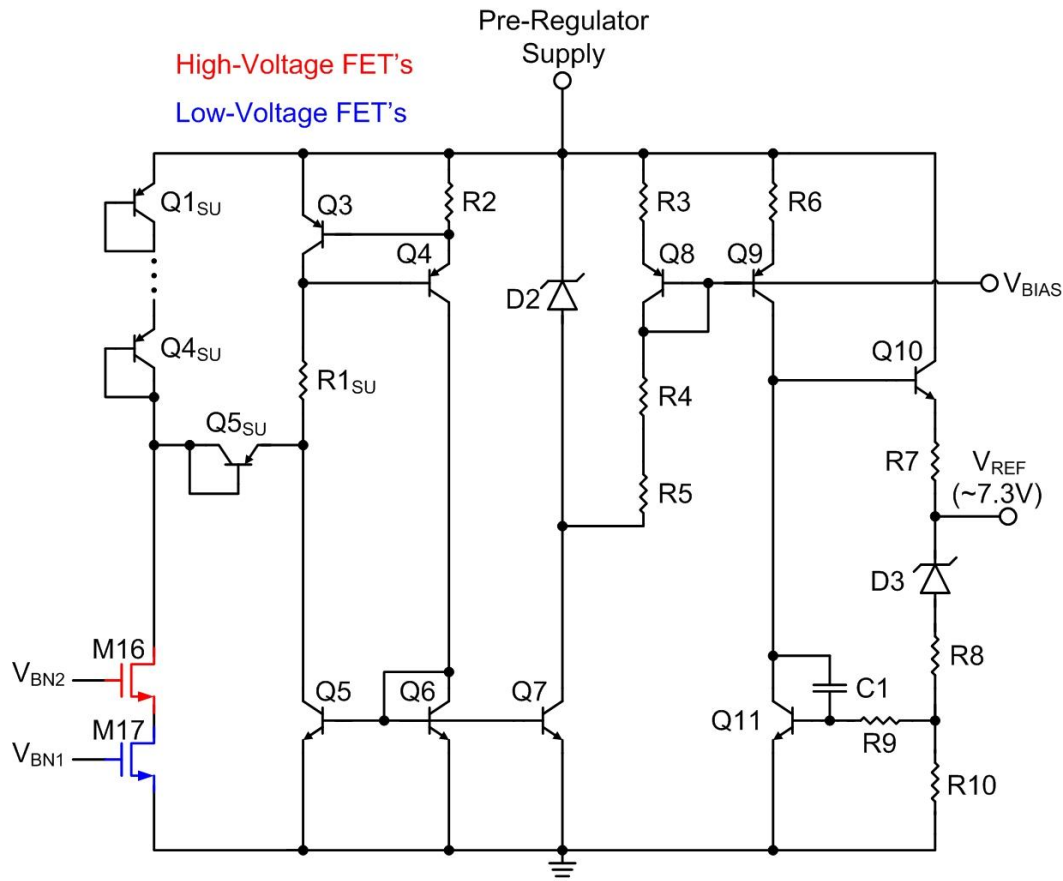


Figure 3.3 – Reference Generator Circuit

$D2$  establishes a reference voltage drop across  $R3$ - $R5$  and  $Q8$ , resulting in a bias current in  $Q8$  governed by Equation 3.4 [4].

$$I_{C8} = \frac{V_{D2,BD}}{R3+R4+R5} \quad (\text{Equation 3.4})$$

$R3$  and  $R4$  possess complementary temperature coefficients and are used to compensate the temperature dependence of  $V_{EB8}$ . The bias current through  $Q8$  is mirrored throughout the reference generator and op-amp circuits. As seen in the LM723 discussion,  $Q10$  provides current bias through  $D3$ .  $D3$  in series with  $R8$  and  $R10$  establish the temperature-compensated reference voltage  $V_{REF}$ .  $R8$  is sized to provide additional compensation to the inherent temperature compensation of  $D3$ . The Darlington pair in the LM723 reference generator is removed because a  $V_{DDH}$  of 10 V does not allow enough headroom between the reference voltage to the pre-regulator voltage. Loading effects on the output of the reference generator are carefully considered due to the removal of the Darlington pair common collector stage [8]. Table 3.2 summarizes the devices used in the reference generator circuit. These device sizes imply a bias current through  $Q3$ - $Q6$  of about 10  $\mu\text{A}$  based on Equation 3.5 and the technology parameters given in the commercially-available, 0.8-micron process documentation.

$$I_{C3} = \frac{V_{EB3}}{R2} \quad (\text{Equation 3.5})$$

The bias current through  $Q7$  is set 2x the current through  $Q5$ - $Q6$  by doubling the emitter area of  $Q7$ . The current through  $Q8$  is established at about 10  $\mu\text{A}$ .  $R10$  establishes a bias current through  $D3$  of approximately 10  $\mu\text{A}$  (Equation 3.6).

$$I_{D3} = \frac{V_{BE11}}{R10} \quad (\text{Equation 3.6})$$

The temperature-dependent reference voltage is described by Equation 3.7.

$$V_{REF}(T) = V_{D3,BD}(T) + V_{BE11}(T) + R8(T) \cdot I_{D3}(T) \quad (\text{Equation 3.7})$$

Substituting Equation 3.6 into Equation 3.7 yields Equation 3.8. The first-order temperature coefficients are estimated by taking the first derivative of Equation 3.8.

**Table 3.2 – Reference Generator Device Specifications**

Device	Device Type	Device Property
<i>M16</i>	45-V N-Channel LDMOS	$\frac{20 \mu}{3.2 \mu}$
<i>M17</i>	Low-Voltage NMOS	$\frac{3.2 \mu}{1.6 \mu}$
<i>Q1<sub>SU</sub>-Q5<sub>SU</sub></i>	Lateral PNP	1x (unit transistor)
<i>Q3-Q4, Q8-Q9</i>	Lateral PNP	4x
<i>Q5-Q6, Q11</i>	Lateral NPN	4x
<i>Q7, Q10</i>	Lateral NPN	8x
<i>D2, D3</i>	Zener	8x
<i>R1<sub>SU</sub></i>	Poly2	110 kΩ
<i>R2</i>	Poly2	68 kΩ
<i>R3, R6</i>	Poly2	2 kΩ
<i>R4</i>	Poly2	380 kΩ
<i>R5</i>	PWell	170 kΩ
<i>R7</i>	N+	160 Ω
<i>R8</i>	Poly2	18 kΩ
<i>R9</i>	Poly2	32 kΩ
<i>R10</i>	Poly2	42 kΩ
<i>C1</i>	MOSCAP	4 pF

$$V_{REF}(T) = V_{D3,BD}(T) + V_{BE11}(T) + V_{BE11}(T) \cdot \frac{R8(T)}{R10(T)} \quad (\text{Equation 3.8})$$

Equation 3.9 defines the first-order temperature coefficient of the reference voltage as a function of device temperature coefficients.

$$\frac{\partial}{\partial T} V_{REF}(T) = \frac{\partial}{\partial T} V_{D3,BD}(T) + \frac{\partial}{\partial T} V_{BE11}(T) + \frac{\partial}{\partial T} V_{BE11}(T) \cdot \frac{R8_o}{R10_o} \quad (\text{Equation 3.9})$$

$R8$ ,  $R10$  temperature coefficients cancel yielding Equation 3.10, where the nominal resistor values ( $R8_o$ ,  $R10_o$ ) are chosen to minimize the reference voltage temperature coefficients.

$$\frac{R8_o}{R10_o} = \frac{-\left(\frac{\partial}{\partial T}V_{D3,BD}(T) + \frac{\partial}{\partial T}V_{BE11}(T)\right)}{\frac{\partial}{\partial T}V_{BE11}(T)} \quad (\text{Equation 3.10})$$

Equation 3.10 serves as a first order approximation; therefore, second order temperature effects are still present in the generated reference voltage [5]. Using the devices shown in Table 3.2 and device information provided with the commercially-available, 0.8-micron process PDK, a nominal reference voltage of  $\sim 7.3$  V is established by the reference generator. Using Equation 3.10, the  $R8/R10$  ratio is set to 0.4 based on a  $V_{D3,BD}$  temperature coefficient of 2.8 mV/ $^{\circ}$ C and a  $V_{BE}$  temperature coefficient of  $-2$  mV/ $^{\circ}$ C [5].

### 3.1.3 – Operational Amplifier

In order to properly regulate the output voltage under a load condition, the reference voltage is fed to an error amplifier [4]. To combat the inherently low  $\beta$  values for the BJT devices ( $\sim 50$  for NPN,  $\sim 10$  for PNP at room temperature) this amplifier is composed of three stages as opposed to the two used in the LM723 topology. This topology provides a high DC gain, which reduces offset error and improves regulation [8]. Because the op-amp for this regulator has narrow bandwidth requirements (due to use of an external output capacitor), the compensation scheme reduces the bandwidth quite low to accommodate phase margin concerns (the affects of this compensation scheme on transient response are addressed in later sections). Reducing the bandwidth of the feedback loop allows the three-stage amplifier to remain stable [8]. Figure 3.4 shows the implemented three-stage operational amplifier. The compensation node has moved from the differential pair (as in the LM723) to the common-emitter stage. Another modification to the operational amplifier is that the reference voltage is resistively divided before being fed to the operational amplifier input. The 7.3-V reference voltage used to generate  $V_{DD}$  must be resistively divided to approximately 5 V, which requires the operational amplifier to operate in unity gain. Figure 3.4 demonstrates this configuration with the feedback resistor  $R_F$  used to reduce mismatch offset related to the input bias currents. All bias currents in the op-amp are set to  $I_{C8}$  (of the reference generator) except for  $I_{C16}$  and  $I_{C22}$  which are double  $I_{C8}$ .

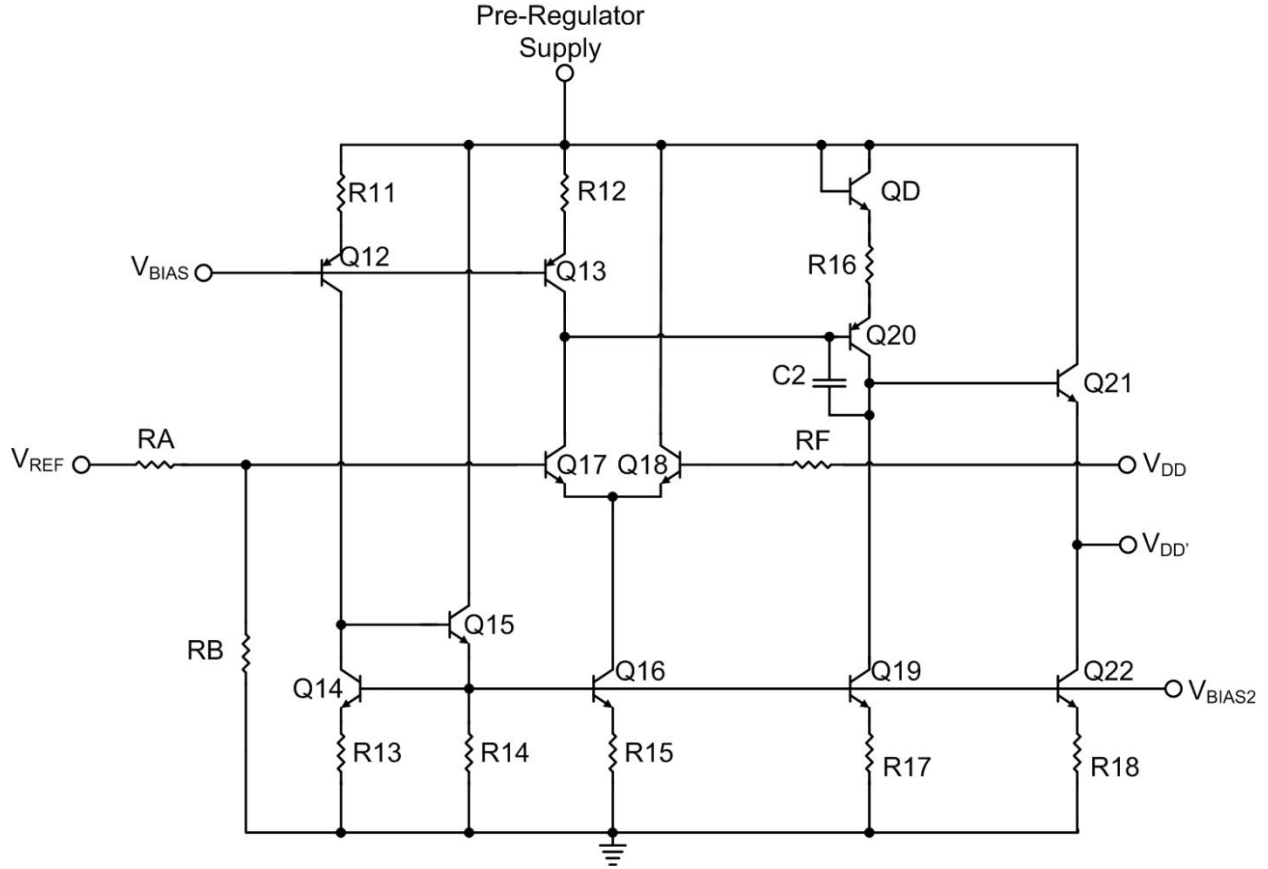


**Figure 3.4 – Operational Amplifier Circuit**

$I_{C16}$  is doubled to provide current bias for  $Q17$  and  $Q18$ , while  $I_{C22}$  is doubled to increase the drive capability of the common collector stage.  $QD$  and  $R16$  are added to allow  $Q13$  to remain in forward-active mode by pulling the emitter voltage of  $Q20$  down from the pre-regulator voltage rail. The resistance seen in the emitter of  $Q20$  ( $R16$  and  $r_{eD}$ ) is sized to allow  $Q20$  to remain the dominant gain stage. The DC loop transmission is found to be approximately 85 dB using Equation 3.11 ( $A_{diff} \sim 25$  dB,  $A_{CE} \sim 60$  dB using defined device values).

$$T_o = \frac{|v_o|}{|v_i|} = A_{diff} \cdot A_{CE} = \frac{g_{m17}}{2} (R_{o17} || R_{LEQ17}) \cdot -g_{m20} \cdot \frac{R_{LEQ20}}{R16} \quad (\text{Equation 3.11})$$

The Miller capacitor  $C2$  provides loop stability by pole splitting [7]. The pole created at the common-emitter stage ( $Q20$ ) is compensated to take advantage of the 60 dB gain at that stage. The expression for the loop transmission can be seen in Equation 3.12. Assuming  $C2$  dominates parasitic capacitances,  $\tau_l$  in Equation 3.12 is established by the gain of the common emitter stage,  $C2$ , and the equivalent load seen by  $Q17$ .

$$T(s) = T_o \left( \frac{1}{1 + \frac{s}{\tau_1}} \right) \left( \frac{1}{1 + \frac{s}{\tau_2}} \right) \quad (\text{Equation 3.12})$$

Similarly,  $\tau_2$  is established by the capacitance at the base of *Q18* and the equivalent resistance at the base of *Q18*. Both poles in the two-pole approximation are subject to the Miller effect. The gain of the common-emitter amplifier is set to dominate the gain of the differential input pair, which allows pole-splitting to ensure stability.

$$\tau_1 = \left( R_{in,20} \parallel R_{out,17} \parallel R_{out,13} \right) \cdot C_2 \cdot A_{CE} \quad (\text{Equation 3.13a})$$

$$\tau_2 = \left( R_{in,18} \parallel (R_F + (R_{out,21} + R_{out,22})) \right) \cdot C_{in,18} \cdot A_{diff} \quad (\text{Equation 3.13b})$$

The resulting phase margin is over 70° which allows for stable operation. Table 3.3 lists the devices used in the operational amplifier circuit. This simple op-amp design provides stable voltage regulation over the full range of operating conditions.

**Table 3.3 – Operational Amplifier Device Specifications**

Device	Device Type	Device Property
<i>Q12-Q13, Q20</i>	Lateral PNP	4x
<i>Q14-Q15, Q17-19, QD</i>	Lateral NPN	4x
<i>Q16, Q21-Q22</i>	Lateral NPN	8x
<i>R11-R13, R16-R17</i>	Poly2	2 kΩ
<i>R14</i>	Poly2	58 kΩ
<i>R15, R18</i>	Poly2	1 kΩ
<i>RA</i>	Poly2	200 kΩ
<i>RB</i>	Poly2	440 kΩ
<i>RF</i>	Poly2	140 kΩ
<i>C2</i>	MOSCAP	100 pF

### 3.1.4 – Output Stage

In addition to the common-collector stage at the output of the op-amp, an output device capable of driving large currents and regulating large input/output voltage differentials is required at the last stage of the voltage regulator. To prevent load current from being drawn from the pre-regulator (increasing the no load supply current), this pass device draws its current directly from the input voltage ( $V_{DDH}$ ). The insufficient open-base collector-emitter breakdown voltage of the BJT devices necessitates the use of a high-voltage NMOS device for the output device. The schematic for the output stage is depicted in Figure 3.5.  $Q23$  provides a small bias current to allow  $M18$  to regulate the output voltage under no load conditions. Using an NMOS transistor as the pass device allows the load current to be drawn from  $V_{DDH}$ , but the “on” resistance associated with this device degrades the load regulation this voltage regulator could potentially demonstrate [5]. Due to the high drain voltage imposed on  $M18$ , this device is always saturated; and therefore, the output voltage is a function of the load current [8]. To decrease this effect as much as possible, the width of  $M18$  is set quite large. Table 3.4 lists the devices used in the output stage of the voltage regulator design.

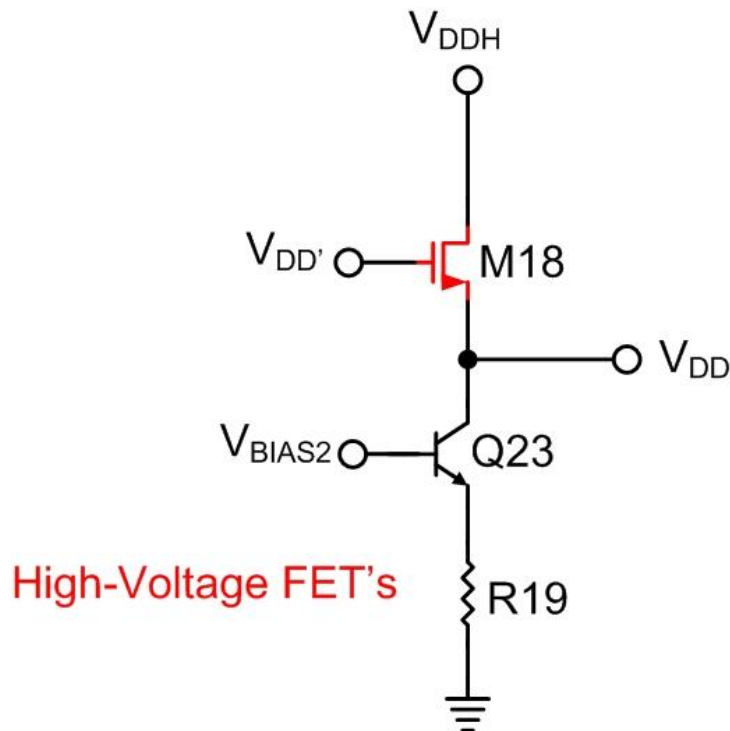


Figure 3.5 – Output Stage

**Table 3.4 – Output Stage Device Specifications**

Device	Device Type	Device Property
<i>M18</i>	45-V N-Channel LDMOS	$\frac{3000 \mu}{3.2 \mu}$
<i>Q23</i>	Lateral NPN	4x
<i>R19</i>	Poly2	2 k $\Omega$

### 3.2 – Voltage Regulator Simulation

#### 3.2.1 – Operational Amplifier

For the operation amplifier loop transmission simulation,  $V_{DD'}$  is connected directly to  $V_{DD}$ , which allows the op-amp performance to be isolated. Loop transmission simulations for the operational amplifier closely match the predicted loop transmission as evident in Figure 3.6. The simulated DC loop gain of the op-amp is over 86 dB. The op-amp loop transmission is dominated by a two-pole response ( $f_1 \sim 10$  Hz,  $f_2 \sim 500$  kHz) with a gain-bandwidth product of about 200 kHz. Some higher order effects are visible but occur well past  $f_{un}$  and have minimal effect on the op-amp operation. Stable op-amp operation is ensured due to the ample phase and gain margins ( $P.M. \sim 72$ ,  $G.M. \sim 10$  dB). The operational amplifier provides stable operation, low offset, and accurate regulation due to the high gain and phase margin. The transient response of the operational amplifier is limited due to the low bandwidth of the design. The use of an external output capacitor reduces the bandwidth requirement of the voltage regulator by providing charge storage to respond to a load transient. The settling time of the regulated output voltage will be slow, but the total deviation from nominal  $V_{DD}$  will be minimal. The load transients presented by the gate driver have very narrow pulse widths, and therefore, the total charge required during a transient will be small. A relatively small output capacitor can supply the charge required during these events effectively reducing the load presented to the voltage regulator. Using this design, the operational amplifier is able to exhibit high DC gain while remaining stable for all operating conditions.



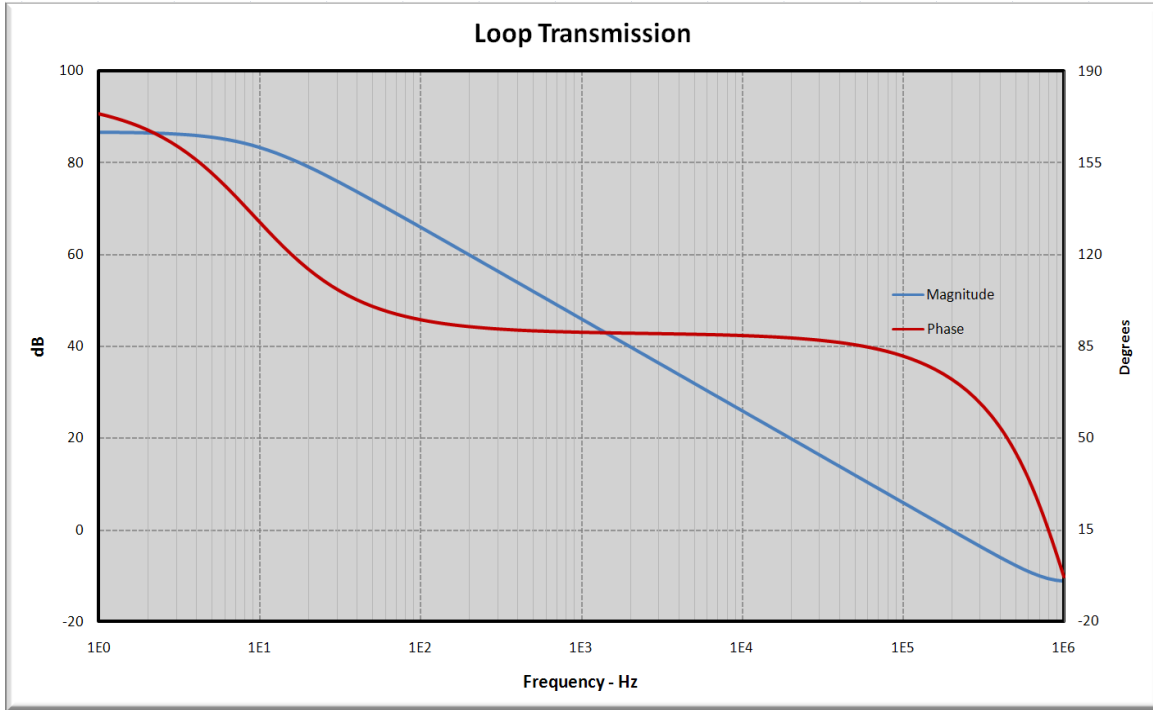


**Figure 3.6 – Operational Amplifier Loop Transmission**

### 3.2.2 – Input Voltage Start-Up

Voltage regulator start-up occurs when the Zener diode,  $D3$ , reaches its breakdown voltage, and the reference voltage is properly regulated. This start-up voltage is one of the fundamental limits of the LM723 topology. Historically, silicon Zener diodes with a breakdown voltage of about 5.6 V have been shown to offer minimized temperature coefficients (the voltage at which the Zener effect and the avalanche effect cancel). In the commercially-available 0.8 micron process, a 6.3 V Zener diode is available. In order for the designed voltage regulator to start-up, Equation 3.14 must be satisfied ( $R7$  is negligible).

$$V_{PRE} \geq V_{D3,BD} + 2V_{BE} + I_{D3} * (R7 + R8) \quad (\text{Equation 3.14})$$

The input voltage must be greater than the sum of the breakdown voltage of the Zener diode and all voltage drops in series with the Zener diode. Typically, the LM723 topology has a higher start-up voltage than other series linear regulator designs. The large start-up voltage of LM723-based voltage regulator designs is a significant design trade-off that must be considered. For the gate driver project, input voltages are always above 10 V allowing the use of the LM723 topology. Input start-up simulation shows a start-up voltage around 8.3 V (Figure 3.7).

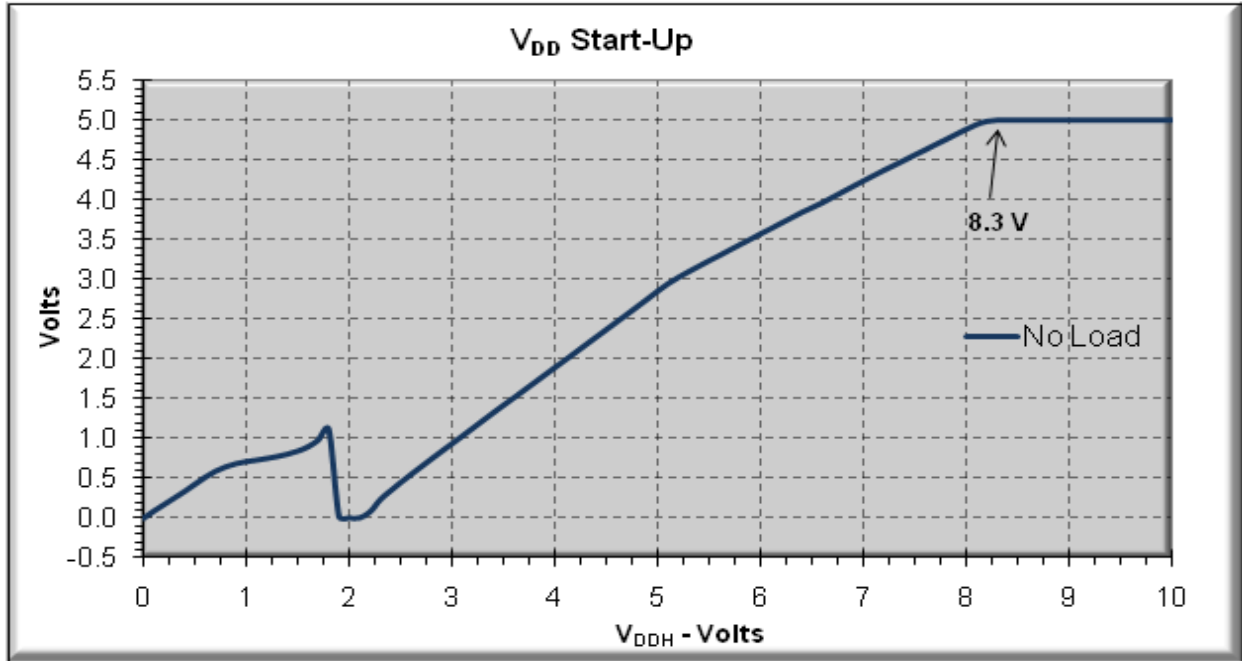


**Figure 3.7 – Simulated Voltage Regulator Start-Up**

### 3.2.3 – Line Regulation

Line regulation is a very important consideration for any voltage regulator design due to the variability of input voltages. Line regulation is simulated at room temperature for both the no load condition and a 10-mA load condition over a  $V_{DDH}$  range of 10 V – 35 V. Figures 3.8 - 3.11 illustrate line sweep simulation results for  $V_{DD}$ ,  $V_{PRE}$ ,  $V_{REF}$ , and  $I_{REG}$ , respectively. As Figure 3.8 demonstrates, the line regulation of  $V_{DD}$  is extremely small for either load condition; the inherent supply rejection of the LM723 topology and the use a pre-regulator circuit account for this simulated line regulation. This line regulation (on the order of ppb/V) far exceeds any foreseeable application demand. Adding a 10-mA load current to the output of the voltage regulator induces a slight increase in the input sensitivity of  $V_{DD}$  most likely arising from the “on” resistance of the pass device. Figure 3.9 shows the pre-regulator voltage in response to the input voltage sweep. The line regulation of  $V_{PRE}$  is not on the order of  $V_{DD}$  (an expected result), but the pre-regulator still regulates  $V_{DDH}$  on the order of ppm/V. Loading the voltage regulator exhibits virtually no change in the line regulation of  $V_{PRE}$ . The observed proportionality of  $V_{PRE}$  to  $V_{DDH}$  is related to channel length modulation of the MOSFET devices used in the pre-regulator circuit. Figure 3.10 examines the reference voltage as a function of input voltage. The reference

voltage (ideally independent of input voltage) is found to have a very small, proportional relationship to input voltage (ppb/V). This proportionality comes from the relationship of Zener breakdown voltage Zener diode current. Generating both the reference voltage and bias current with Zener diodes (as is done in this voltage regulator topology) reduces this effect. This, seemingly simple concept of the LM723 topology, allows for very predictable reference voltages to be generated over a wide range of input voltages. The line regulation of the output voltage,  $V_{DD}$ , is limited by the line regulation of  $V_{REF}$ , so design choices in the reference generator circuit are carefully considered in the overall voltage regulator design. Generating a reference voltage with a line regulation on the order of ppb/V is the main reason that the output voltage demonstrates extreme resistance to input variation. Load current variation reveals virtually no change in the line regulation of  $V_{REF}$  (due to the low output impedance of the op-amp). The regulator bias current generated from the Zener reference current source is indirectly related to input voltage (through  $V_{PRE}$ ) due to the Early effect (Figure 3.11), but the coefficient of this relationship is on the order of pA/V and has little effect on regulator performance. Load current variation has no discernable effect on  $I_{REG}$  line sensitivity.

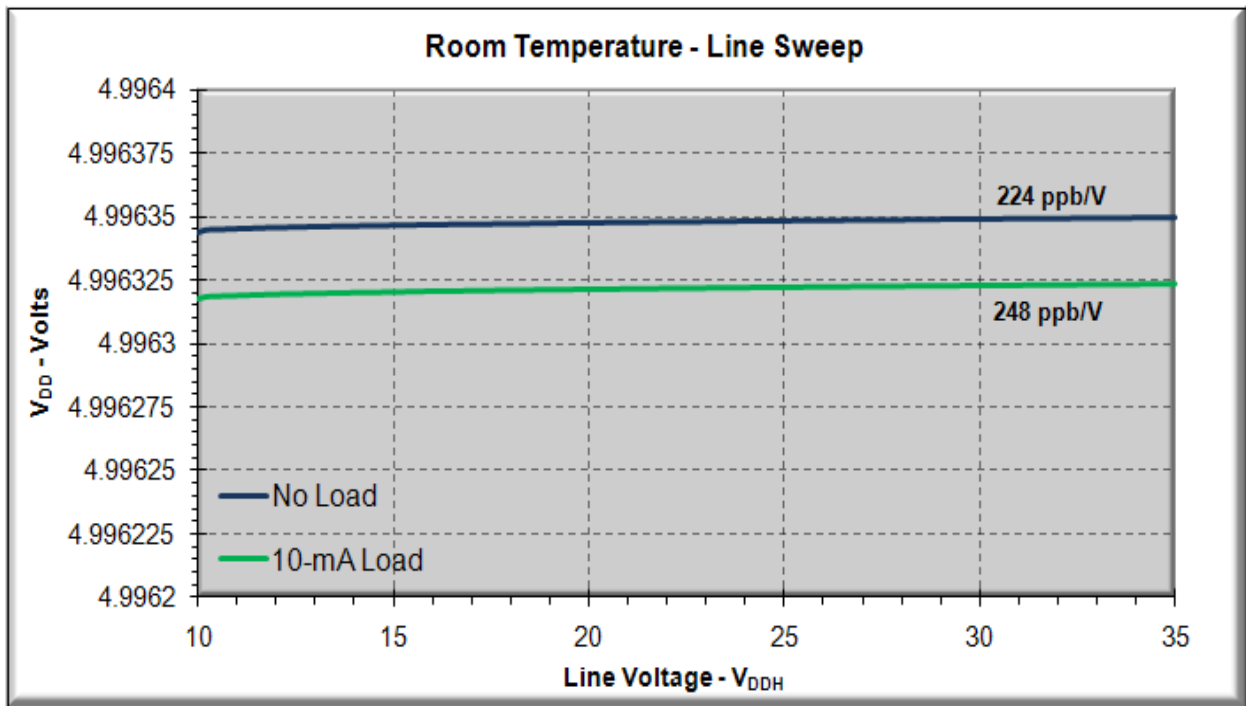
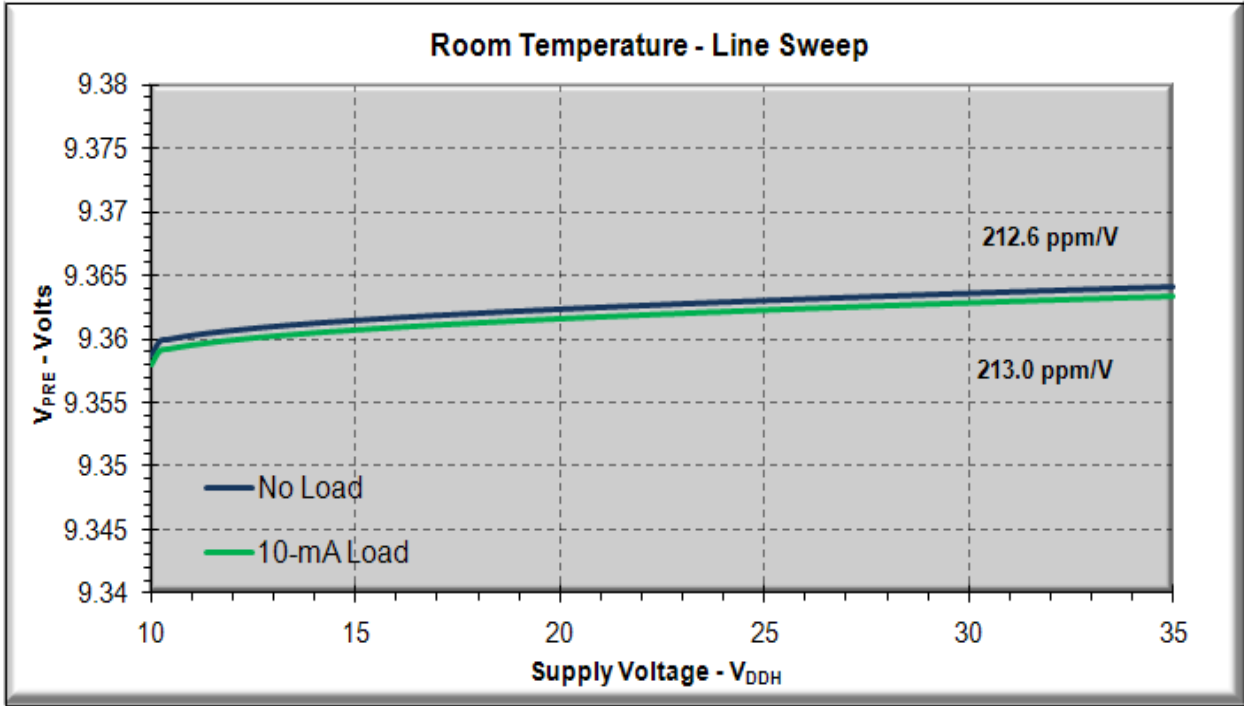
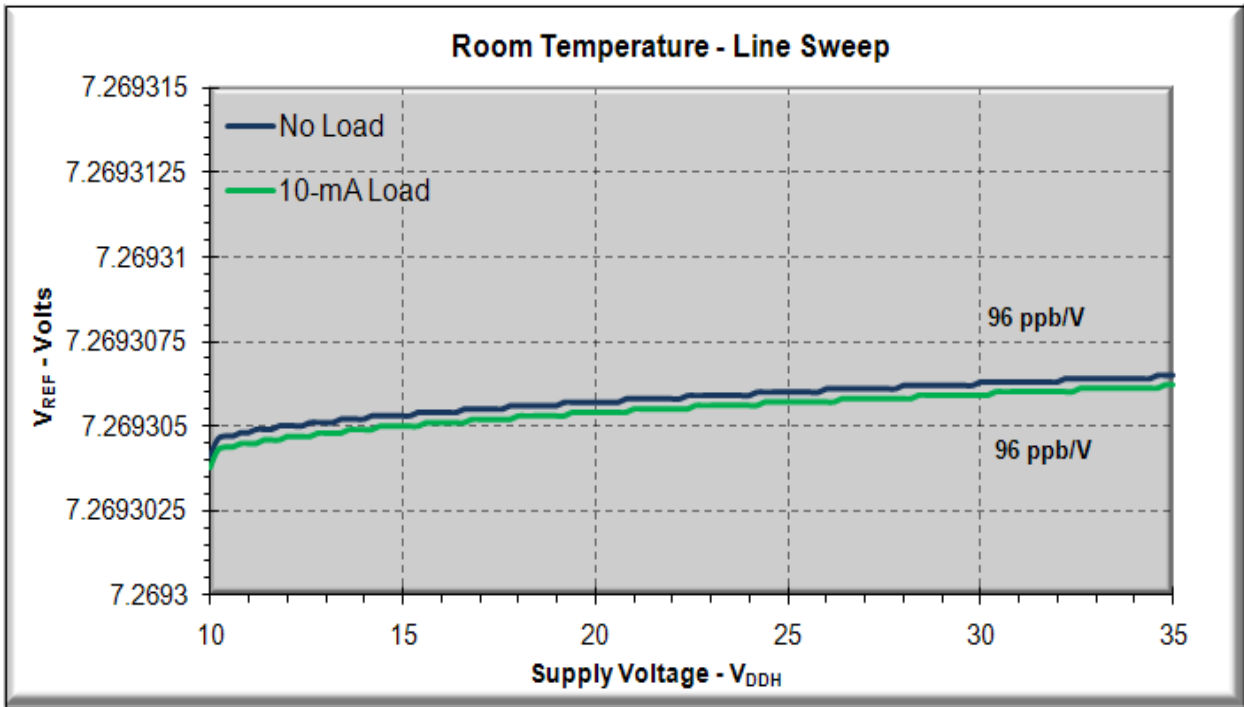


Figure 3.8 – Simulated  $V_{DD}$  Line Regulation



**Figure 3.9 – Simulated  $V_{PRE}$  Line Regulation**



**Figure 3.10 – Simulated  $V_{REF}$  Line Regulation**

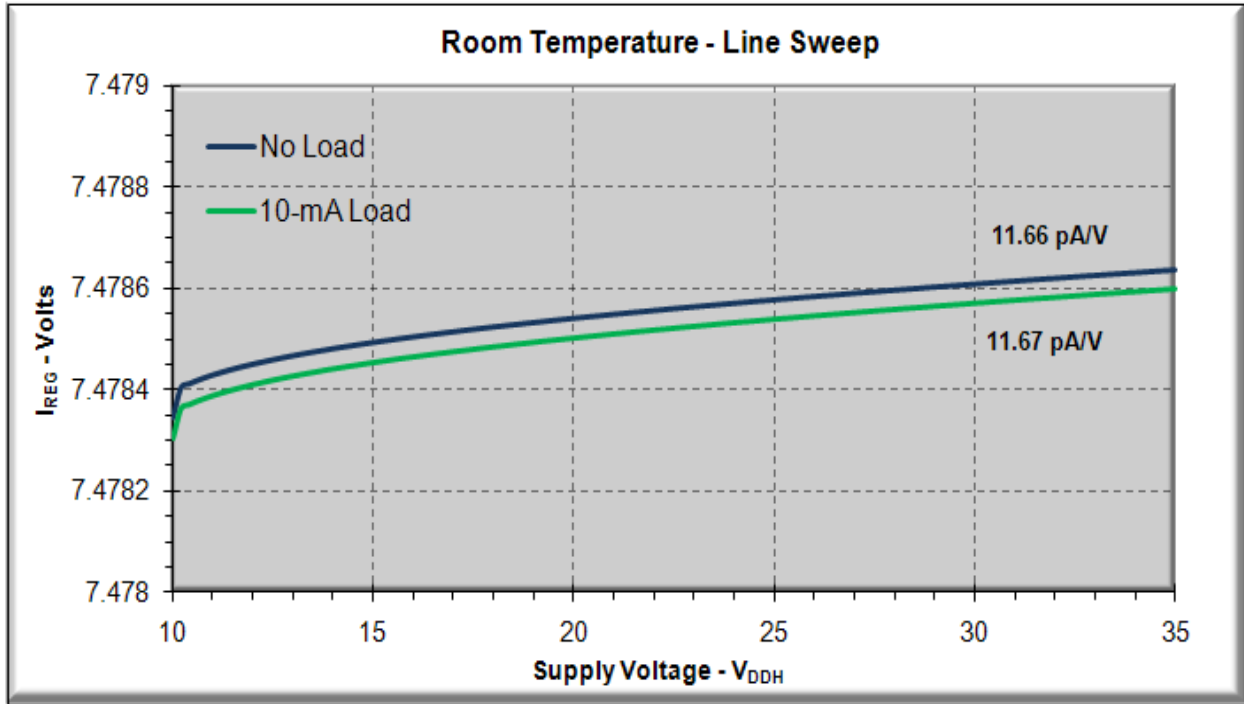


**Figure 3.11 – Simulated  $I_{REG}$  Line Regulation**

### 3.2.4 – Load Regulation

Load regulation is another critical parameter on which voltage regulators are evaluated. The ability to supply a wide range of load currents without a minimal change in output voltage allows the voltage regulator to be implemented in a myriad of applications. Some circuits (especially analog circuits) have very strict supply voltage constraints and demand the ability to draw current linearly with virtually no change in supply voltage. Digital circuits (such as the circuits in the gate driver application) are less sensitive to changes in supply voltage but impose very fast load transients on the voltage regulator. Analog and digital circuits present their own unique challenges when design voltage supplies for these circuits. This voltage regulator is designed to accommodate both types of electronic devices. DC load regulation simulations are performed at room temperature for input voltages of 10 V, 20 V, and 30 V. Figures 3.12 - 3.16 display load sweep simulation results for  $V_{DD}$ ,  $V_{PRE}$ ,  $V_{REF}$ ,  $I_{PRE}$ , and  $I_{REG}$ , respectively. Over a load current range of 0 to 10 mA,  $V_{DD}$  is found to vary only a few  $\mu\text{V}/\text{mA}$  for all  $V_{DDH}$  voltages (Figure 3.12). The complementary dependence of  $V_{DD}$  on load current is due to the “on” resistance of the pass device, but this coefficient is quite small and allows for undisturbed performance over a wide

range of load currents. This load current vs.  $V_{DD}$  relationship is linear, and can be extrapolated for load currents exceeding 200 mA. For all input voltages,  $V_{PRE}$  has an inverse, linear proportionality to  $V_{DDH}$  (Figure 3.13). This relationship results from the increasing  $I_{DI3}$  current required by the regulator circuits. The complementary relationship between  $V_{DDH}$  and  $V_{REF}$  (Figure 3.14) arises from the Early effect imposed on the regulator devices from the pre-regulator voltage load sensitivity. However,  $V_{REF}$  is nearly independent of load current through the use of an operational amplifier in the LM723 topology. The operational amplifier prevents loading effects from being referred to the reference voltage node. No measurable correlation between  $I_{PRE}$  and load current is discernable for any  $V_{DDH}$  voltage (Figure 3.15). This result is expected as  $I_{PRE}$  is generated using a threshold referenced current source. The Early effect on the BJT devices (as mentioned in reference to  $V_{REF}$  load regulation results) results in a complementary relationship between  $I_{REG}$  and load current (Figure 3.16). Overall, the voltage regulator shows excellent load regulation at each stage of the design. The load current can be increased up to 300 mA without risk of circuit damage.

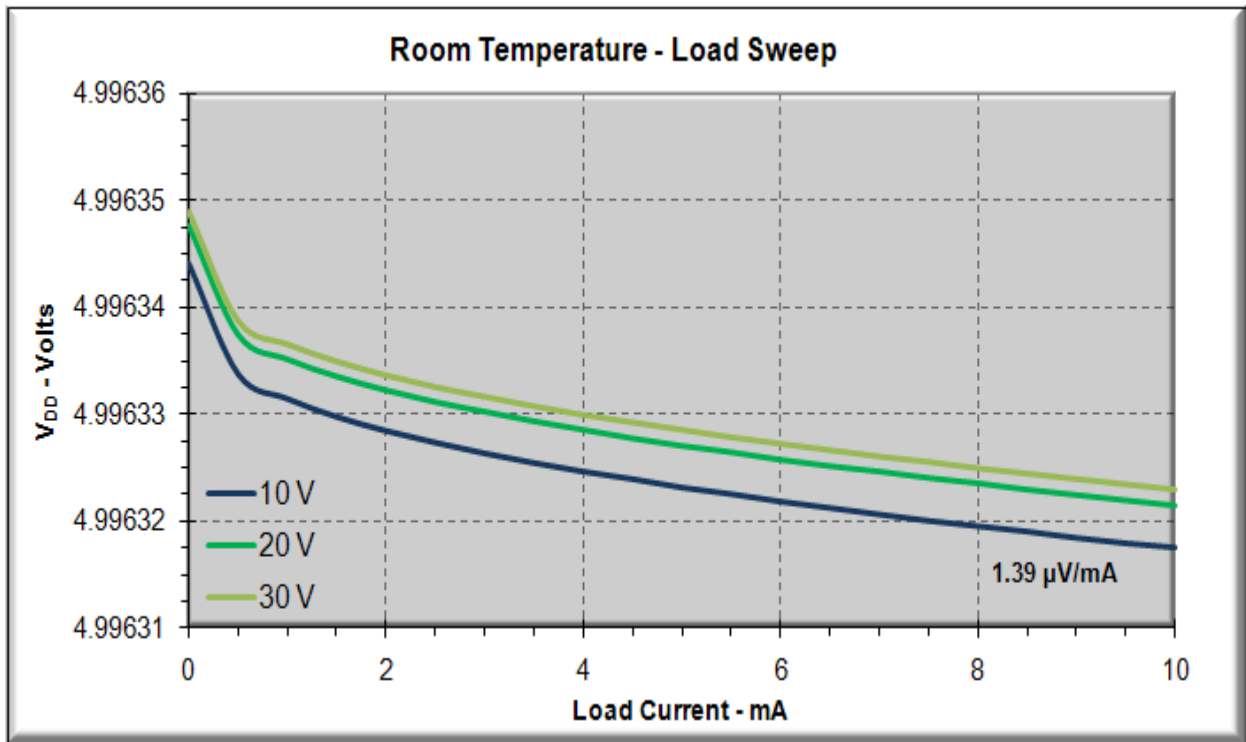


Figure 3.12 – Simulated  $V_{DD}$  Load Regulation

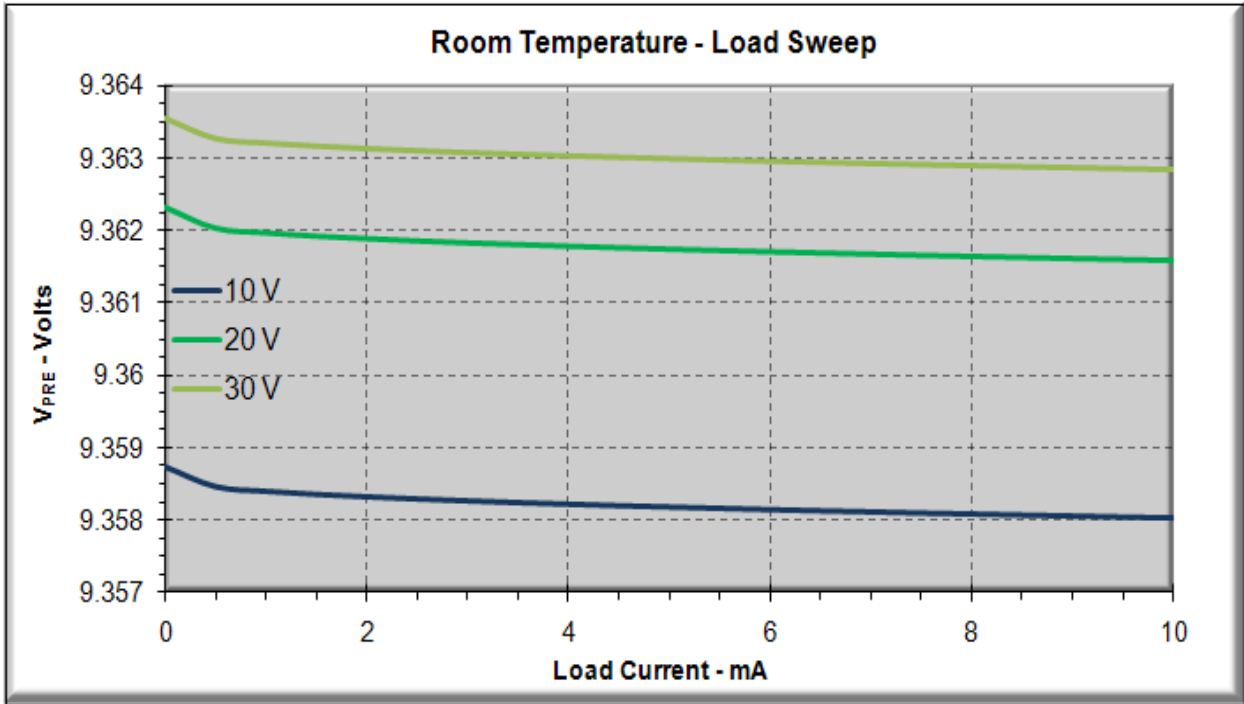


Figure 3.13 – Simulated  $V_{PRE}$  Load Regulation

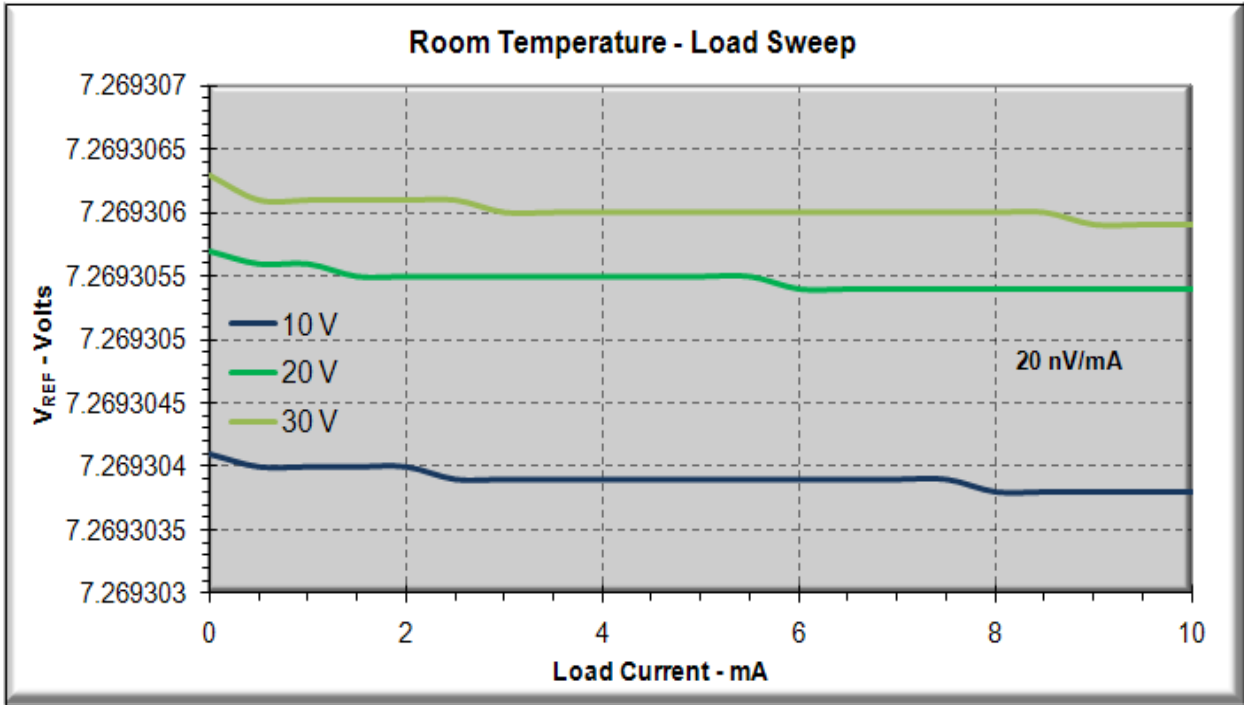


Figure 3.14 – Simulated  $V_{REF}$  Load Regulation

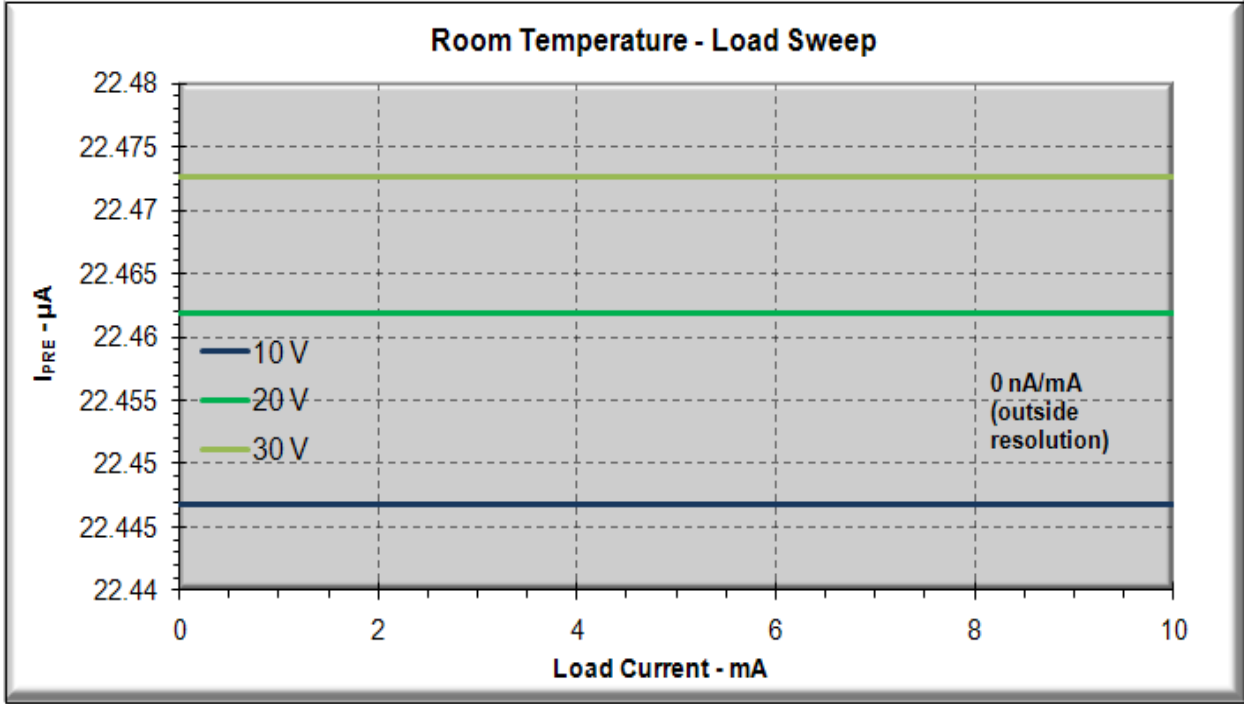


Figure 3.15 – Simulated  $I_{PRE}$  Load Regulation

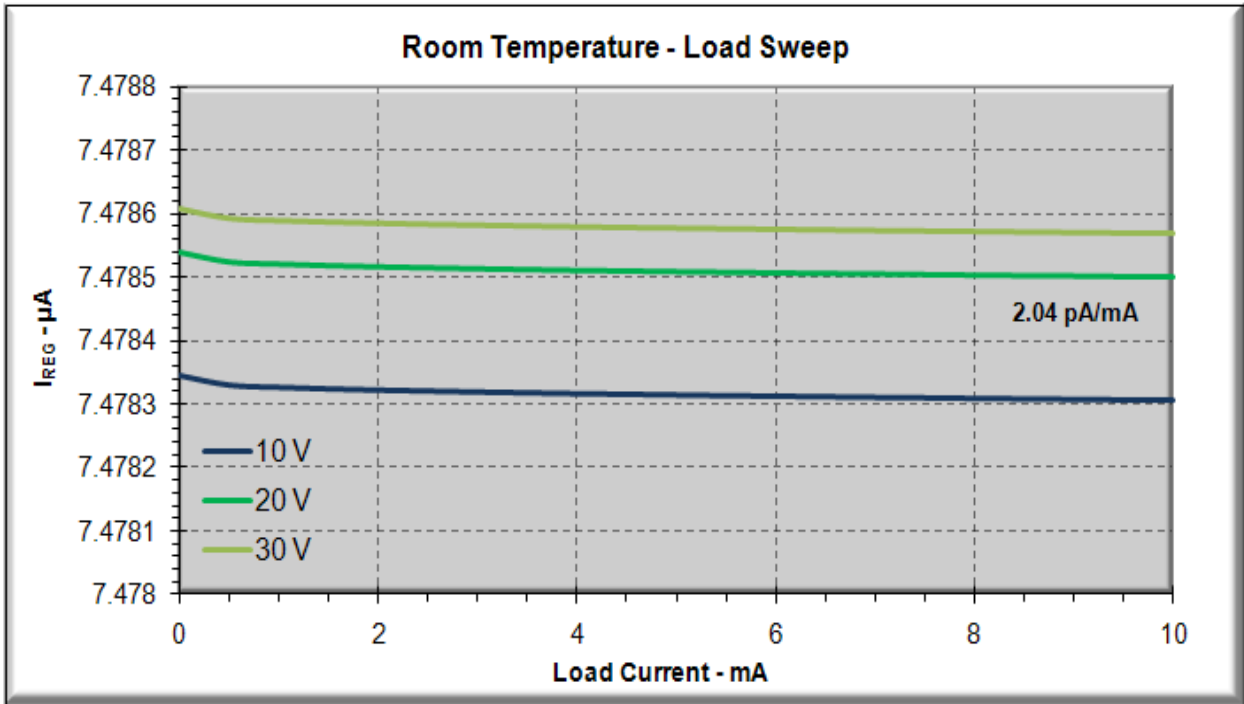


Figure 3.16 – Simulated  $I_{REG}$  Load Regulation



### 3.2.5 – Temperature Characteristic

One of the main initiatives in developing this gate driver project is the requirement for all circuits to operate up to 200 °C. Current LM723 designs offer temperature ratings up to 125 °C, which is substantially less than the environment imposed by hybrid electric engines. This voltage regulator design is simulated over a wide temperature range (–50 °C to 200 °C) to ensure all environmental conditions have been examined. Figures 3.17 - 3.22 demonstrate temperature sweep simulation results for  $V_{DD}$ ,  $V_{PRE}$ ,  $V_{REF}$ ,  $I_{PRE}$ ,  $I_{REG}$ , and  $I_{SUPPLY}$ , respectively. As Figure 3.17 illustrates,  $V_{DD}$  varies less than 7 mV over the full 250 °C temperature range (regardless of changes in  $V_{DDH}$  or load current). The Zener reference topology along with the additional temperature compensation described in section 3.1.2 allow for the small temperature dependence observed. The temperature compensation resistor  $R8$  in Figure 3.3 takes advantage of temperature coefficient of the current through  $D3$  by providing a voltage drop with a temperature coefficient complementary to that of the Zener diode breakdown voltage. In addition to the small temperature dependence of  $V_{DD}$ , the consistency of the temperature characteristic of  $V_{DD}$  for all  $V_{DDH}$  voltages and load currents allows for predictable operation in nearly any application. The temperature characteristic of  $V_{PRE}$  shows a significant dependence on  $V_{DDH}$  while load condition has an insignificant effect.  $V_{DDH}$  variation demonstrates an alteration of the temperature characteristic for  $V_{DDH}$  values close to  $V_{PRE}$ . For  $V_{DDH}$  voltages greater than ~11 V, the supply voltage has an insignificant effect on temperature characteristic. The combination of the temperature coefficients of  $V_{PRE}$  and  $V_{DS,SAT}$  of the p-channel LDMOS devices  $M13$  and  $M14$  result in the observed temperature curves (Figure 3.18). Just as was the case with  $V_{DD}$ , the temperature characteristic of  $V_{REF}$  illustrates virtually no dependence on  $V_{DDH}$  or load current (see Figure 3.19).  $V_{REF}$  exhibits only a 17 mV variation over the full 250 °C simulation. Figure 3.20 reveals that  $V_{DDH}$  and load current have an insignificant effect on temperature characteristics for  $I_{PRE}$ . This bias current varies about 5  $\mu$ A over the full temperature sweep. This variation is due to the temperature dependence of  $V_{TH}$  and the temperature dependence of the resistivity of the poly2 layer. Changes in pre-regulator bias current do not affect the remaining regulator stages as long as the current demand of the regulator circuits on the pre-regulator does not exceed  $I_{D13}$ . In the event that regulator current demand exceeds the current available from  $M13$ - $M14$ ,  $D1$  will not have a bias current to establish  $V_{PRE}$ . Under this condition, the regulator circuits would be subject to unpredictable line voltages and circuit operation would be erratic.

To avoid this potential pitfall,  $I_{D13,14}$  is set well above the worst case current draw of the regulator circuit. The regulator bias current temperature characteristic also exhibits little variability with  $V_{DDH}$  and load current changes (Figure 3.21). The  $I_{REG}$  temperature coefficient is a result of the temperature dependence of  $V_{BE}$ , poly2 resistivity, and p-well resistivity. The temperature coefficient of  $I_{REG}$  is actually advantageous, as the  $I_{REG}$  curve cancels the inherent temperature curve of the Zener diode. This complementary behavior illustrates the advantage of using Zener diodes to establish both the bias currents and reference voltage. The supply current draw visible in Figure 3.22 is the summation of the bias currents of all four voltage regulator stages. The maximum supply current draw is 324  $\mu\text{A}$  at 100  $^{\circ}\text{C}$ , for a 30-V input. The voltage regulator is designed so that  $I_{SUPPLY}$  is parabolic with respect to temperature. The parabolic temperature characteristic results in the lowest possible variability in current draw over temperature. The power requirements of this voltage regulator are, therefore, very predictable. Figure 3.22 also shows that supply current is proportional to supply voltage. For a load condition, total supply current is the direct sum of the no load supply current and the load current.

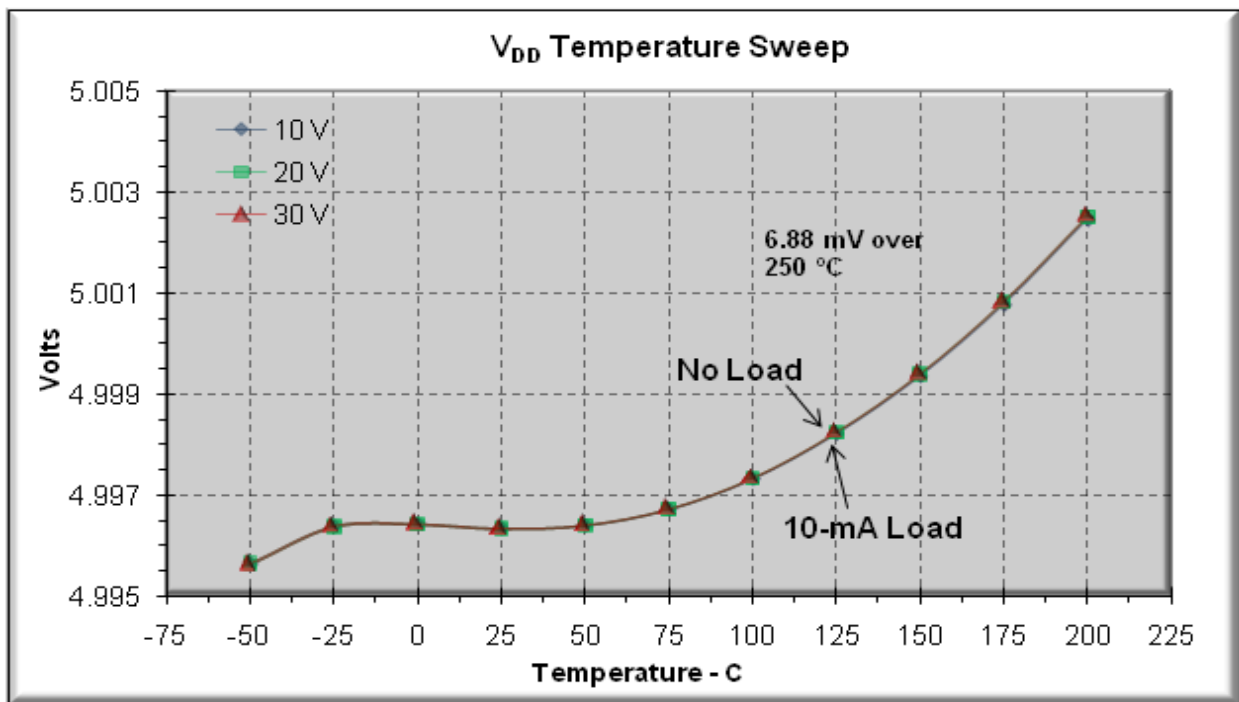


Figure 3.17 – Simulated  $V_{DD}$  Temperature Characteristic

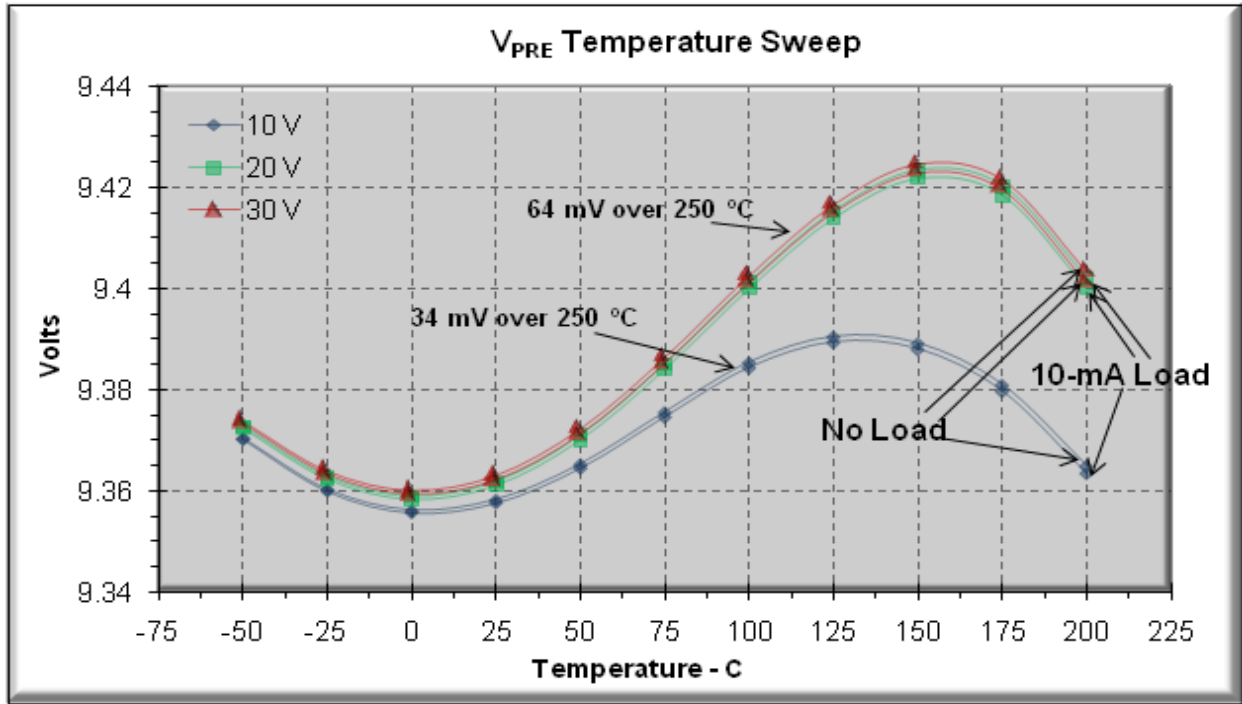


Figure 3.18 – Simulated  $V_{PRE}$  Temperature Characteristic

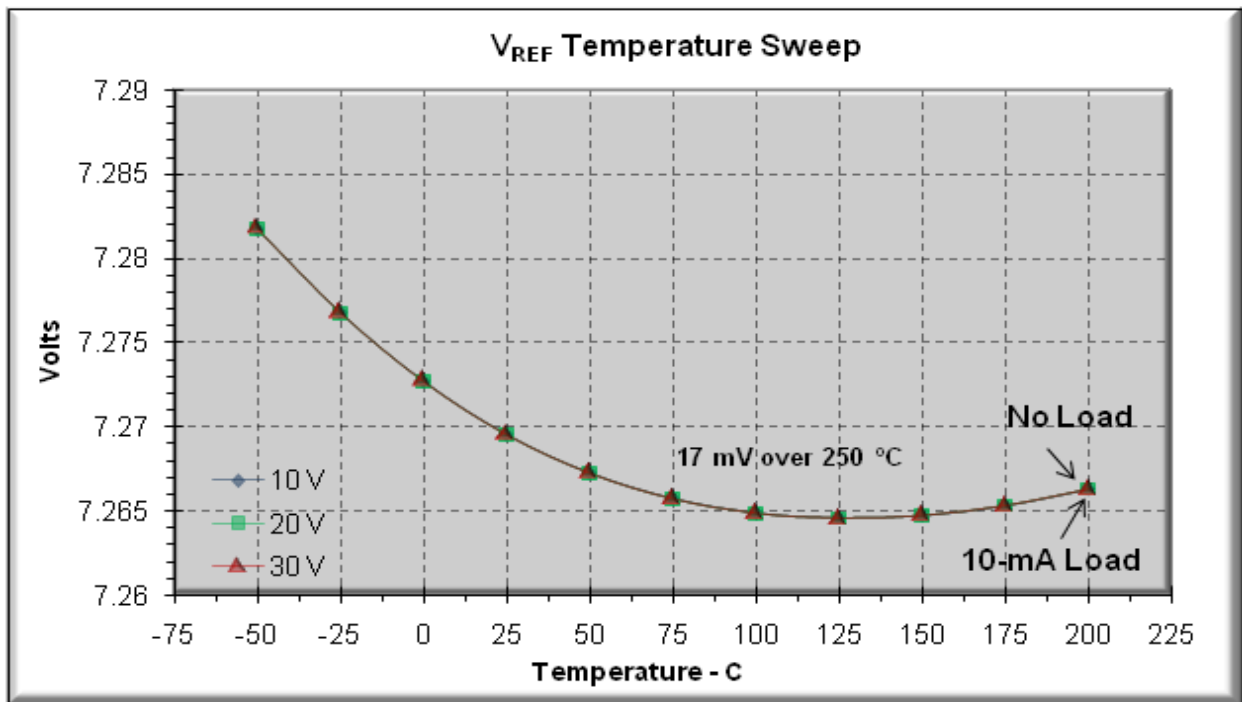


Figure 3.19 – Simulated  $V_{REF}$  Temperature Characteristic

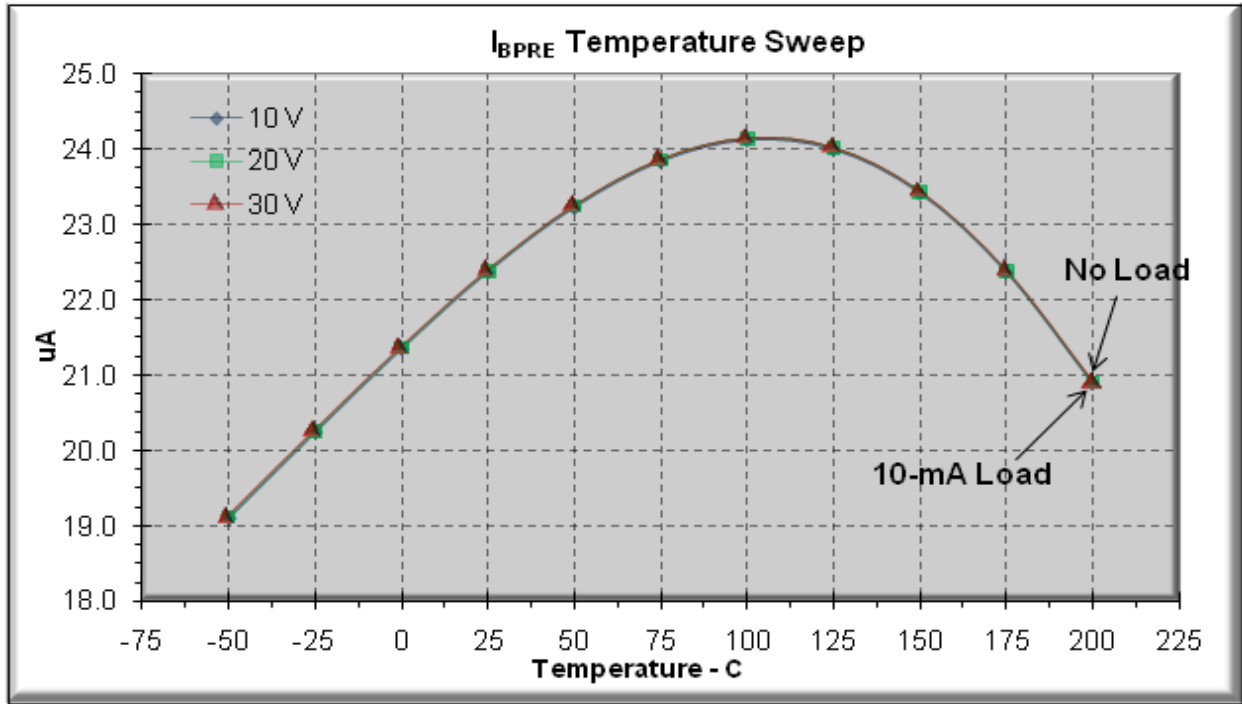


Figure 3.20 – Simulated  $I_{PRE}$  Temperature Characteristic

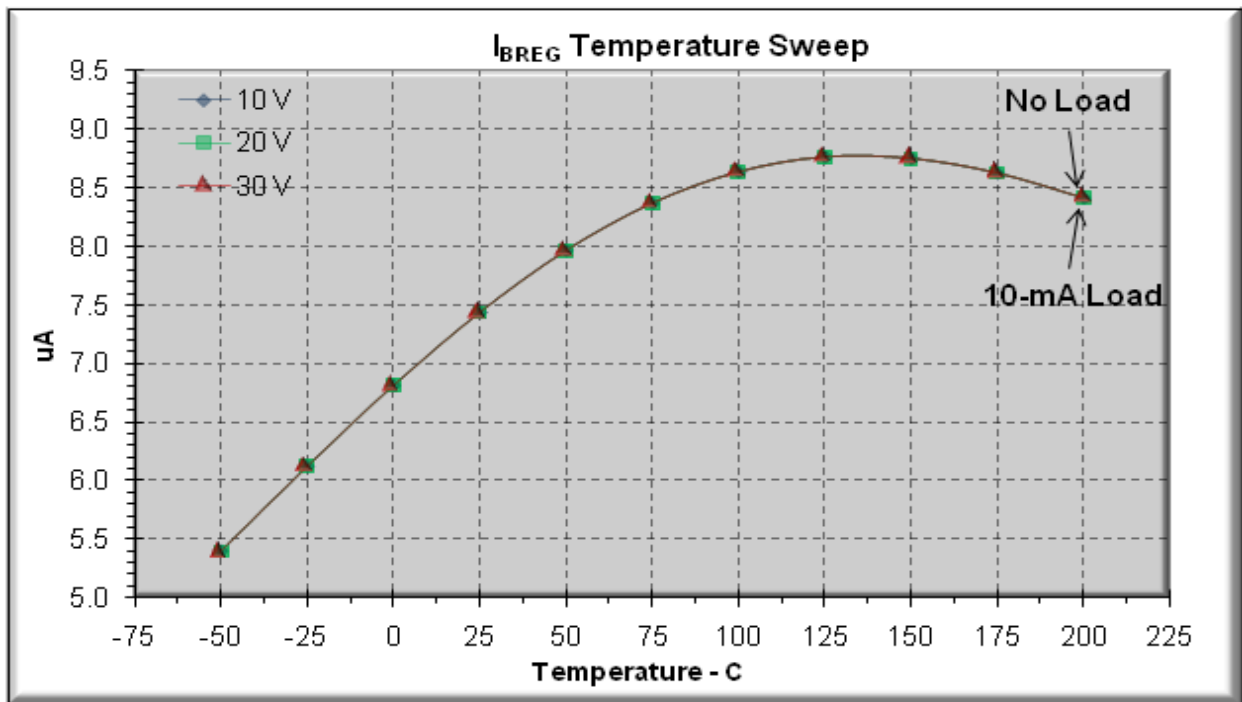
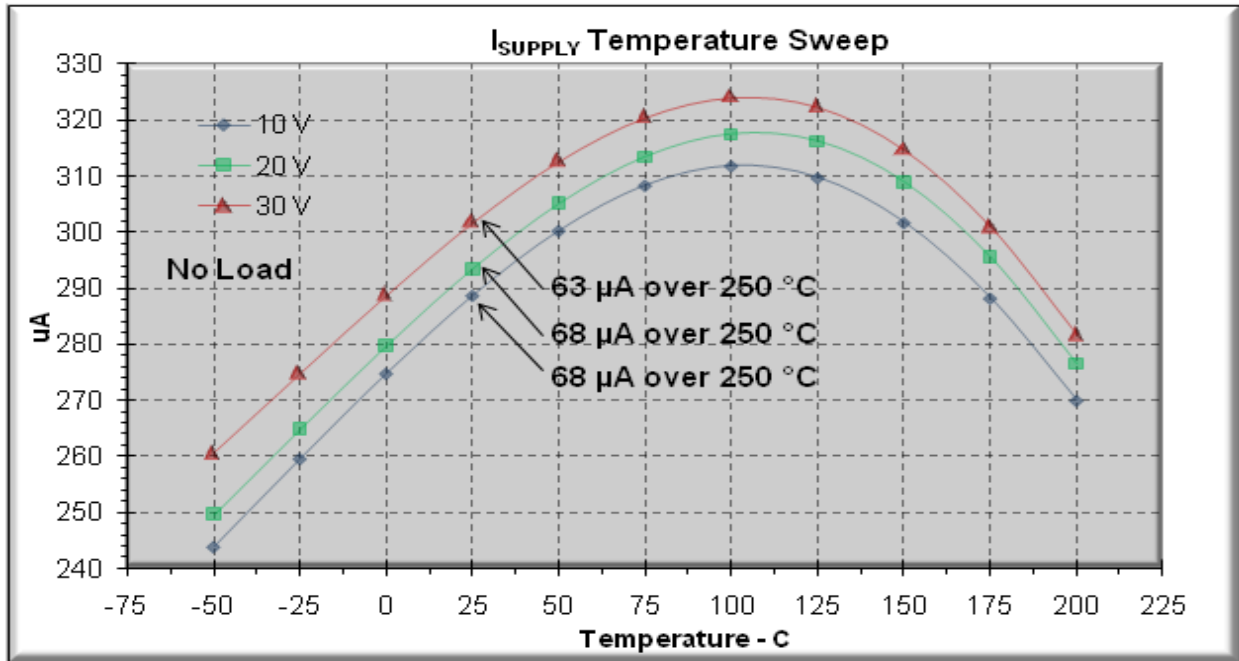


Figure 3.21 – Simulated  $I_{REG}$  Temperature Characteristic



**Figure 3.22 – Simulated  $I_{SUPPLY}$  Temperature Characteristic**

### 3.2.6 – Load Transient

Figures 3.23-3.25 are the simulation results of the voltage regulator in response to a 220-mA load transient at  $-50\text{ }^{\circ}\text{C}$ ,  $25\text{ }^{\circ}\text{C}$ ,  $200\text{ }^{\circ}\text{C}$ , respectively.  $V_{DDH}$  is set to 20 V, and an output capacitor of  $3.8\text{ }\mu\text{F}$  is used as a charge storage device.  $V_{DD}$  and  $V_{PRE}$  drop linearly during the 220-mA current draw as the load capacitor discharges and current demands on  $V_{DD}$  increase. In the gate driver application, the transient loads have a much shorter pulse width than demonstrated in these simulations (several orders of magnitude shorter). The shorter pulse widths remove the linear drop of  $V_{DD}$  and  $V_{PRE}$  seen in these simulations.  $V_{REF}$  exhibits extreme resistance to load transients, which is consequential to the use of the operational amplifier (essentially a buffer). Throughout the load transient, the regulator is able to restrict the output voltage to within 99.6 % of nominal  $V_{DD}$ . The load transient effect on  $V_{DD}$  is nearly independent of temperature. The load transient effect on  $V_{PRE}$  is pronounced at the extreme ends of the temperature range; however, the worst-case effect is still limited to under a mV total displacement. The response observed on  $V_{REF}$  to a load transient increases with temperature; the worst case for the load transient response of  $V_{REF}$  is under  $100\text{-}\mu\text{V}$  total displacement.

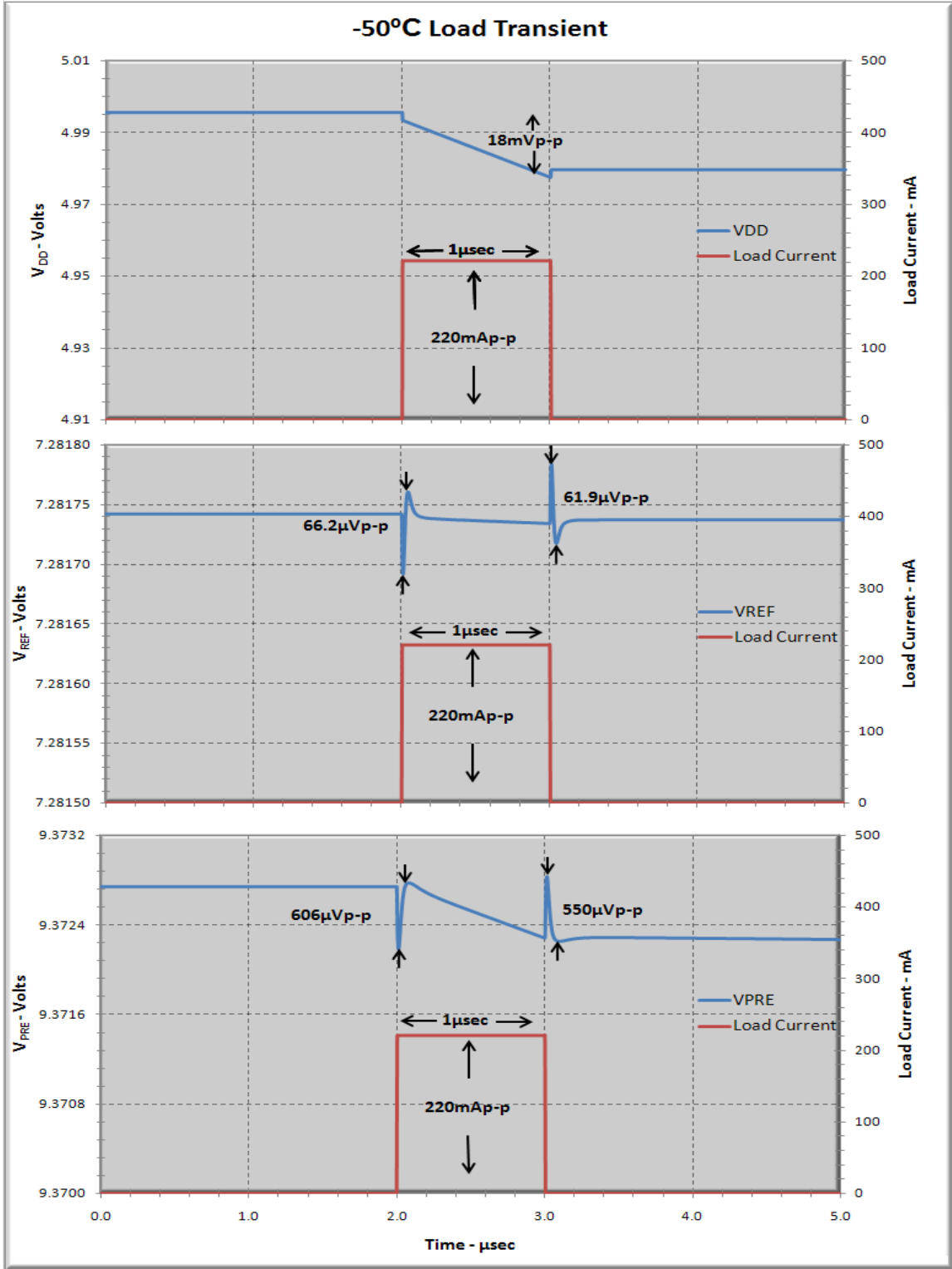


Figure 3.23 – Simulated  $-50^\circ\text{C}$  Load Transient

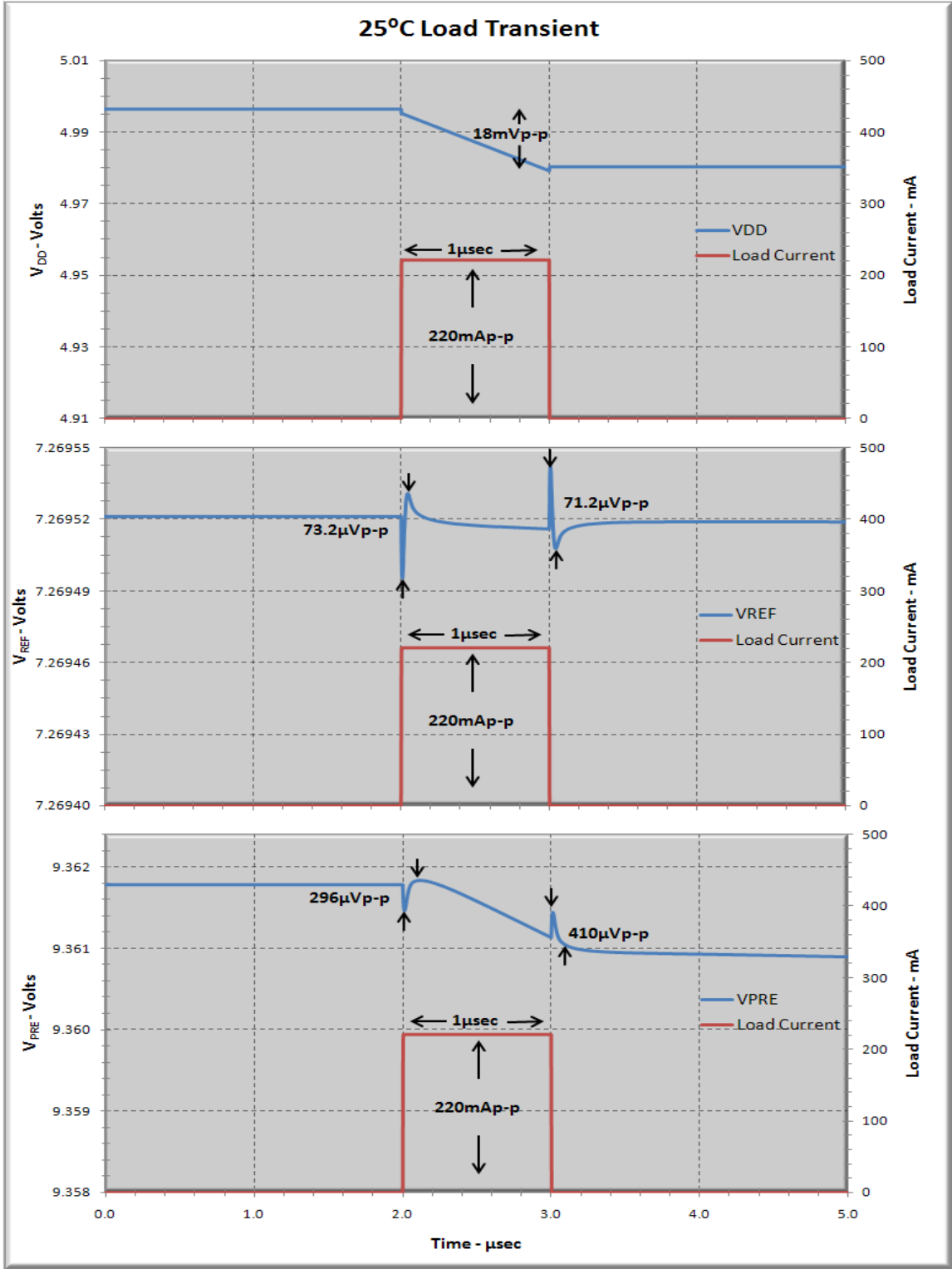


Figure 3.24 – Simulated 25 °C Load Transient

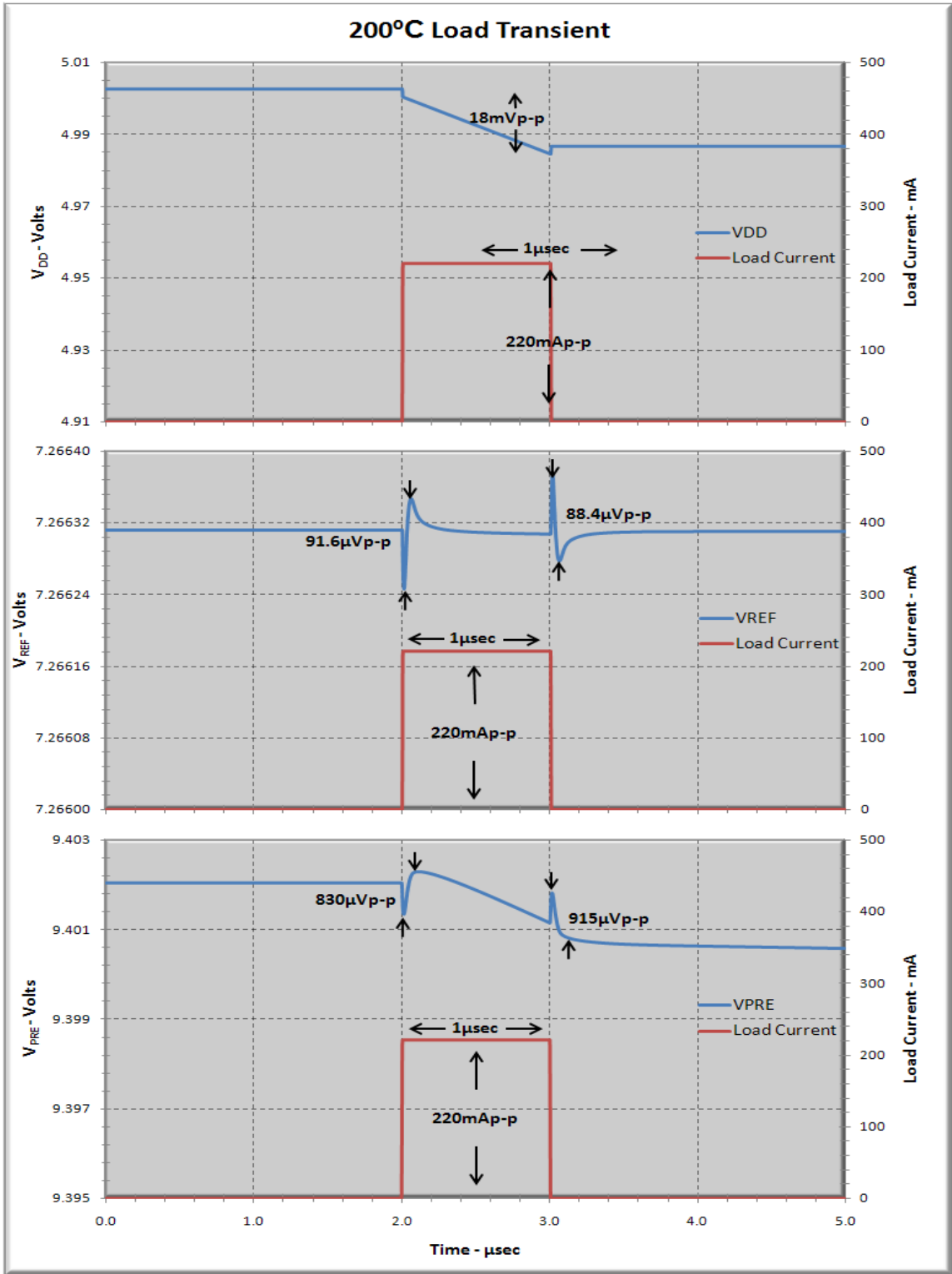


Figure 3.25 – Simulated 200 °C Load Transient



### 3.2.7 – Line Transient

Figures 3.26-3.28 examine the simulated voltage regulator response to a line transient of  $5 V_{p-p}$  at  $-50\text{ }^{\circ}\text{C}$ ,  $25\text{ }^{\circ}\text{C}$ ,  $200\text{ }^{\circ}\text{C}$  respectively. In this simulation,  $V_{DDH}$  switches between 20 V and 25 V with fast edges as demonstrated in the figures. The line transient simulation reveals small transient pulses in both the pre-regulator voltage and the reference voltage at both rising and falling edges of a line transient. The amplitude of these pulses is greatest in the first stage of the circuit and is attenuated throughout the remaining voltage regulator stages.  $V_{DD}$  exhibits no susceptibility to a falling edge line transient (due to the class-A output stage) and shows only a modest change in output voltage in response to a rising edge transient. The amplitudes of  $V_{DD}$  during a line transient are inversely proportional to temperature.  $V_{DD}$  is regulated to within 99.97 % of nominal  $V_{DD}$  even under the worst case ( $-50\text{ }^{\circ}\text{C}$ ) line transient.  $V_{PRE}$  exhibits a significant line transient response (on the order of  $V_{p-p}$ ) with a complementary relationship to temperature. This result is expected, as  $V_{PRE}$  is directly connected to  $V_{DDH}$ . The resistance to line transients in the remaining voltage regulator stages is attributable in part to the resistance to line transients found in  $V_{PRE}$ . The line transient response of  $V_{REF}$  is directly related to the response of  $V_{PRE}$ . An attenuated effect of  $V_{PRE}$  is visible in  $V_{REF}$ , resulting in a similar temperature dependence. The ability of the voltage regulator to perform well in the presence of line transients allows the voltage regulator to be implemented in applications where reliable power supplies may not be available (almost any embedded application). Reducing the restrictions on supply voltage required by a regulator widens the potential applications for the voltage regulator, and therefore, improves the marketability of the voltage regulator.

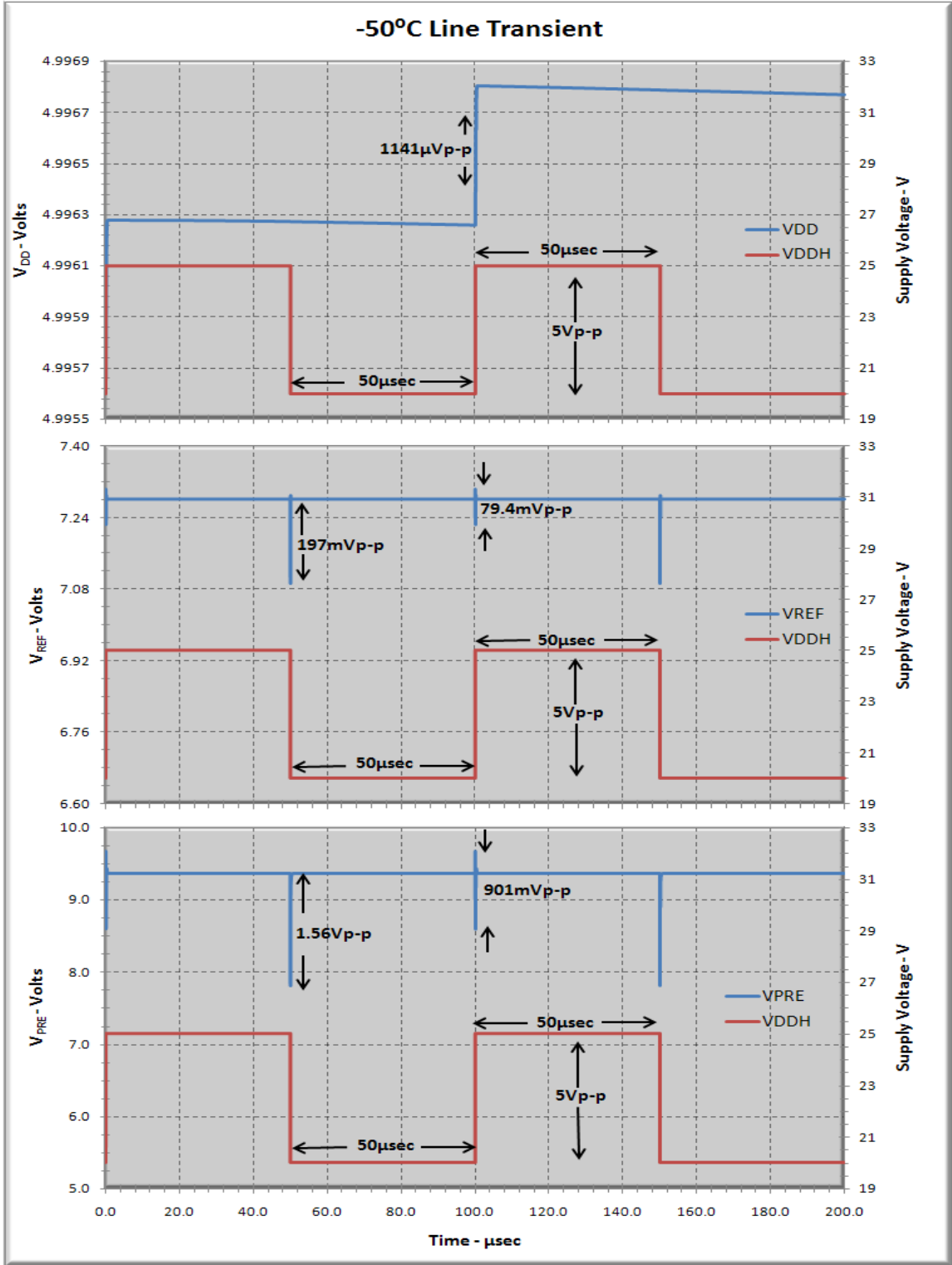


Figure 3.26 – Simulated -50 °C Line Transient

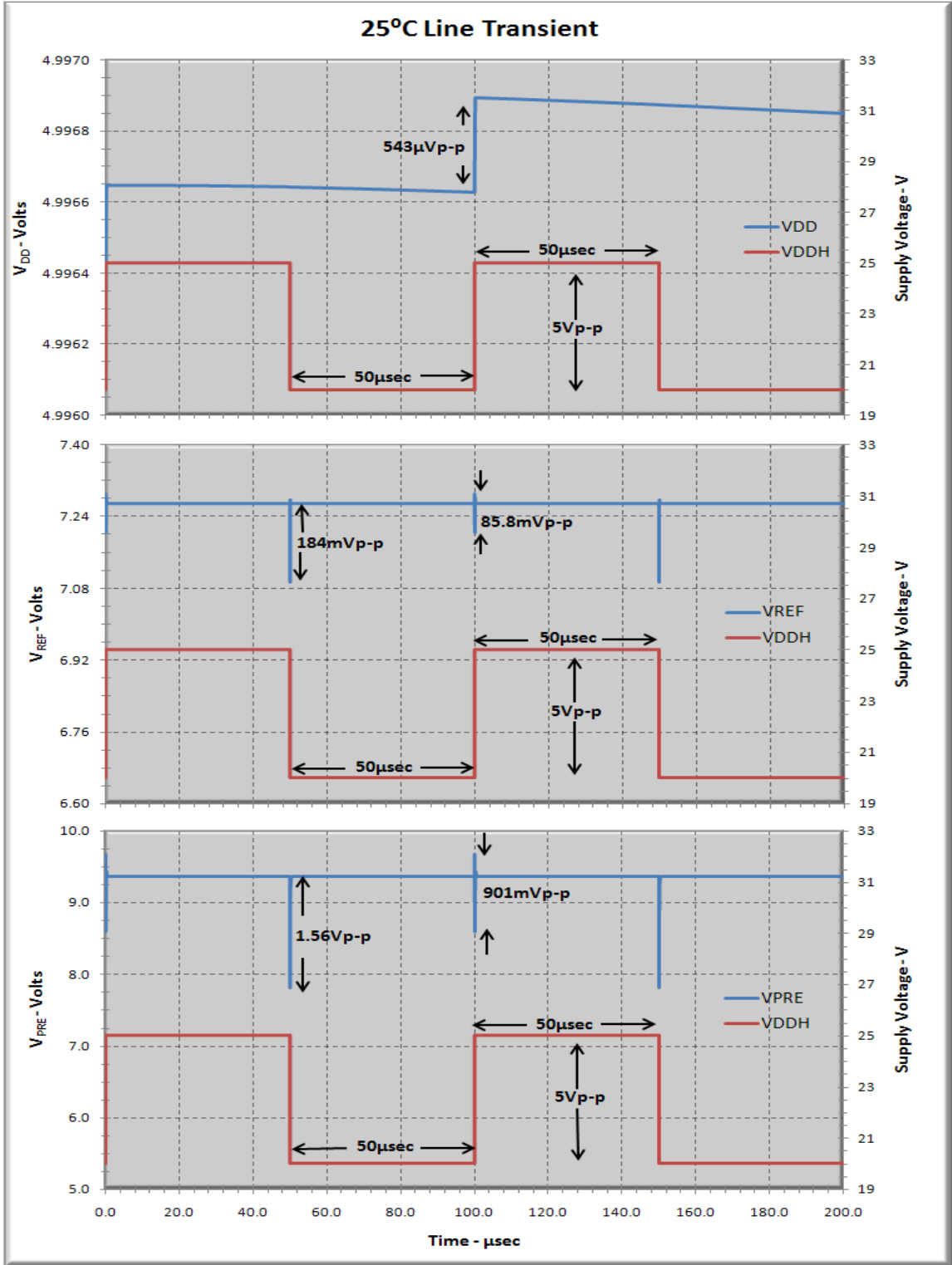


Figure 3.27 – Simulated 25 °C Line Transient

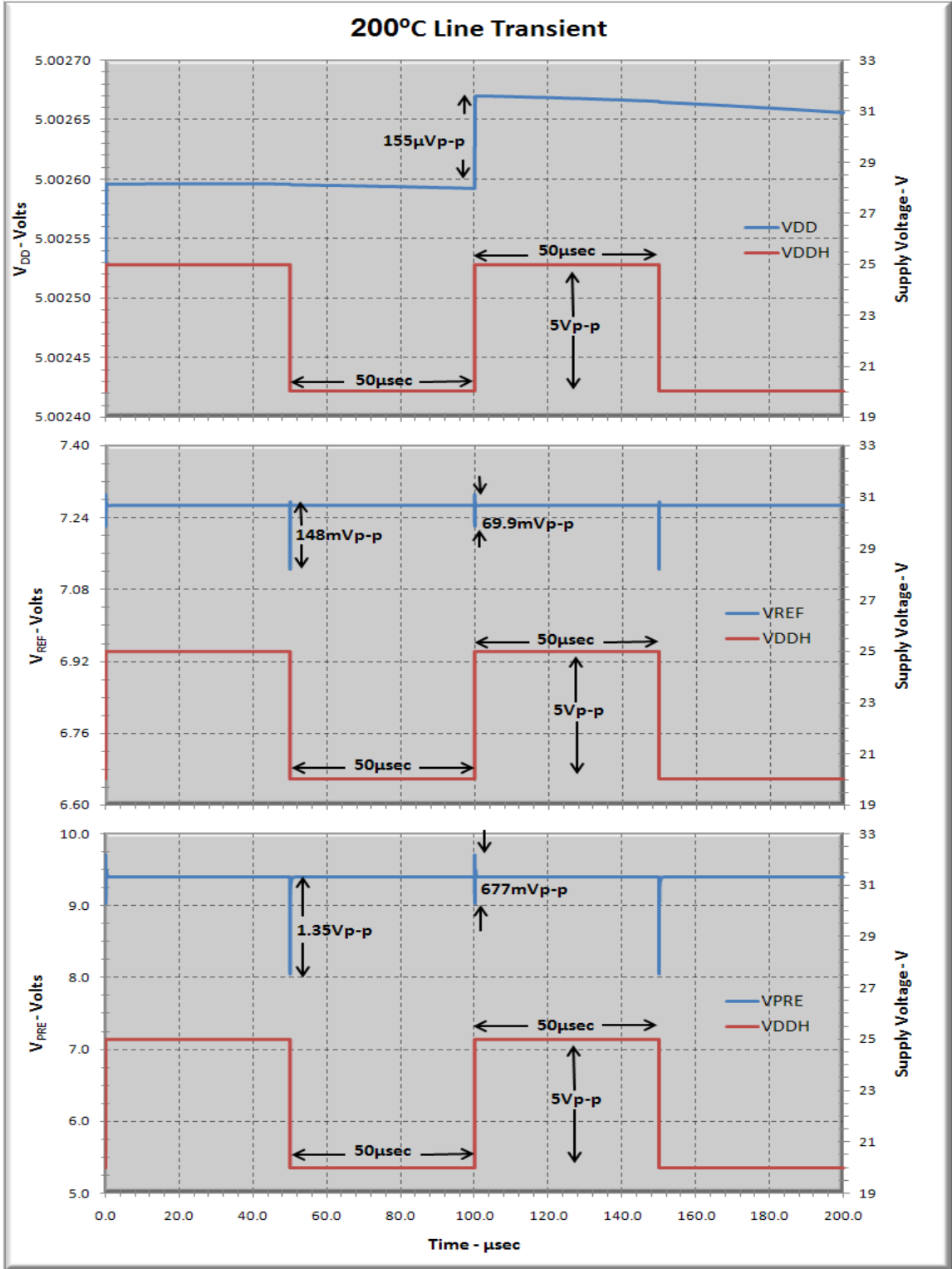


Figure 3.28 – Simulated 200 °C Line Transient

## 4. Post-Fabrication Verification

### 4.1 – Voltage Regulator Testing Set-Up

The voltage regulator layout in Figure 4.1 segregates each circuit stage in the voltage regulator design. Device matching is impossible for all BJT, LDMOS, and MOSCAP devices due to the non-self aligned nature in this SOI-process. The overall layout is compact which minimizes chip area and process variation. Figure 4.2 shows the fabricated chip in contrast to the layout image. The total device area for the voltage regulator design is less than  $0.5 \text{ mm}^2$ . A large portion of this chip area is used for on-chip capacitors. This capacitor area can be greatly reduced to accommodate smaller die areas in future fabrications. High-voltage ESD for pins exceeding 5 V is implemented using a gate-source connected, high-voltage LDMOS. Low voltage ESD for pins within 5 V is implemented using standard Zener diode ESD pads. Measurement data is obtained through a printed-circuit board (PCB) test set-up, using high-temperature components. Figure 4.3 shows the complete test board. The 4-layer PCB is fabricated with polyimide dielectric, immersion gold contact finish, and PSR-9000 FXT solder resist for optimal high-temperature performance.

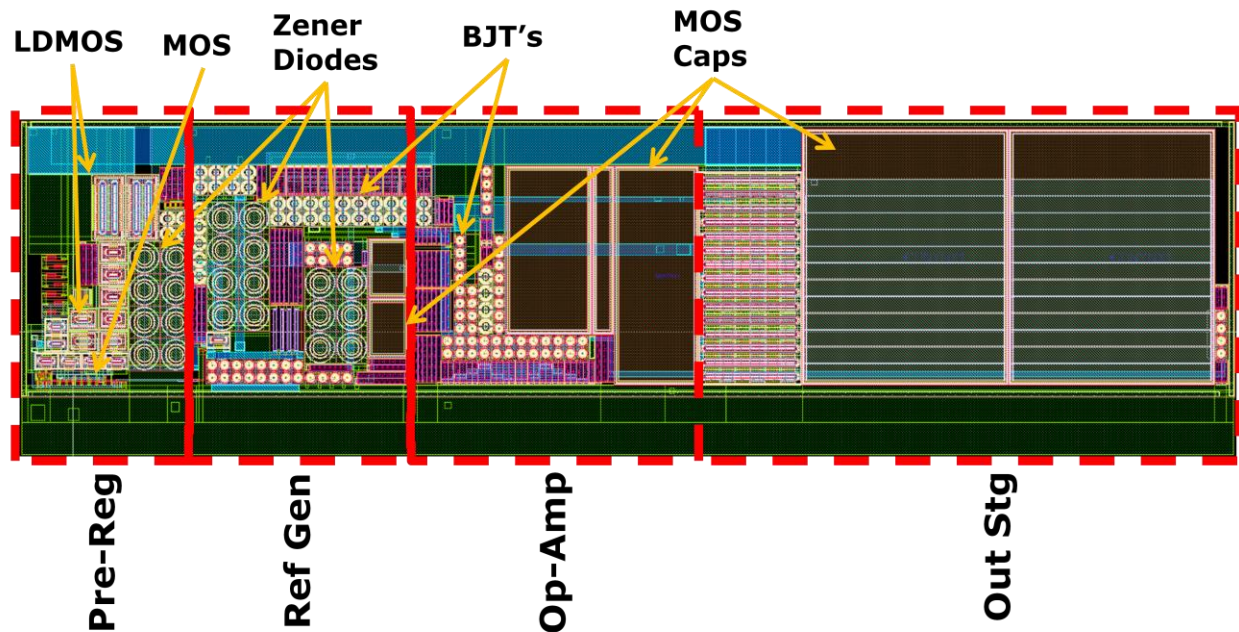


Figure 4.1 – Voltage Regulator Layout



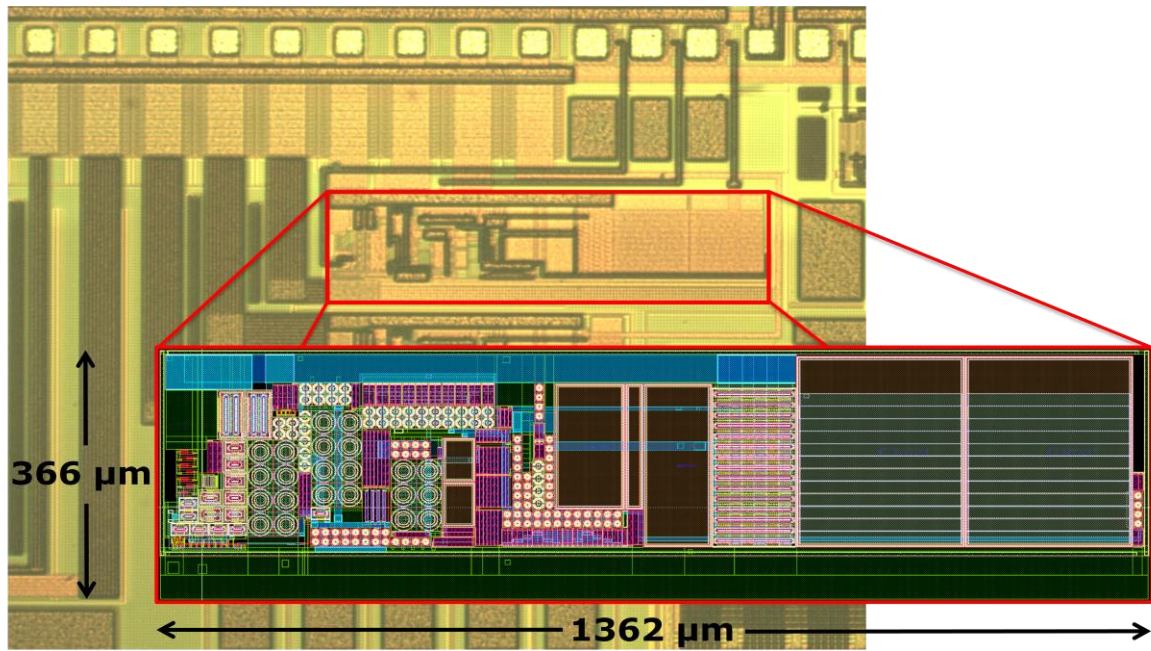


Figure 4.2 – Voltage Regulator Post-Fabrication

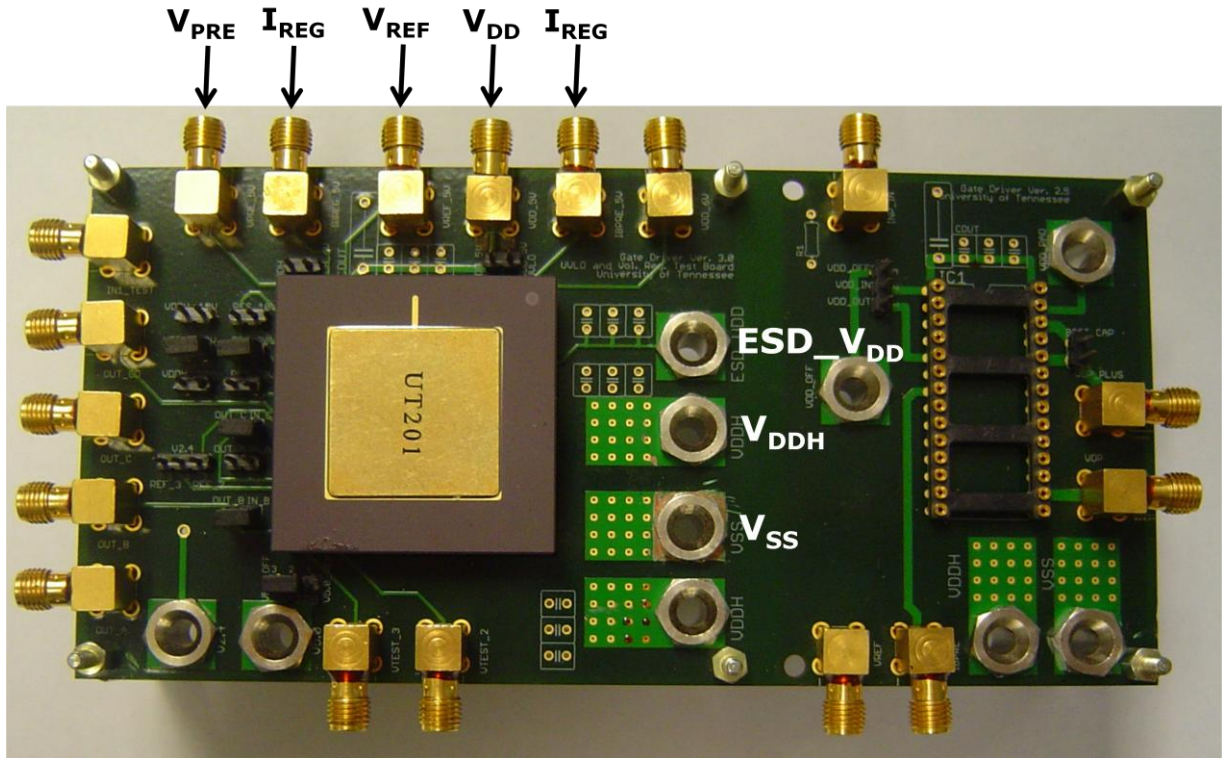


Figure 4.3 – Voltage Regulator Test Board

High-temperature, Teflon-insulated, gold-plated SMA connectors are used to route signals to and from the test board. Power is supplied via banana plugs and high-temperature, Teflon wire. On-board capacitance is provided by NPO ceramic capacitors, which provide a stable capacitance over temperature. This test board is designed to support independent or collaborative testing of the voltage regulator and the under voltage lock out circuits (a sub-circuit on the gate driver project). The DC testing (input start-up, line regulation, load regulation, and temperature testing) is performed using Labview 8.5-controlled Hewlett-Packard E3631A power supplies, Agilent 34401A multimeters, and Keithley 2400 ammeters. During each iteration of a test, the Labview code sets the independent variable for the specific test (load current or supply voltage), measures each instrument, writes the data to arrays, and increments the independent variable. After the final iteration, the arrays of each measurement are compiled and written to a text file.

#### 4.2 – Input Voltage Start-Up

Figure 4.4 illustrates the voltage regulator performance during start-up. Results similar to simulations are observed, as the voltage regulator is functional for  $V_{DDH}$  voltages greater than 8.3 V. This result is consistent with predicted and simulated start-up values. The 8.3 V start-up voltage verifies voltage regulator functionality for a  $V_{DDH}$  voltage of 10 V (the lower limit).

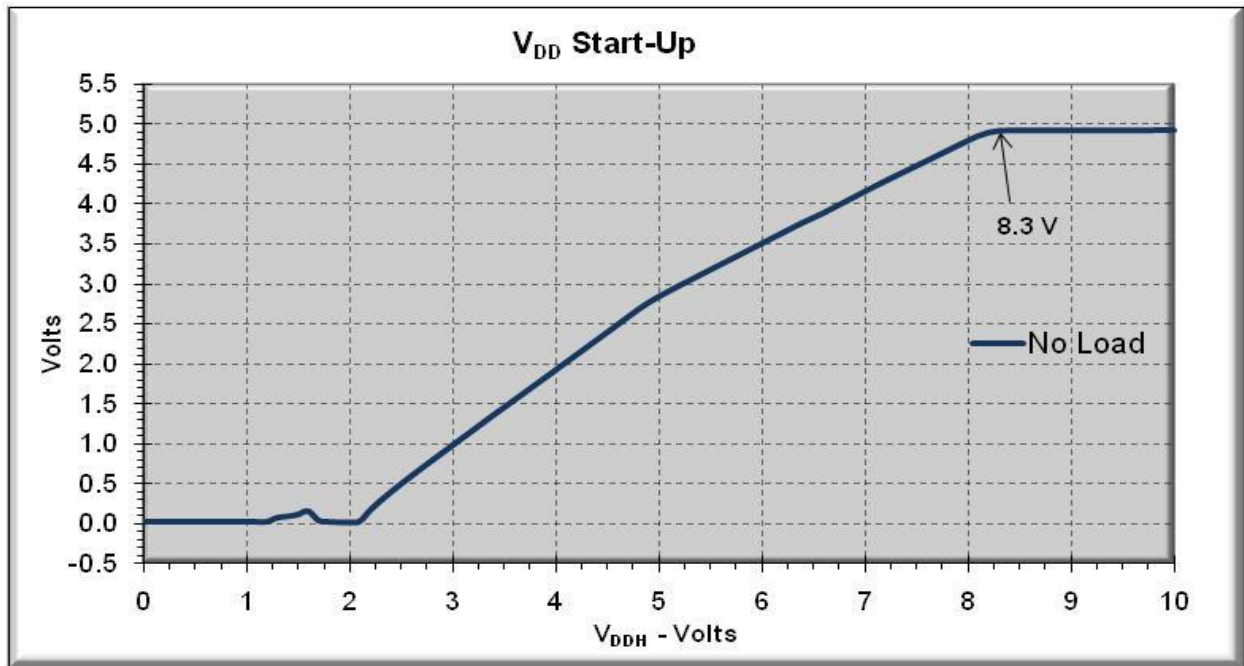


Figure 4.4 – Measured Voltage Regulator Start-Up

### 4.3 – Line Regulation

The designed voltage regulator is functional on a  $V_{DDH}$  range of 8.3 V to 35+ V. Figures 4.5-4.8 reveal the voltage regulator response to a  $V_{DDH}$  voltage sweep under no load and 10-mA load conditions. As seen in simulation results,  $V_{DD}$  possesses a proportional relationship with  $V_{DDH}$  for both loading conditions. Comparing measured results to simulations, a significant decrease in calculated line regulation is observable; however, noise limits the measurable resolution of  $V_{DD}$  to well above the order of ppb found in simulation results. The actual line regulation for the voltage regulator is not accurately measurable using the equipment described in section 4.1. The relationship between  $V_{DD}$  and  $V_{DDH}$  is emphasized with a 10-mA load present, but still well within design constraints. As predicted in simulations, the “on” resistance of the pass transistor causes  $V_{DD}$  line sensitivity, but self-heating of the voltage regulator under a load condition increases this effect. Noise renders accurate readings of  $V_{PRE}$  difficult (Figure 4.6), but the general trend of  $V_{PRE}$  as a function of  $V_{DDH}$  is visible as a proportional relationship (due to channel length modulation). Self-heating of the voltage regulator under a load condition affects  $V_{PRE}$  in a manner similar to  $V_{DD}$ . The measured line regulation of  $V_{PRE}$  matches the simulated line regulation fairly well with only small, constant deviations.  $V_{REF}$  is almost independent of supply voltage under the no load condition; however, an inversely proportional relationship is demonstrated during a DC load condition (Figure 4.7). Self-heating is again responsible for the decrease in line regulation  $V_{REF}$  shows in the presence of a load.  $V_{REF}$  still exhibits a line regulation on the order of ppm/V, and has minimal effect on the voltage regulator operation. The simulated vs. measured results of  $V_{DD}$ ,  $V_{PRE}$ , and  $V_{REF}$  correlate well, which implies a robust design.  $I_{REG}$  exhibits similar line regulation characteristics to  $V_{REF}$  during an input voltage sweep (Figure 4.8). The regulator bias current is essentially independent of  $V_{DDH}$  under a no load condition, but the bias current increases proportionally to supply voltage in the presence of a DC load due to self-heating. As with  $V_{REF}$ , the small line sensitivity of  $I_{REG}$  will have a negligible effect on the voltage regulator performance. Overall, the voltage regulator demonstrates remarkable line regulation (for both no load and DC load current) at all circuit stages.



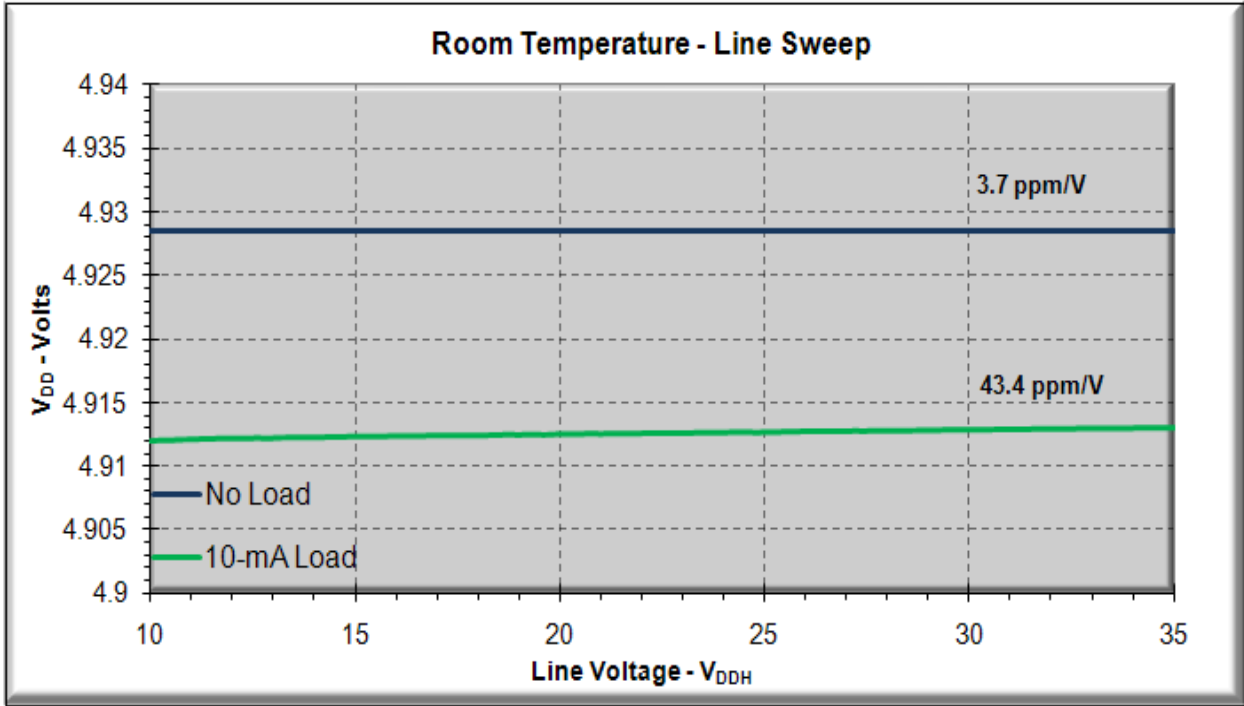


Figure 4.5 – Measured  $V_{DD}$  Line Regulation

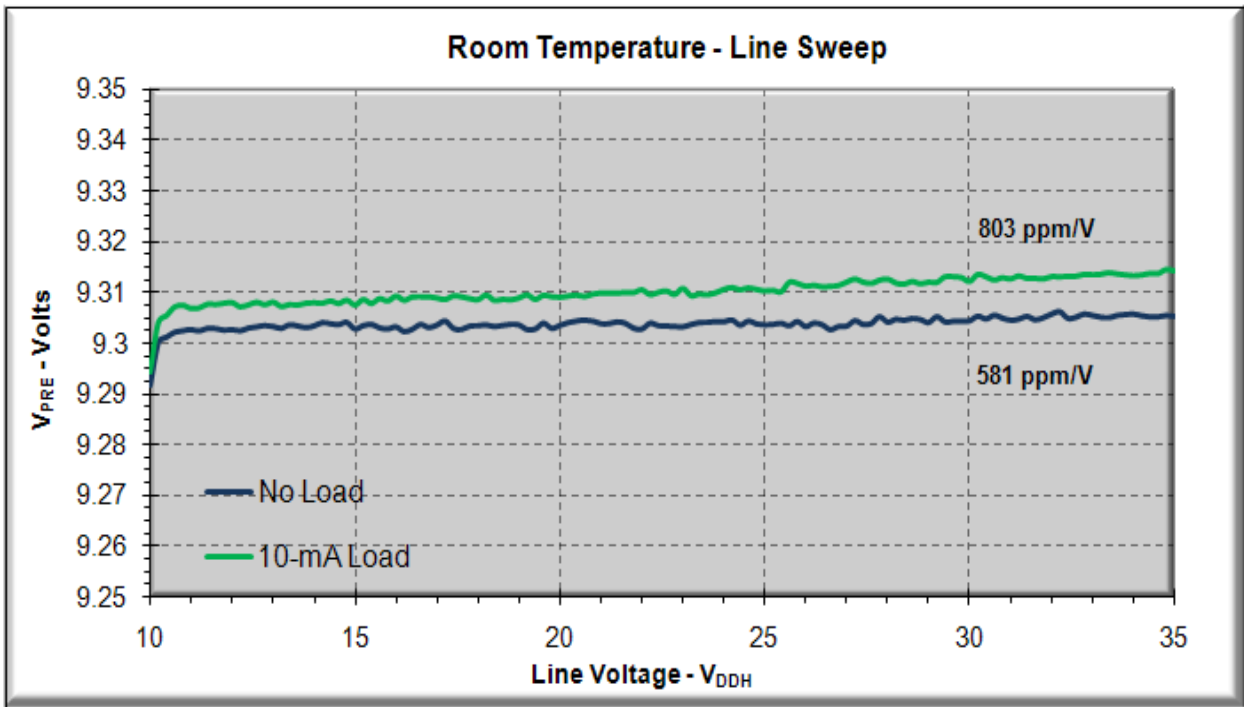
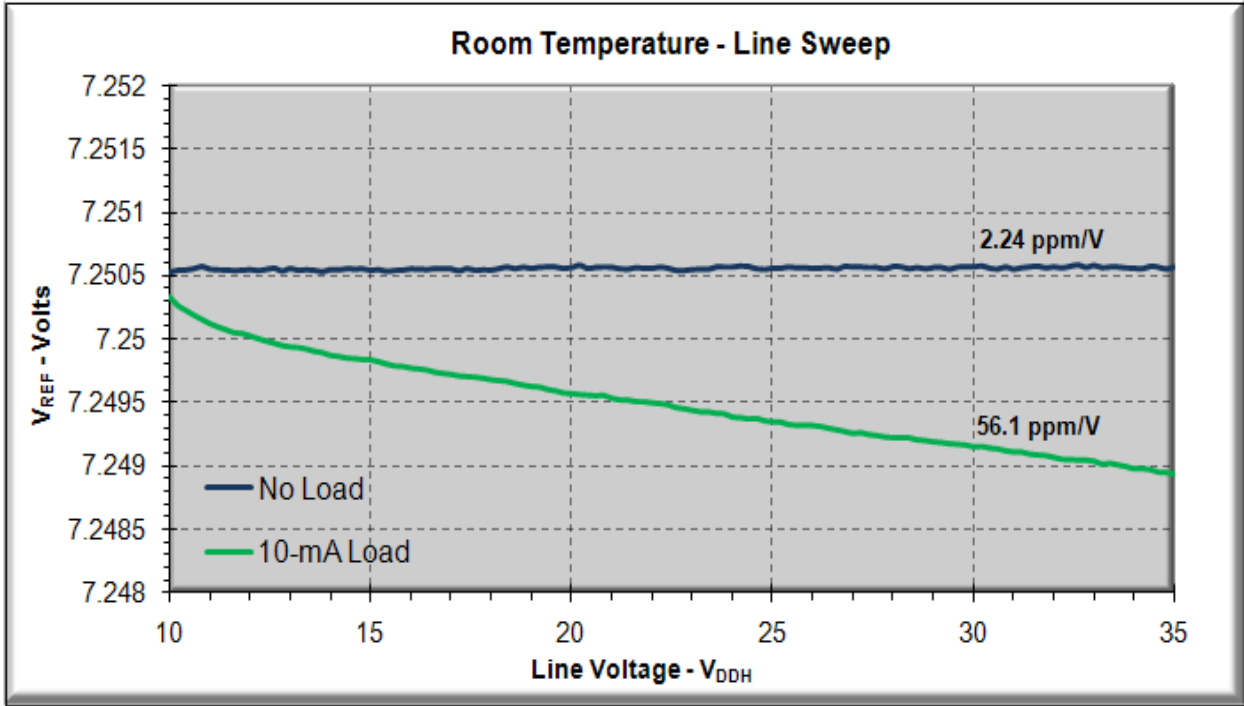
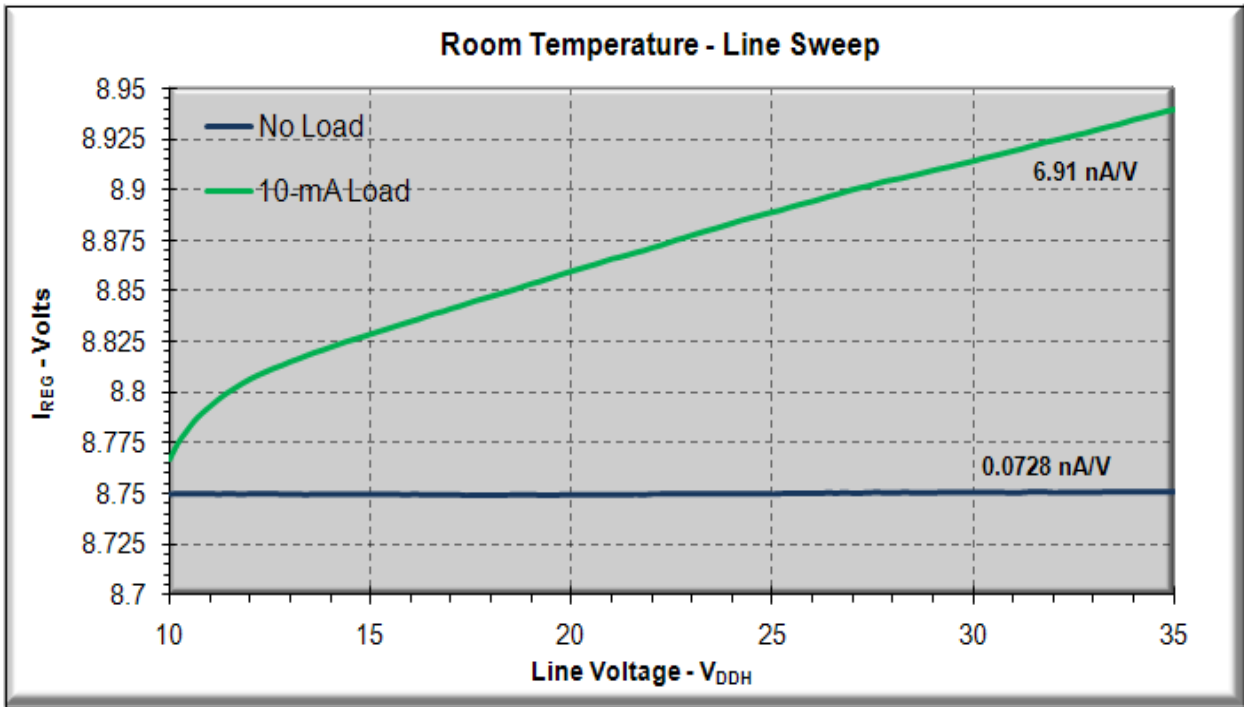


Figure 4.6 – Measured  $V_{PRE}$  Line Regulation



**Figure 4.7 – Measured  $V_{REF}$  Line Regulation**



**Figure 4.8 – Measured  $I_{REG}$  Line Regulation**

## 4.4 – Load Regulation

The gate driver specifications for this voltage regulator require only about 250- $\mu$ A DC current capability; however, the output is subject to transient load currents of 200 mA. To ensure reliable operation, the voltage regulator is capable of safely supplying over 300 mA of DC current. For testing purposes, the load regulation measurements are only performed to 10 mA, which is well below the capability of the regulator but well above the design requirements. Figures 4.9-4.13 illustrate the voltage regulator response to the load current sweep for 10-V, 20-V, and 30-V input voltages. In Figure 4.9,  $V_{DD}$  displays a linear relationship to load current indicating a linearly decaying  $R_{DS}$  of the pass transistor. This resistance is inversely proportional to load current and induces a small voltage drop, which reduces the overall output voltage.  $V_{DD}$  decays as load current increases at the rate much higher than simulations predicted. This rate of change decreases very slightly as  $V_{DDH}$  increases. The discrepancy between measured and simulated load regulation most likely arises from model inaccuracies of the high-voltage NMOS device (used as the pass device). The annular gate used in these devices is difficult to accurately model for simulation. The  $R_{DS}$  resistance can be decreased by increasing the width of the pass device, or by increasing gate overdrive. For this project, the DC current requirements do not require a strict DC load regulation; the measured load regulation is acceptable for most applications. A small, proportional relationship between  $V_{PRE}$  and load current is illustrated in Figure 4.10. This relationship is predominantly due to the effects described in simulation results, but self-heating as load current increases also contributes to the observed response.  $V_{REF}$  (Figure 4.11) possesses an extreme resistance to load current which is consistent with simulation results. The observable effects of  $V_{DDH}$  on the load regulation of  $V_{REF}$  (Figure 4.11) stem from increased power dissipation at higher  $V_{DDH}$  voltages. Figure 4.12 reveals a linear relationship between pre-regulator bias current and load current. In this case, the heat generated from load current lowers the threshold voltage of the NMOS devices in the threshold referenced current source of the pre-regulator and increases the generated bias current. Figure 4.13 examines the relationship between the regulator bias current and load current which is found to be similar to the relationship found in the pre-regulator bias current. Neglecting self-heating, measured load regulation results match simulated load regulation results at all voltage regulator stages, save  $V_{DD}$ . Overall, the regulator performs well under a wide range of load conditions.

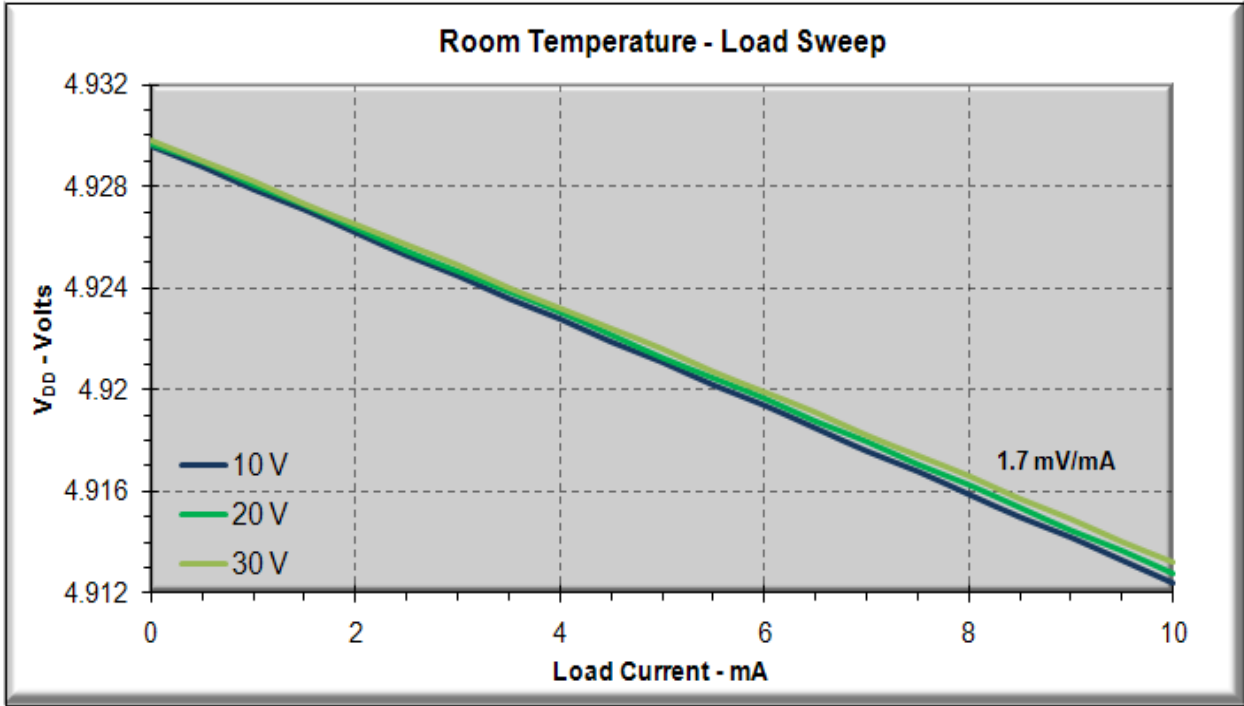


Figure 4.9 – Measured  $V_{DD}$  Load Regulation

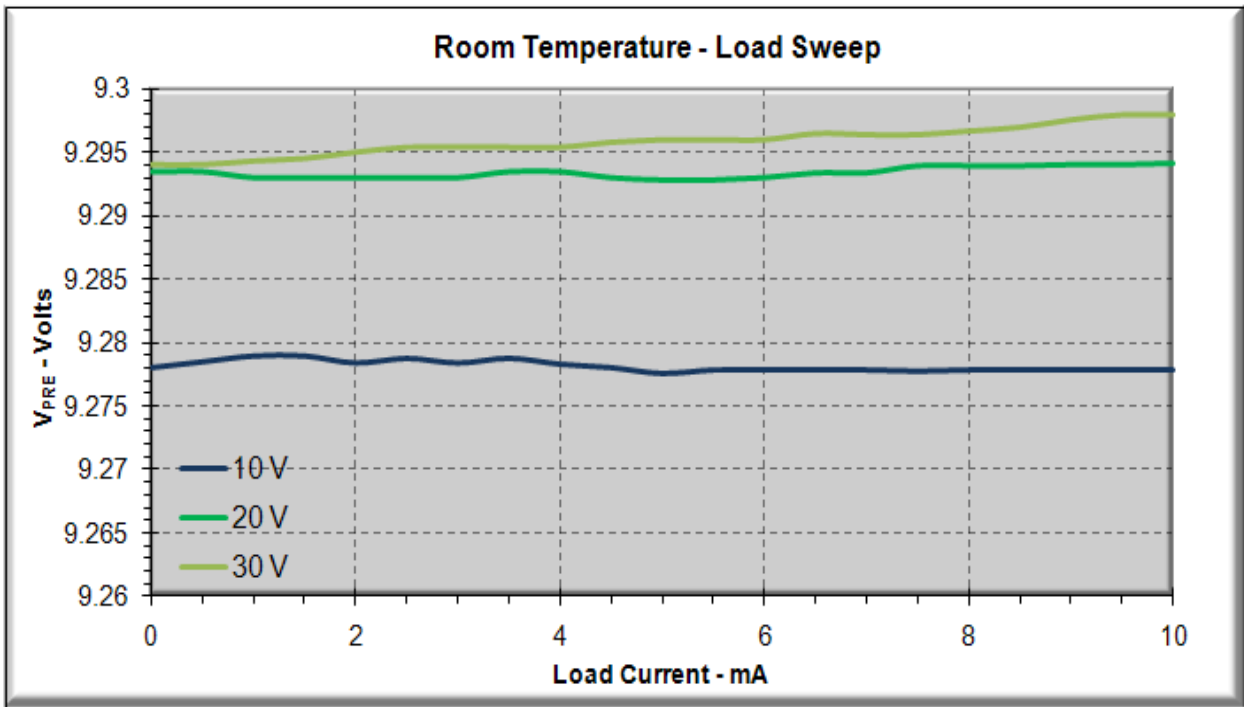


Figure 4.10 – Measured  $V_{PRE}$  Load Regulation

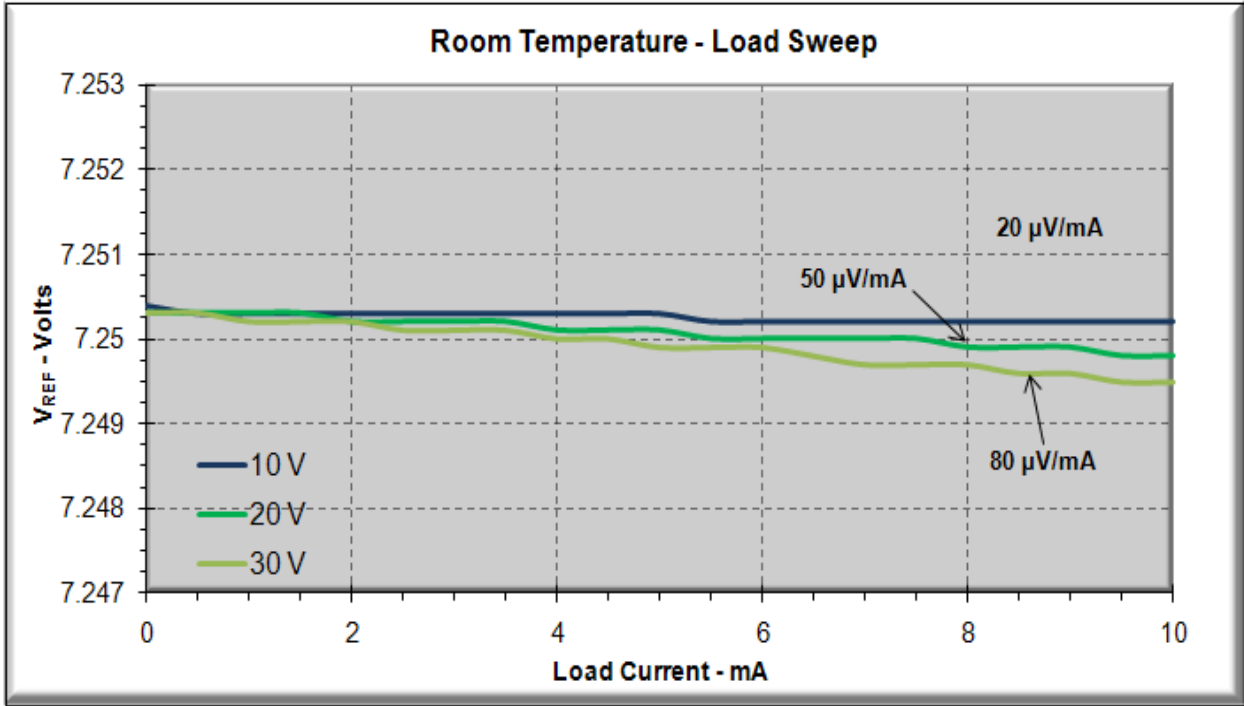


Figure 4.11 – Measured  $V_{REF}$  Load Regulation

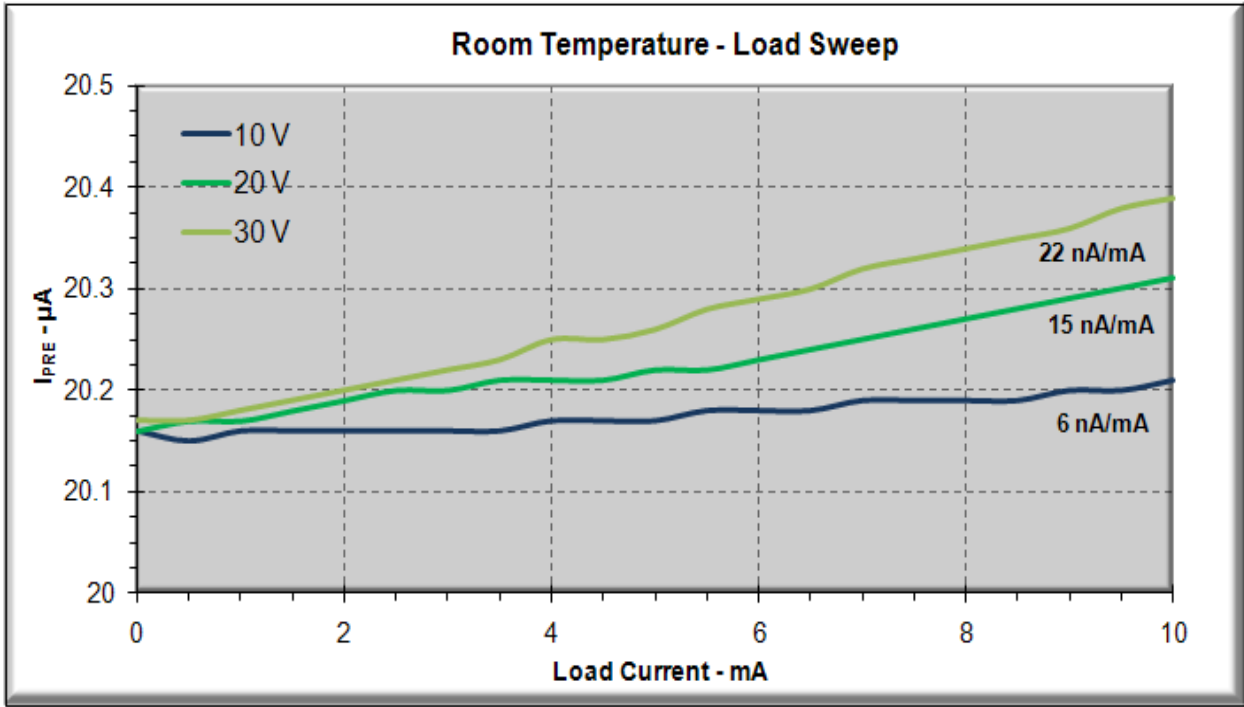


Figure 4.12 – Measured  $I_{PRE}$  Load Regulation

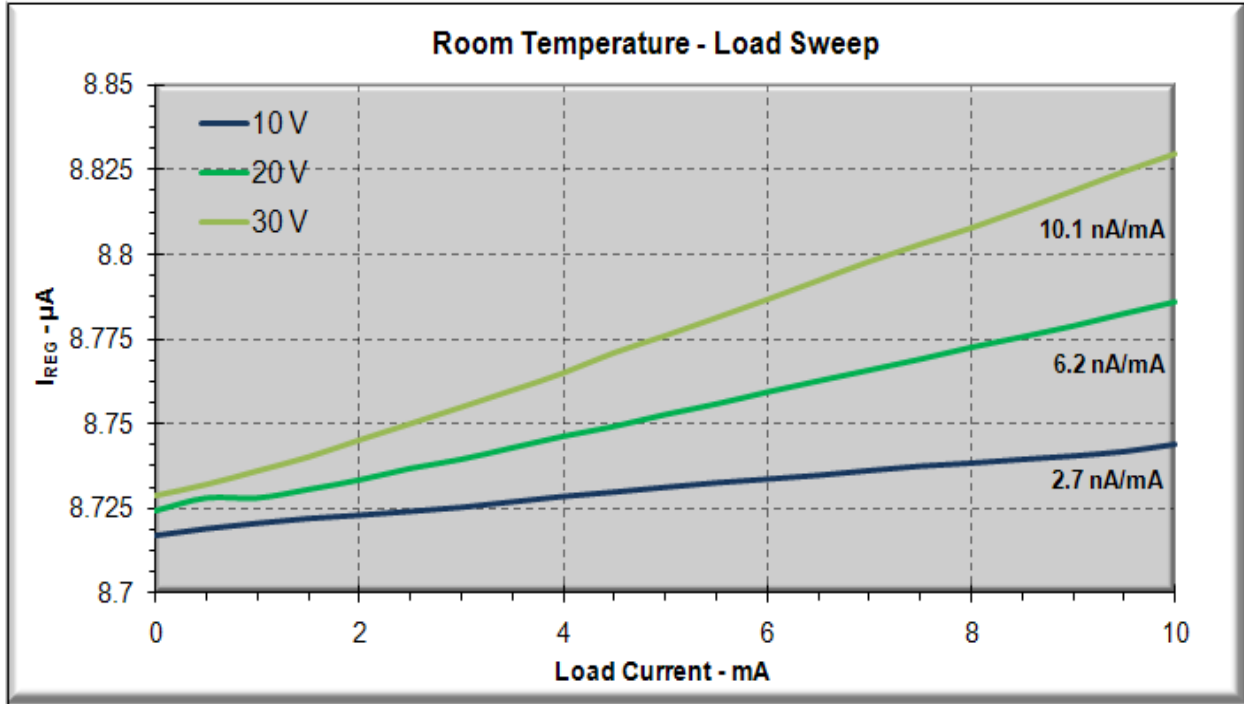


Figure 4.13 – Measured  $I_{REG}$  Load Regulation

#### 4.5 – Temperature Characteristic

The voltage regulator is tested in a Delta Design 9023 Environments Chamber over a temperature range of  $-50\text{ }^{\circ}\text{C}$  to  $200\text{ }^{\circ}\text{C}$  with a sample taken every  $25\text{ }^{\circ}\text{C}$ . Figures 4.14-4.19 show the temperature characteristics of  $V_{DD}$ ,  $V_{PRE}$ ,  $V_{REF}$ ,  $I_{PRE}$ ,  $I_{REG}$ , and  $I_{SUPPLY}$  with 10-V, 20-V and 30-V input voltages and no load and 10-mA load conditions. Under no load, the output voltage exhibits a nearly uniform, parabolic relationship to temperature while varying only a few mV over the  $250\text{ }^{\circ}\text{C}$  range (Figure 4.14). Supply voltage variation from 10-30 V reveals no discernable effect on the temperature characteristic of  $V_{DD}$ . Under a 10-mA load condition, a similar parabolic relationship is observable but with a less uniform correlation. The effects of temperature on  $R_{DS}$  cause an increased drop in  $V_{DD}$  as temperature increases. This effect is due to the proportional relationship of  $R_{DS}$  to temperature. In spite of the temperature effect on  $R_{DS}$ , the total variation of  $V_{DD}$  over a  $250\text{ }^{\circ}\text{C}$  temperature sweep remains modest for either load condition. Supply voltage variation effects on  $V_{DD}$  with a 10-mA load display an inverse relationship to temperature; however, the effect is small.  $V_{PRE}$  relationship to temperature is demonstrated in Figure 4.15. The temperature coefficients of MOSFET threshold voltages and

poly2 resistivity combine to form this temperature dependence. A load condition results in a very small decrease in pre-regulator voltage, which is consistent across temperature. The proximity effect as  $V_{DDH}$  approaches  $V_{PRE}$  observed in simulations presents in measurement results as well. The temperature characteristic exhibited in Figure 4.15 differs from the simulation results due to modeling inaccuracies (likely the high-voltage LDMOS devices). At all temperatures, supply conditions, and load conditions the pre-regulator voltage remains well above the turn-on voltage required by the regulator circuits. Figure 4.16 reveals a decaying reference voltage in response to increasing temperature. The magnitude of the simulated  $V_{REF}$  temperature coefficient differs from the temperature characteristic found in measurement results. Once again, model inaccuracies are the most probable cause of the discrepancy. Load condition and supply voltage have minimal effects on  $V_{REF}$  temperature characteristic. Despite deviation from simulated results,  $V_{REF}$  is well-bounded over temperature and will allow for accurate voltage regulation.  $I_{PRE}$  and  $I_{REG}$  (Figures 4.16 and 4.17, respectively) respond to temperature changes as predicted by the simulations. The voltage regulator provides an overall temperature characteristic that out performs most comparable commercially-available voltage regulators.

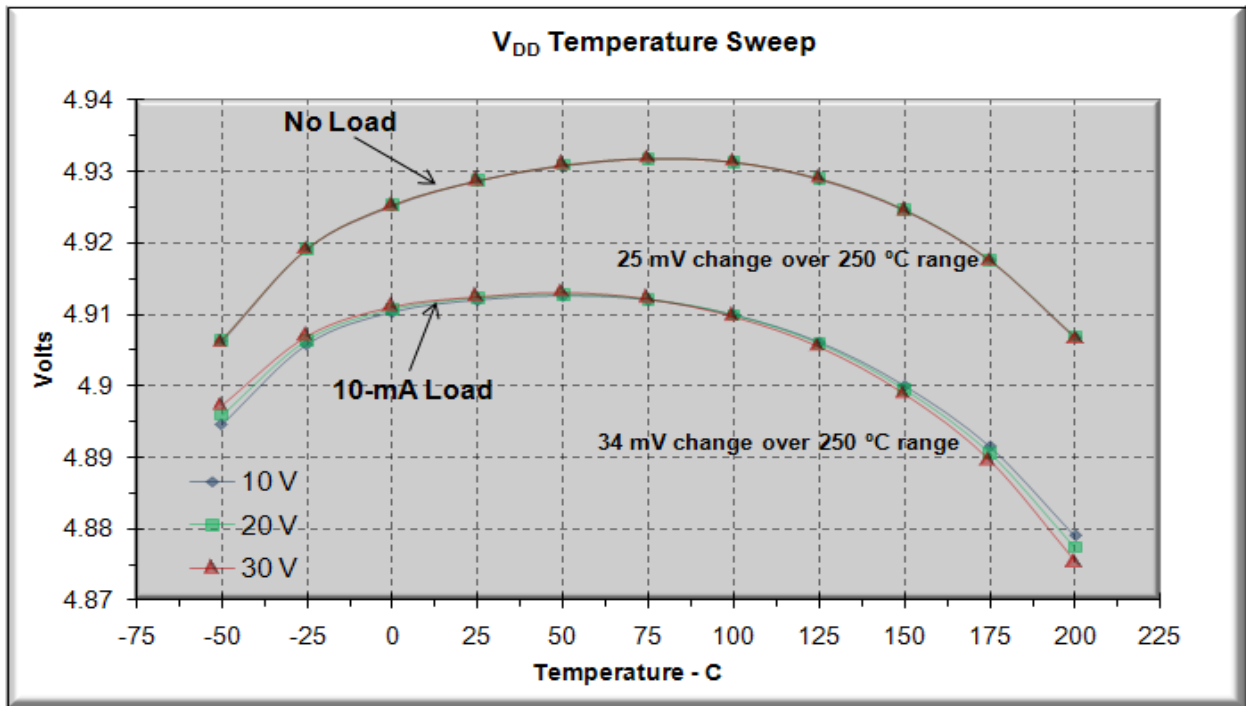


Figure 4.14 – Measured  $V_{DD}$  Temperature Characteristic

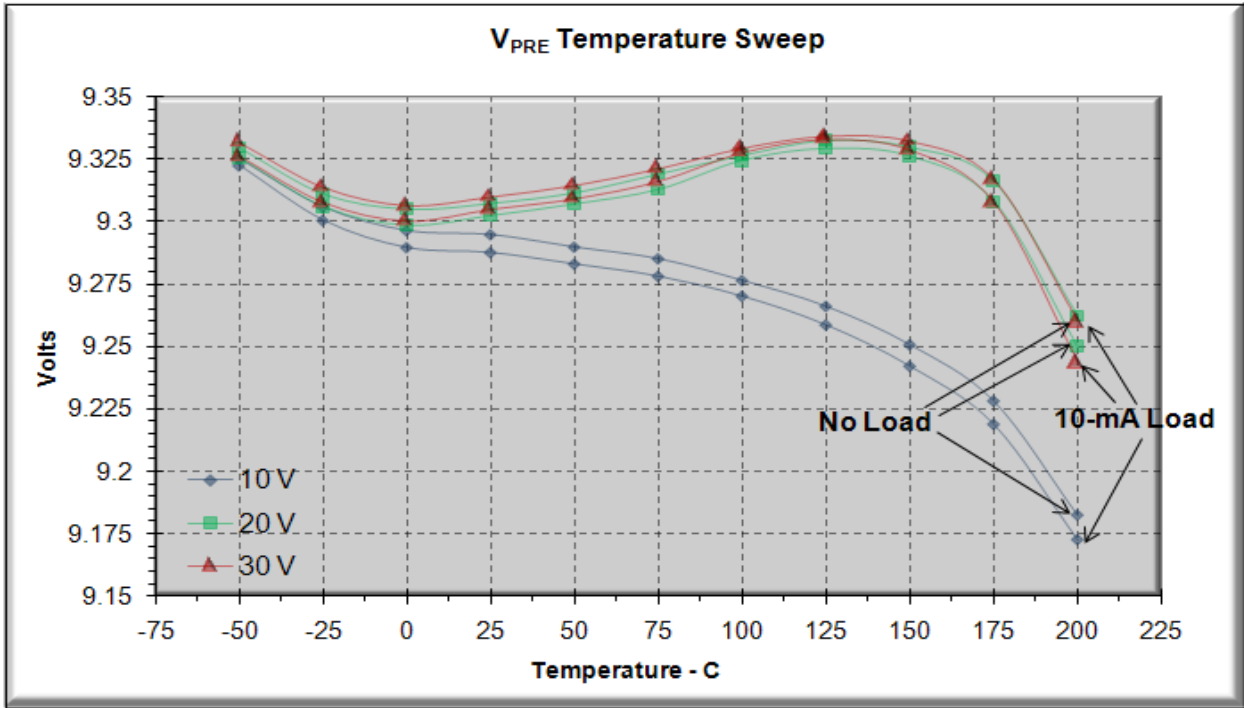


Figure 4.15 – Measured  $V_{PRE}$  Temperature Characteristic

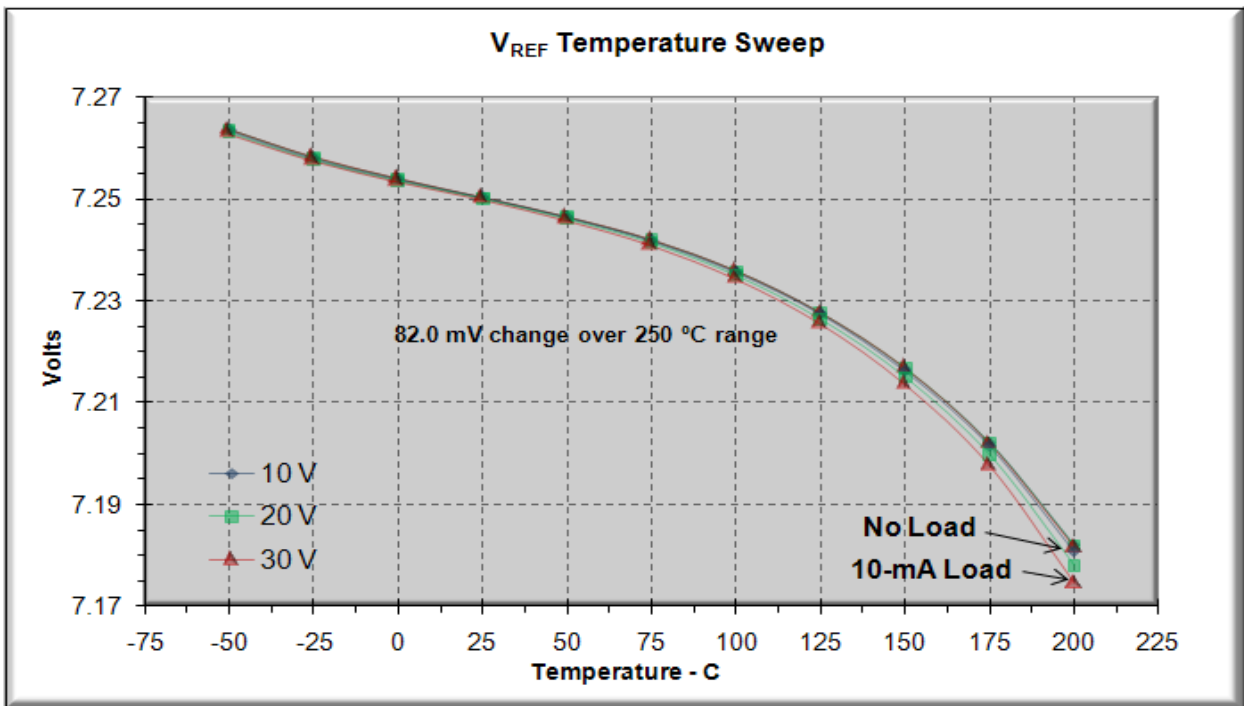


Figure 4.16 – Measured  $V_{REF}$  Temperature Characteristic



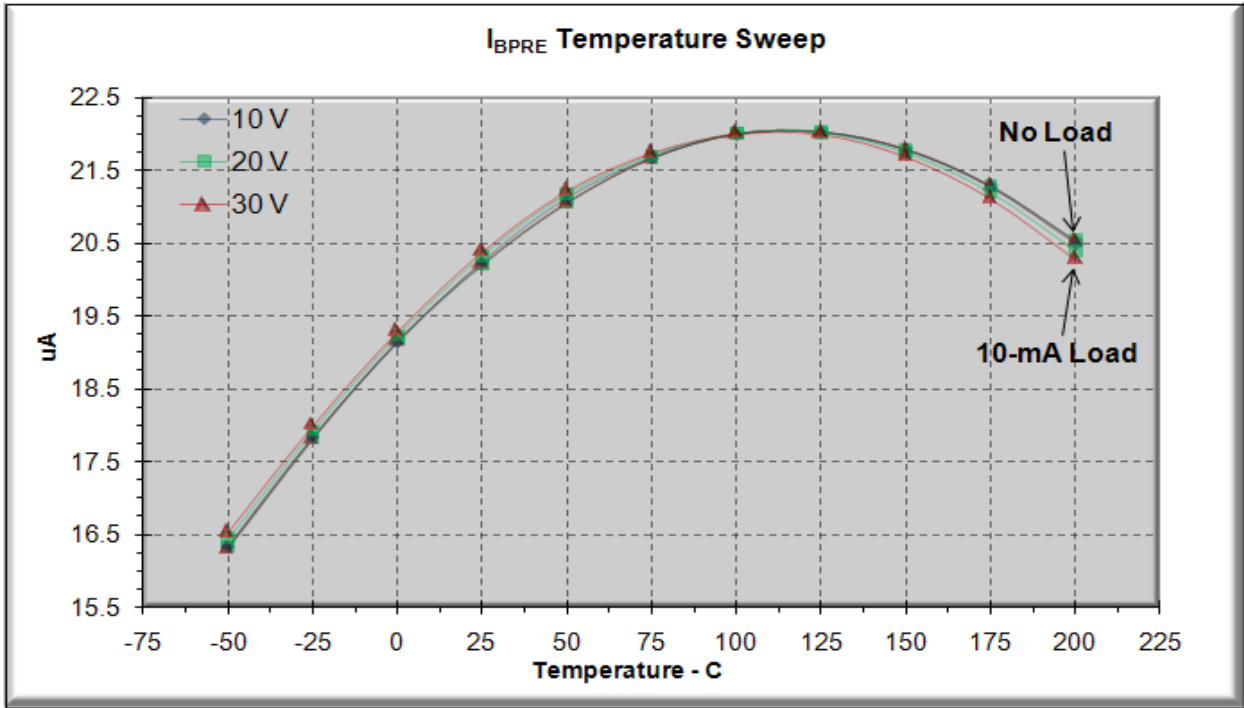


Figure 4.17 – Measured  $I_{PRE}$  Temperature Characteristic

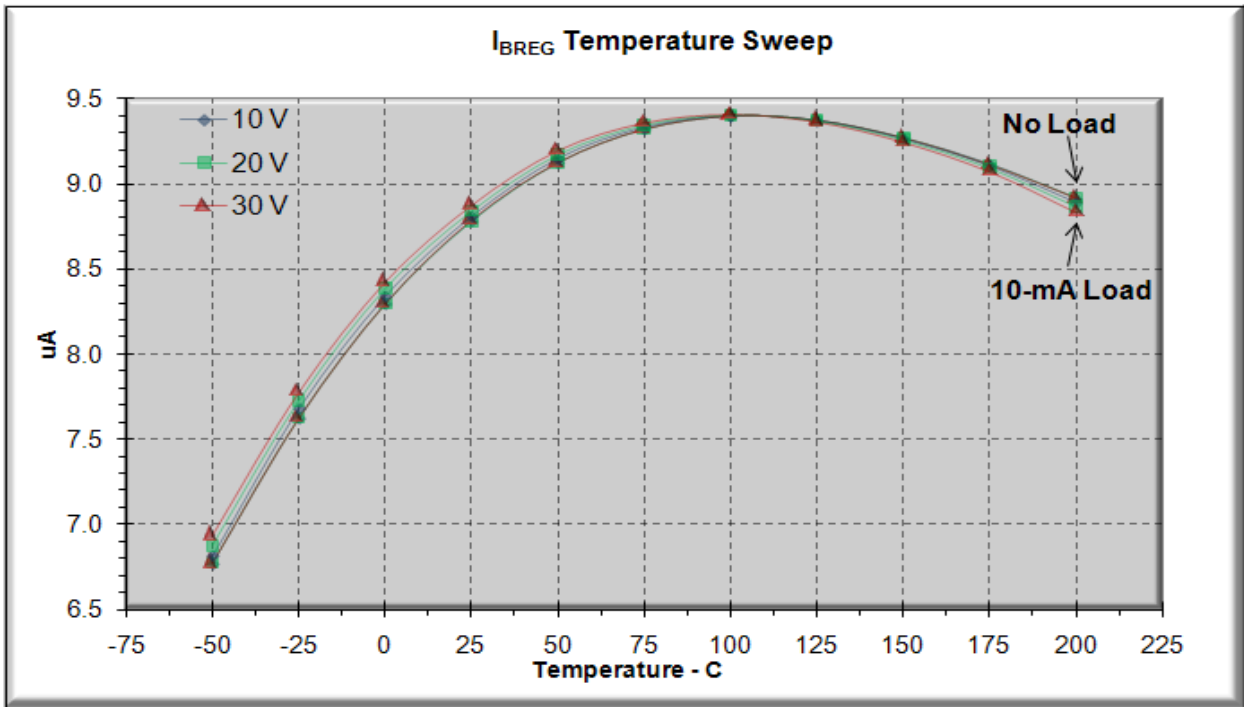


Figure 4.18 – Measured  $I_{REG}$  Temperature Characteristic

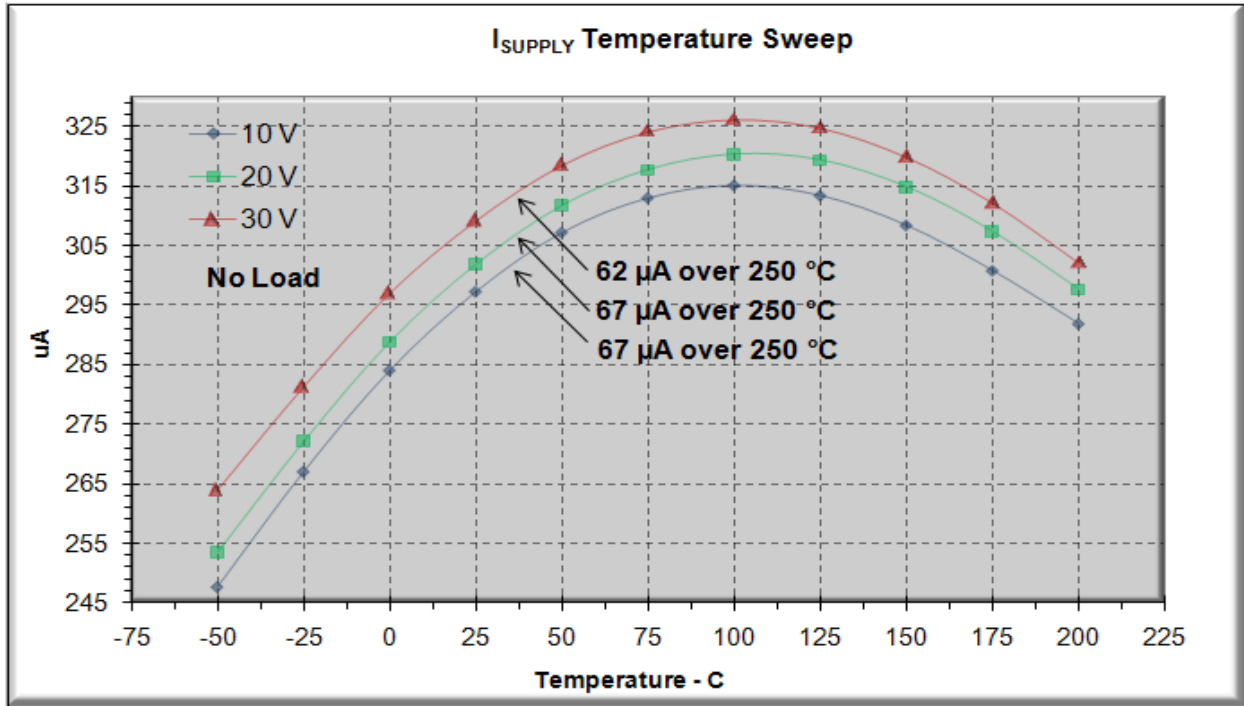
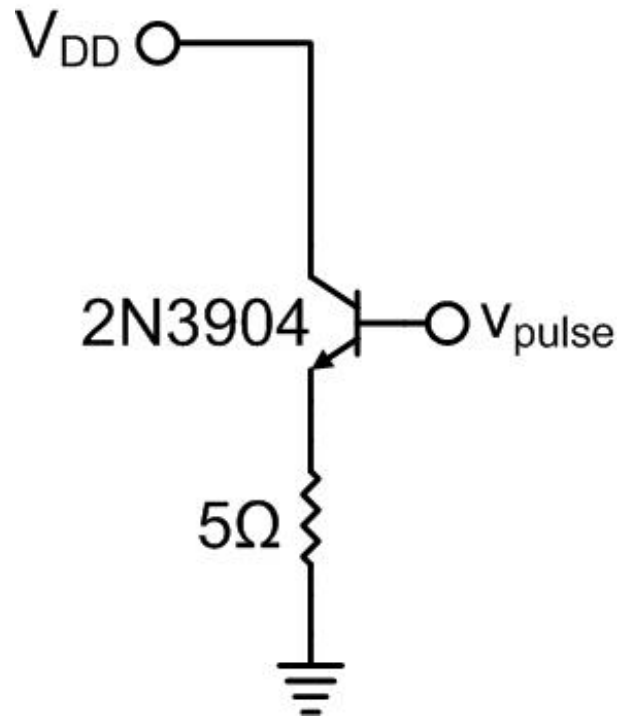


Figure 4.19 – Measured  $I_{SUPPLY}$  Temperature Characteristic

#### 4.6 – Load Transient

Load transient tests are performed at  $-50\text{ }^{\circ}\text{C}$ ,  $25\text{ }^{\circ}\text{C}$ , and  $200\text{ }^{\circ}\text{C}$  with a supply voltage of 20 V. The test set-up for the load transient tests can be seen in Figure 4.20. The load current is obtained by measuring the voltage across the 5- $\Omega$  resistor and using Ohm’s law. The switching signal  $v_{pulse}$  is sourced using an Agilent 33250A waveform generator. An Agilent 54624A oscilloscope is used to capture the various signals. Using the pulse signal described, the load current generated exhibits a 70-nsec rise time and a 60-nsec fall time. These transient times are limited by the speed of the 2N3904 current sink device. As in load transient simulations, a ceramic NP0 load capacitor of 3.8  $\mu\text{F}$  is used as a charge storage device. Parasitic inductance and resistance present in the signal path from the signal routing on chip to the instruments inputs degrade the measureable transient response. Signals probed at different points along the signal path displayed drastic differences in transient response. The transient data obtained best represents the actual transient response; however, improved data may be attainable with packaging, PCB board, and test set-up modifications.



**Figure 4.20 – Load Transient Test Set-Up**

The results of the load transient test for  $-50\text{ }^{\circ}\text{C}$ ,  $25\text{ }^{\circ}\text{C}$ , and  $200\text{ }^{\circ}\text{C}$  are illustrated in Figures 4.21-4.23, respectively. For all temperatures, the total displacement of  $V_{DD}$  is about 50 mV during the load transient. The peak-to-peak  $V_{DD}$  load transient response decreases as temperature increases (consistent with simulation).  $V_{DD}$  settles to its nominal value within 2.5  $\mu\text{sec}$ . This observed settling time decreases with temperature. Small ripple voltages are visible on  $V_{PRE}$  and  $V_{REF}$  at the edges of the transient load. These ripple voltages are on the order of a few  $\text{mV}_{\text{p-p}}$  and have settling times of a few  $\mu\text{sec}$  as exhibited in the respective figures. These disturbances settle relatively quickly and do not cause voltage regulator stability issues. The transient load is coupled through various devices within the voltage regulator, but the main coupling path is through the NMOS pass device. The large width of this device implies large parasitic capacitances, which couple AC signals through the voltage regulator. These effects are not detrimental to the voltage regulator performance and are expected in reaction to such a large load transient. Subtle changes in the load transient responses of  $V_{PRE}$  and  $V_{REF}$  can be seen for different temperatures. The measured load transient results differ slightly from the simulation results due to model inaccuracies (mainly the high-voltage LDMOS devices). In spite of this short coming, the voltage regulator performs admirably in the presence of a load transient.

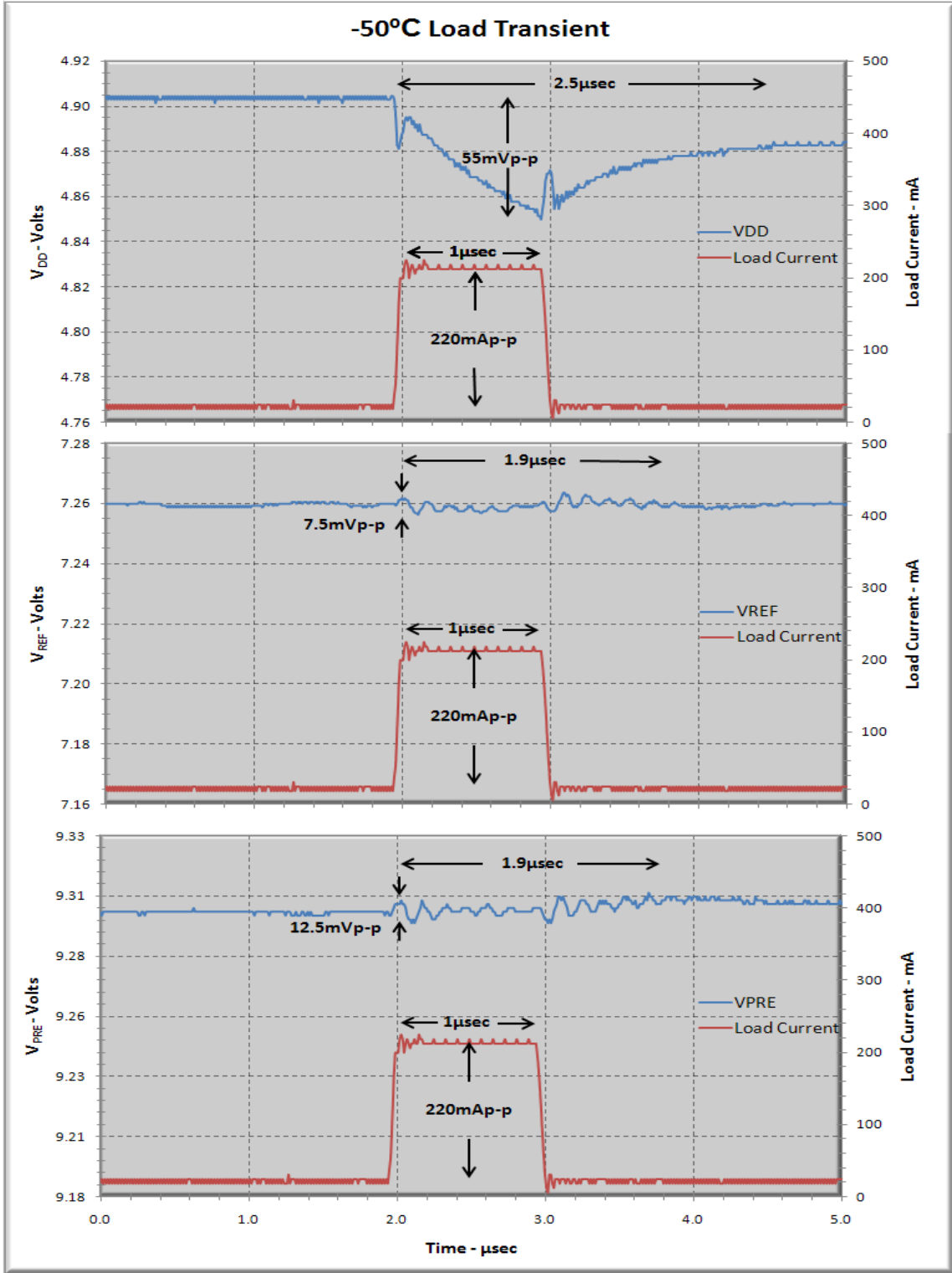


Figure 4.21 – Measured  $-50^\circ\text{C}$  Load Transient

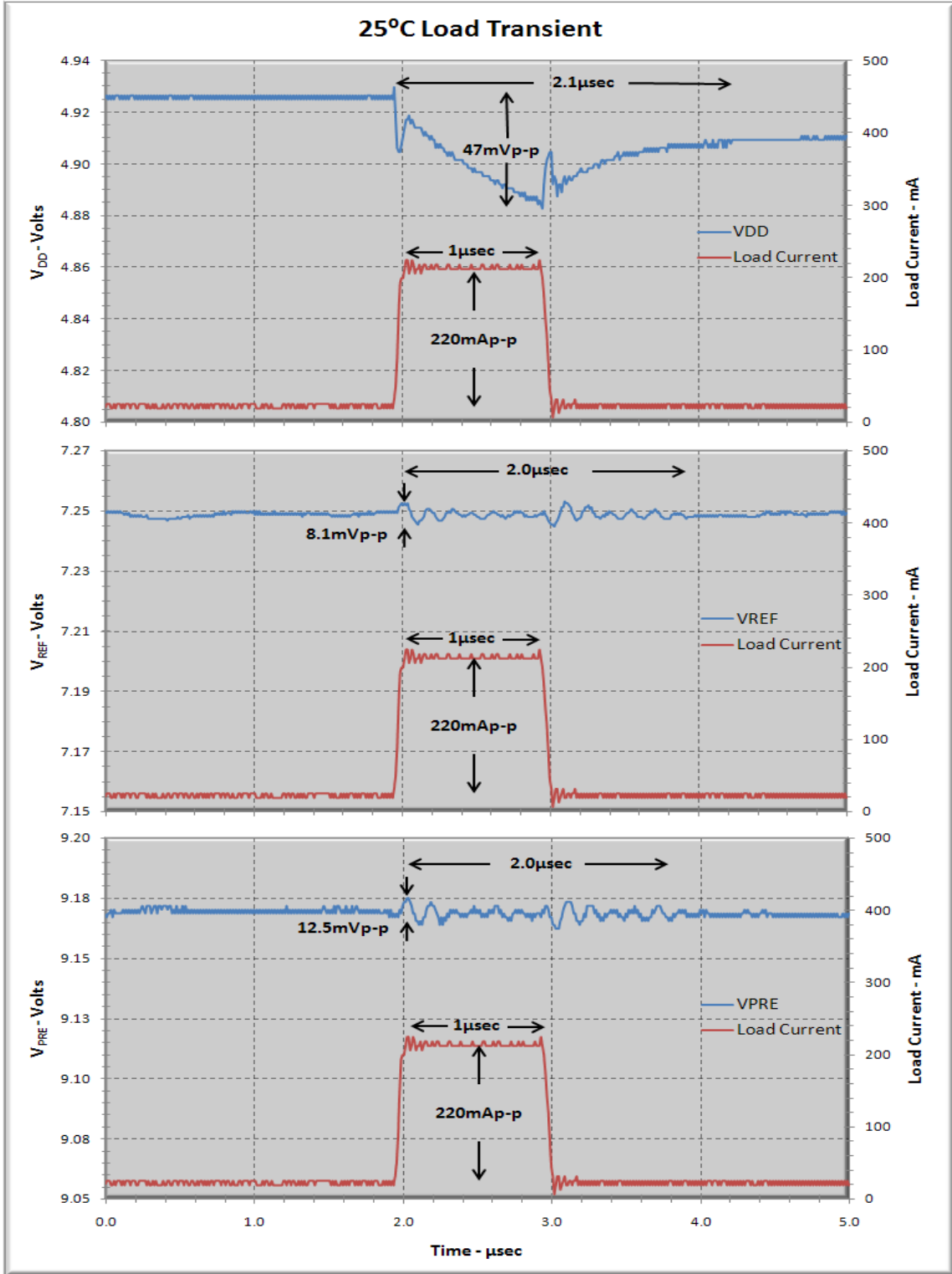


Figure 4.22 – Measured 25 °C Load Transient

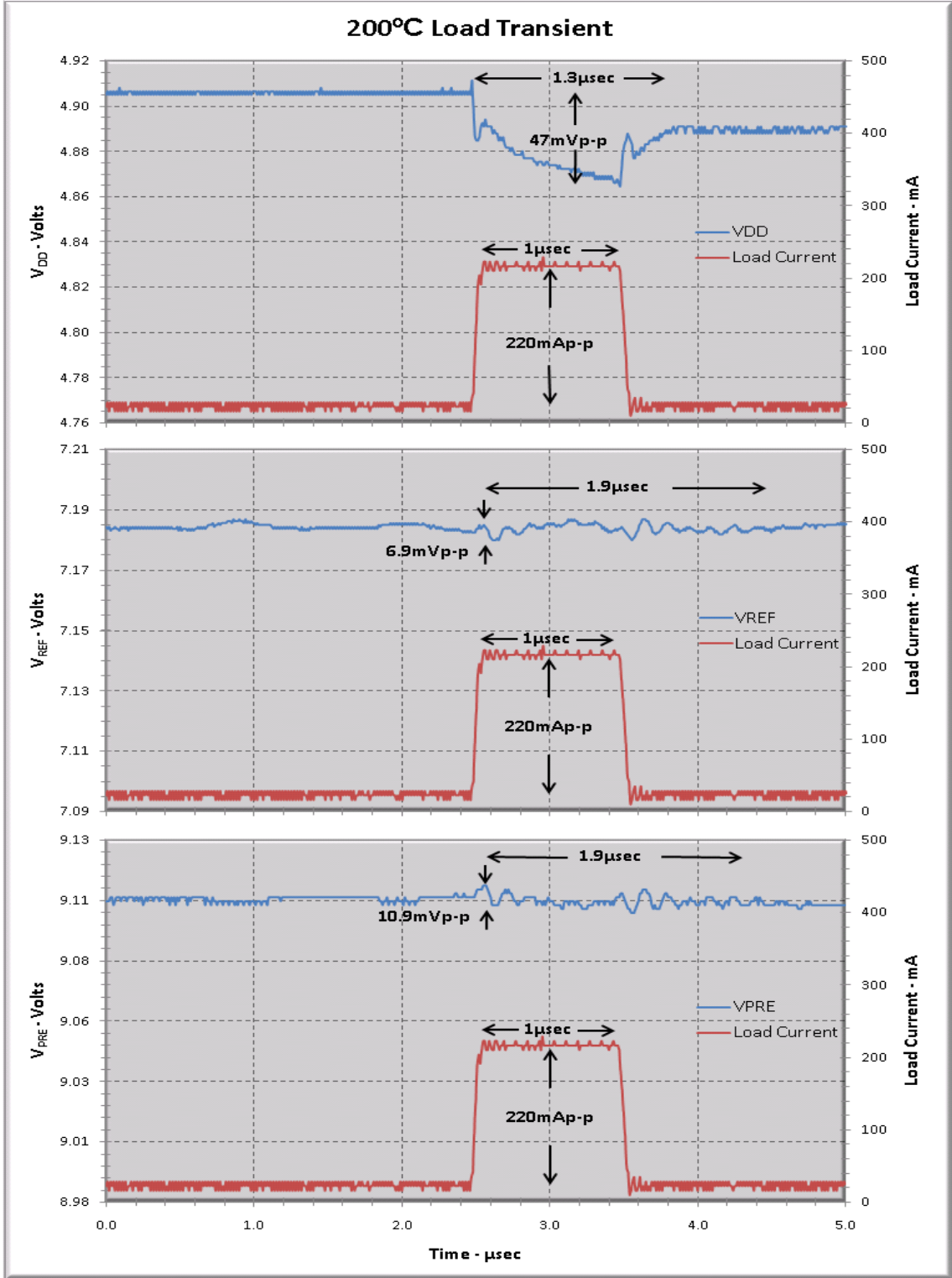


Figure 4.23 – Measured 200 °C Load Transient

## 4.7 – Line Transient

Measured line transient testing is performed using a DC voltage source in series with an AC pulse generator (Figure 4.24). An Agilent 33250A is used to provide the pulse voltage, while an Agilent 54624A oscilloscope is used to capture the various signals. The pulse voltage ( $v_{pulse}$ ) is displayed in Figure 4.25. The pulse voltage is set to 5 Vp-p with a 5-nsec rise time. This test condition greatly exceeds input voltage transients encountered in the gate driver application. This transient supply voltage injects high frequency signals (the edges of the pulse signal) into the voltage regulator. These high frequency signals are coupled through various parasitic capacitors throughout the voltage regulator and are examined at each node in the voltage regulator. The pre-regulator greatly attenuates the line transient imposed on the subsequent voltage regulator circuits (another advantage to implementing the voltage regulator with a pre-regulator circuit). The output capacitor also attenuates the propagated transient signal. As with the load transient test, the accuracy of the measured line transient responses is limited by the parasitic inductance and resistance presented at various points along the signal path.

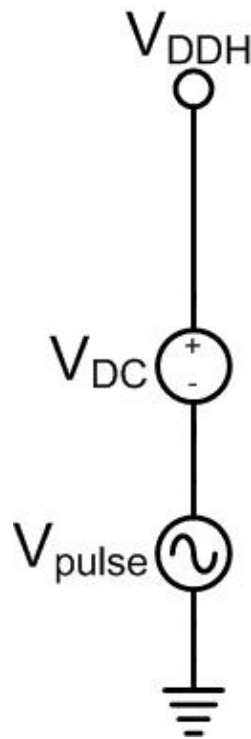
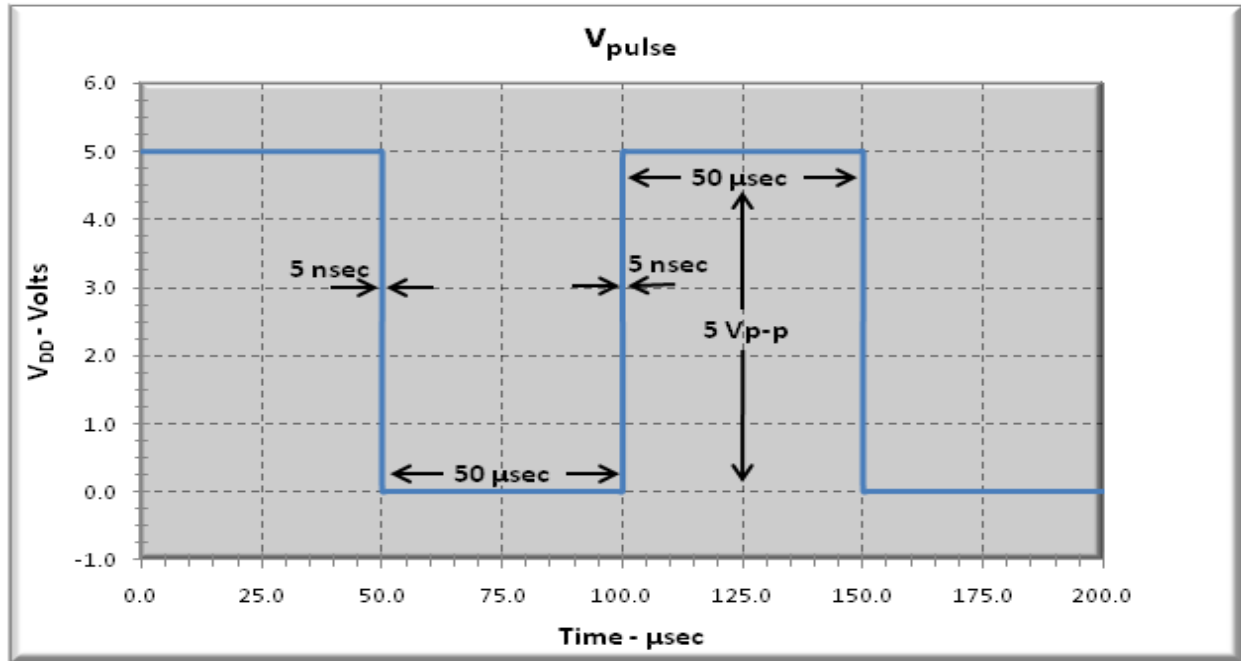


Figure 4.24 – Line Transient Test Set-Up



**Figure 4.25 –  $v_{pulse}$  Line Transient Signal**

The voltage regulator line transient responses can be observed in Figures 4.26-4.28.  $V_{DD}$  varies less than 1 mV during a rising edge transient and does not respond to a falling edge transient (consistent with simulation results). The observed displacement in  $V_{DD}$  increases with temperature but remains quite low even for a large line transient.  $V_{REF}$  shows a transient response at both rising and falling edges of the line transient, but the rising edge response is more pronounced. This transient response in  $V_{REF}$  exhibits narrow pulse widths due to the feedback loop in the reference generator circuit. The amplitude of the  $V_{REF}$  transient response has a parabolic relationship as function of temperature, but only minor differences arise at different temperatures.  $V_{PRE}$  responds to line transients with a proportional voltage step followed by an exponential decay back to the nominal voltage level. The amplitudes and settling times of  $V_{PRE}$  transient response is proportional to temperature. The exponential decay found in  $V_{PRE}$  is attributed to the parasitic capacitances of the two large current source PMOS devices ( $M13$  and  $M14$ ). The pre-regulator greatly improves the voltage regulators ability to reject line transients. Even large line transients do not pose a significant threat to voltage regulator performance as long as the line voltage remains within the input voltage range of the voltage regulator. Measurement results correlate well to simulation results with only small amplitude and time constant variations.



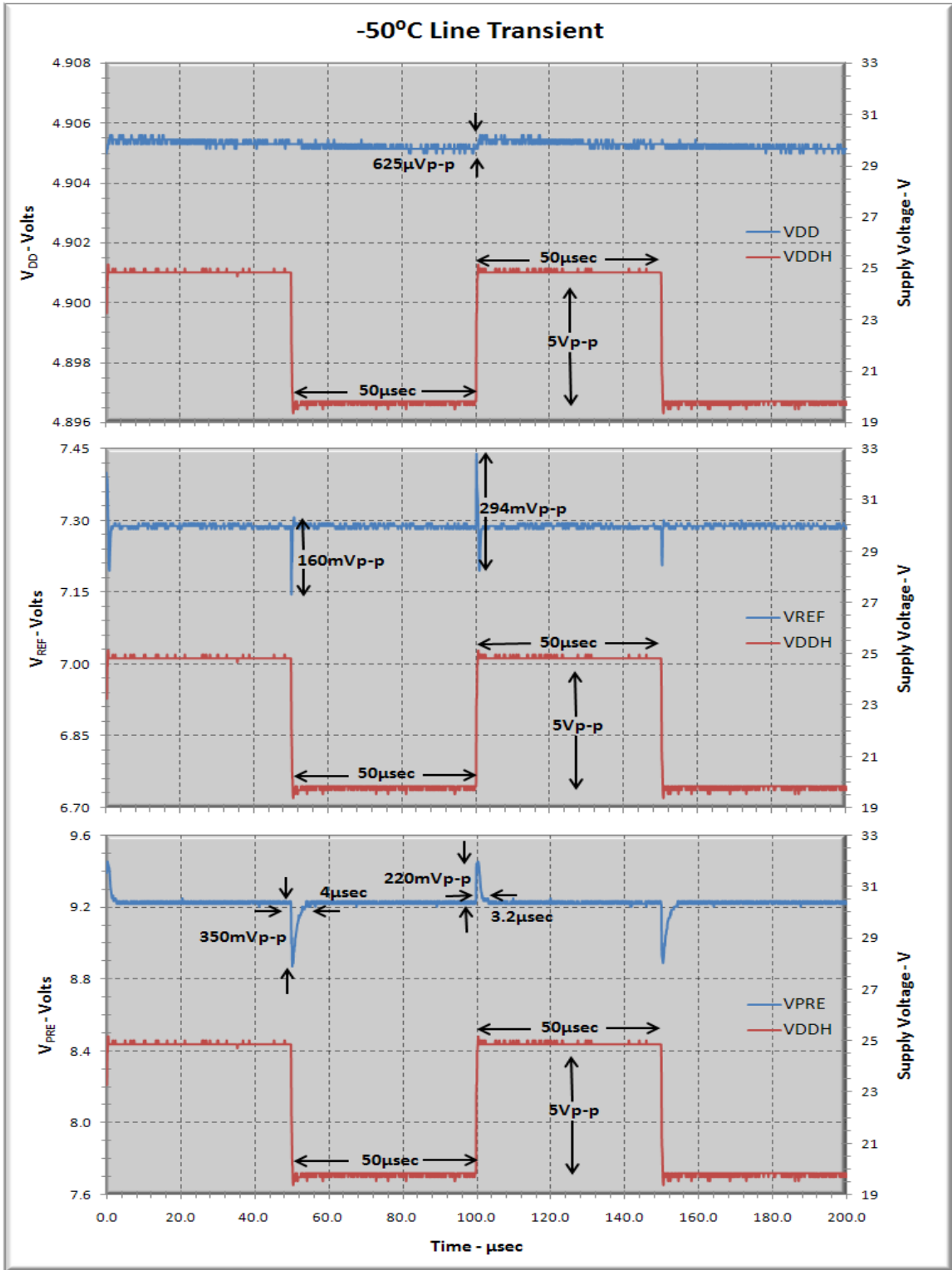


Figure 4.26 – Measured -50 °C Line Transient

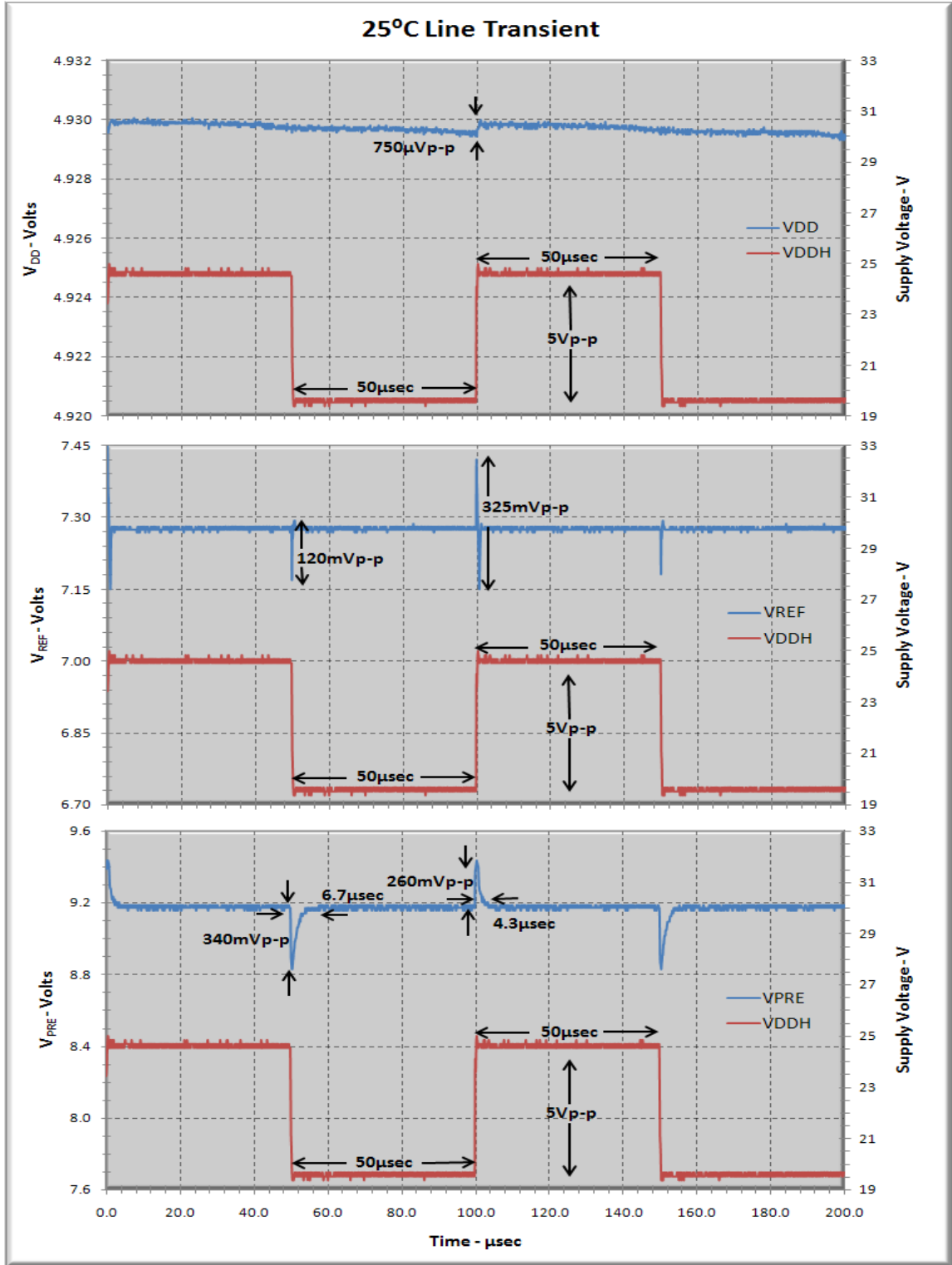


Figure 4.27 – Measured 25 °C Line Transient

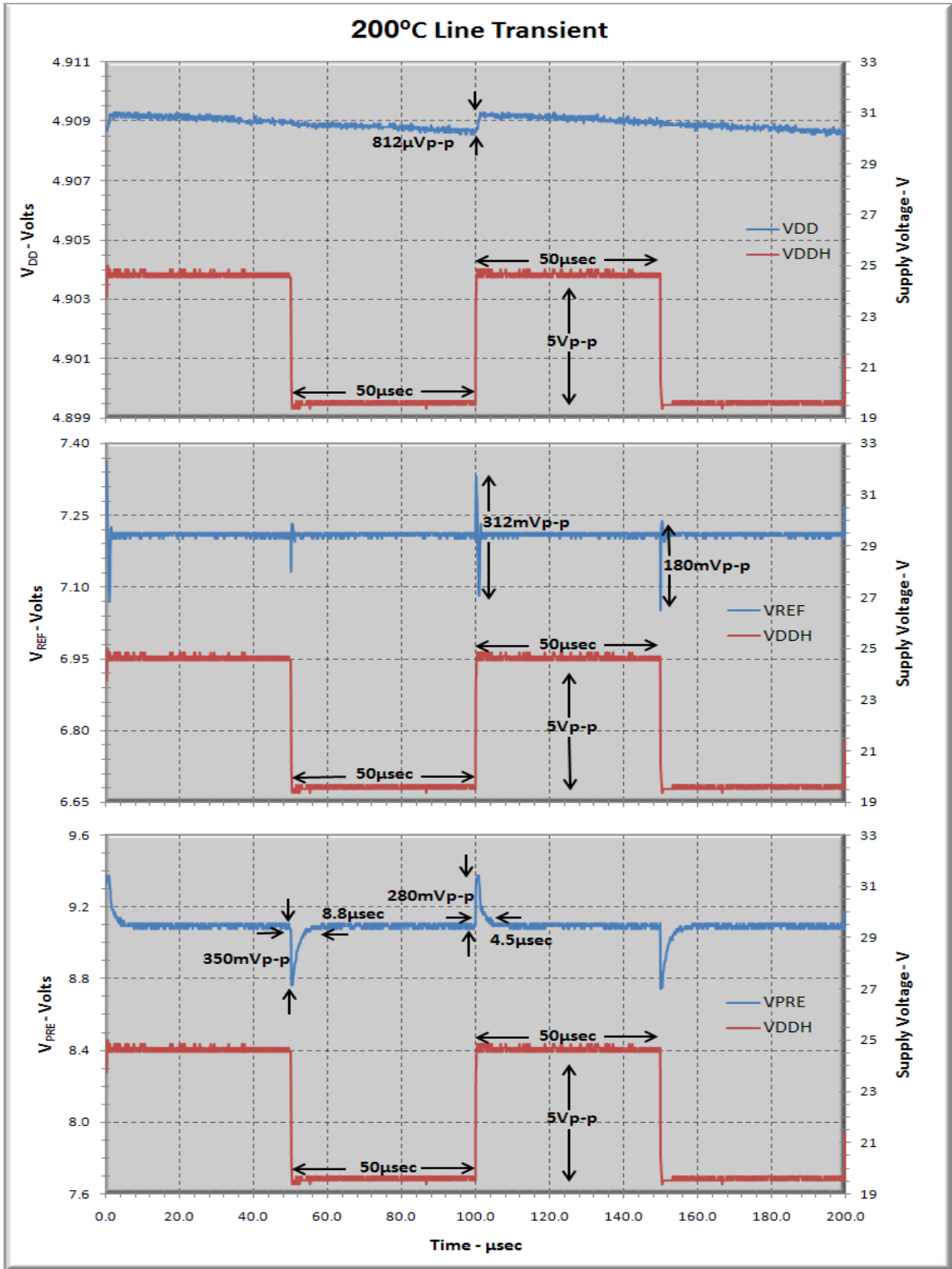


Figure 4.28 – Measured 200 °C Line Transient

## 5. Conclusion

### *5.1– Thesis Summary*

All of the design challenges associated with the high-voltage, high-temperature gate driver project are met by modifying the existing LM723 design. The LM723 is a well-designed, well-tested topology that serves as a strong base for voltage regulator design. The commercially-available, 0.8-micron SOI process greatly enhances the robustness of the design, but the trench isolation of individual devices produces its own unique design challenges (mainly device matching). Device modeling inaccuracies in this process result in simulation vs. measurement discrepancies. By over-designing the voltage regulator, these discrepancies did not significantly detract from the voltage regulator functionality. Overall, the designed voltage regulator performs well over all specified operating conditions. The most pronounced inaccuracy of the voltage regulator is the nominal 70-mV deviation from simulated  $V_{DD}$  voltage. Offset voltage imposed by the inability to match trench isolated devices contributes to this offset. Also, BJT base currents can result in offset as these currents induce voltage drops on the input and feedback voltages of the op-amp differential pair. In spite of these model inconsistencies, the overall performance of the voltage regulator meets or exceeds the demands of gate driver and many other high-temperature applications. The temperature performance of the designed voltage regulator exceeds that of other LM723 based designs. Also, largely due to the implementation of the pre-regulator, the line rejection of the designed voltage regulator (both DC and transient conditions) greatly exceeds most commercial voltage regulators. Load regulation is adequate for most applications (up to 200 mA) but can be improved in future designs.

### *5.2– Future Work*

Future design revisions of this voltage regulator will take advantage of the model information discovered in testing this regulator design and testing of individual devices. One potential modification to this voltage regulator is implementing a BJT-based output stage as opposed to the current LDMOS output stage. The BJT output stage could significantly improve the load regulation and temperature performance. To successfully implement the BJT output stage, the closed-base breakdown voltages of the BJT devices will need to be tested to ensure long term reliability. Modifying the output stage could also result in increased load current capabilities

which would expand the applications of this voltage regulator. An effort will also be made to remove the need for an external output capacitor. Increasing the bandwidth (at the expense of DC gain) and modifying compensation techniques could potentially reduce the need for an output capacitor. Temperature compensation may also be modified as device testing improves simulation accuracy. Due to the limited pin count available and the high demand for pins in this gate driver generation, test points for the voltage regulator are limited. Additional voltage regulator information would be available if future design were capable of allocating more pins for the voltage regulator circuit.

## **References**

# References

- [1] M. A. Huque, B. J. Blalock, C. Su, R. Vijayaraghavan, S. K. Islam, and L. M. Tolbert, "SOI-Based Integrated Circuits for High-Temperature Applications.", International Conference on High-Temperature Electronics, HiTEC, 2008.
- [2] M. A. Huque, L. M. Tolbert, B. J. Blalock, and S. K. Islam, "A High-Temperature, High-Voltage SOI Gate Driver IC with High Output Current and On-Chip Low-Power Temperature Sensor." IIMAPS, 42nd International Symposium on Microelectronics, 2009.
- [3] Chester Simpson, "*Linear and Switching Voltage Regulator Fundamentals.*" National Semiconductor, Power Management Applications, 2004.
- [4] P. R. Gray, P. J. Hurst, S. H. Lewis, and R. G. Meyer, *Analysis and Design of Analog Integrated Circuits 4<sup>th</sup> Edition*, John Wiley & Sons, Inc., 2001.
- [5] Richard C. Jaeger, Travis N. Blalock, *Microelectronic Circuit Design 2<sup>nd</sup> Edition*, McGraw-Hill Inc., 2004.
- [6] National Semiconductor, "*LM723/LM732C Voltage Regulator.*" LM723/LM732C Datasheet, June 1999.
- [7] R. J. Baker, *CMOS: Circuit Design, Layout, and Simulation 2<sup>nd</sup> Edition*, John Wiley & Sons Inc., 2005.
- [8] J. F. Pierce, T. J. Paulus, *Applied Electronics*, Bell & Howell Company, 1972.
- [9] F. Shoucair, "Design Considerations in High-Temperature Analog CMOS Intergrated Circuits," *IEEE Transactions on Components, Hybrids, and Manufacturing Technology*, vol. 9, no. 3, Sept. 1986.
- [10] P. Hong, W. Xiaobo, C. Hai, and H. Binxian, "Power Supply Module Design in the Low Power Consumption Application," *Electron Devices and Solid-State Circuits*, vol. 20, no. 22, Dec. 2007.

# Vita

Benjamin Matthew McCue was born in Oak Ridge, TN on September 6<sup>th</sup>, 1983. He graduated from Karns High School in Knoxville, TN in 2001. Benjamin entered the Engineering School at the University of Tennessee in August of 2002 with a goal of obtaining a B.S. in Electrical Engineering. During his junior year in the electrical engineering program, he interned at the Electric Power Research Institute in Knoxville, Tennessee. As a senior, Benjamin began working for Dr. Benjamin Blalock as a research assistant for the Integrated Circuits and Systems Laboratory (ICASL) research group at the University of Tennessee. It was during this time that he realized he wanted to pursue graduate school to enhance his understanding of his field and widen future career possibilities. In the summer of 2007, Benjamin entered the Masters of Science program at the University of Tennessee. During his work toward achieving a Master's of Science degree, he continued work as a research assistant in the ICASL research group under the instruction of Dr. Blalock. During this time, he worked on several projects including the gate driver project funded by the Oak Ridge National Laboratories (ORNL). After conferral of his Master's degree, Benjamin will continue his education in the pursuit of a Ph.D. degree at the University of Tennessee. During this endeavor, he will continue work as a research assistant for Dr. Blalock in the ICASL research group.